PNWD-3763
WTP-RPT-142, Rev 0

Laboratory Scale Hydraulic Testing of Spherical Resorcinol Formaldehyde Ion Exchange Resins

S. T. Arm
D. L. Blanchard, Jr.
K. P. Brooks
W. C. Buchmiller
B. J. Cook
J. M. Cuta
S. K. Fiskum
Z. Hontz
C. Isackson
A. A. Schepmoes
D. E. Wallace

September 2006

Prepared for Bechtel National Inc.
under Contract No. 24590-101-TSA-W000-00004

WTP-RPT-142, Rev 0

Laboratory Scale Hydraulic Testing of Spherical Resorcinol Formaldehyde Ion Exchange Resins

S. T. Arm
D. L. Blanchard, Jr.
K. P. Brooks
W. C. Buchmiller
B. J. Cook
J. M. Cuta
S. K. Fiskum
Z. Hontz
C. Isackson
A. A. Schepmoes
D. E. Wallace

10/2/06
for W. Tamosaitis

ACCEPTED FOR
WTP PROJECT USE

September 2006

Test specification: 24590-PTF-TSP-RT-04-0002
Test plan: TP-RPP-WTP-359, Rev. 0
Test exceptions: 24590-PTF-TEF-RT-04-00002, 24590-PTF-TEF-RT-04-00004, 24590-PTF-TEF-RT-05-00002, 24590-PTF-TEF-RT-05-00003, 24590-PTF-TEF-RT-05-00006
R&T focus area: Pretreatment
Test Scoping Statement(s): A224

Battelle—Pacific Northwest Division
Richland, Washington 99352

Completeness of Testing

This report describes the results of work and testing specified by test plan TP-RPP-WTP-359, Rev. 0 and test specification 24590-PTF-TSP-RT-04-0002 as modified by test exceptions 24590-PTF-TEF-RT-04-00002, 24590-PTF-TEF-RT-04-00004, 24590-PTF-TEF-RT-05-00002, 24590-PTF-TEF-RT-05-00003 and 24590-PTF-TEF-RT-05-00006. The work and any associated testing followed the quality assurance requirements outlined in the test specification/plan. The descriptions provided in this test report are an accurate account of both the conduct of the work and the data collected. Test plan results are reported. Also reported are any unusual or anomalous occurrences that are different from expected results. The test results and this report have been reviewed and verified.

Approved:

Gordon H. Beeman, Manager
WTP R&T Support Project

9/27/06
Date

Summary

Battelle—Pacific Northwest Division (PNWD) is contracted to Bechtel National Inc. (BNI) on the River Protection Project-Waste Treatment Plant (RPP-WTP) project to perform research and development activities. Unit operations of the WTP process include the separation of cesium-137 by ion exchange from the liquid portion of the waste. SuperLig® 644 (SL644) ion exchange resin was selected by the project to perform the cesium separation. However, an alternative ion exchange resin, spherical resorcinol formaldehyde (RF), available from Boulder Scientific (Boulder, Colorado) and Microbeads AS (Norway), is currently undergoing testing.

Results and Performance Against Objectives

This investigation was conducted according to a test plan[a] in response to a test specification[b] and test scoping statement A224.[c] The test objectives were satisfied. Table S.1 summarizes the test objectives and how they were satisfied.

Table S.1. Test Objective Evaluation

Test Objective	Objective met	Discussion
Measure the bed permeability, particle breakage, and axial and radial pressure resulting from chemical cycling in a bench-scale ion exchange system that simulates full-scale operation. Compare these results for RF resin variations produced by different production conditions and by different vendors.	Yes	Three resins from the development vendor were tested, BRF14, BRF15, and BRF18. No particle breakage was observed for these resins. The permeability of these resins was $\sim 3.2\times10^{-10}$ m^2. Radial and axial pressures during down-flow regeneration of these resins were up to ten times that of the differential pressure indicative of the residual stresses arising from constrained bed expansion. The ratio of these pressures indicates an angle of internal friction of 25°. The resins exhibited radial and axial pressures approximately five times that of the differential pressure when processing simulated low-activity waste (LAW) again indicative of the residual stresses arising from constrained bed re-expansion after its initial contraction.

(a) ST Arm. 2004. *Small Scale Hydraulic Testing of Spherical Resorcinol Formaldehyde Ion Exchange Resins.* TP-RPP-WTP-359, Battelle—Pacific Northwest Division, Richland, WA.

(b) MR Thorson. 2004. *Small Scale Hydraulic Testing of Spherical Resorcinol Formaldehyde Ion Exchange Resin.* 24590-PTF-TSP-RT-04-0002, RPP-WTP project, Richland, WA.

(c) MR Thorson, RA Peterson, and GT Wright. 2002. *Alternative Ion Exchange Resin Supplemental Research and Technology Plan - Case 20*. 24590-PTF-PL-RT-02-002 (business sensitive), RPP-WTP project, Richland, WA.

Table S.1. Test Objective Evaluation

Test Objective	Objective met	Discussion
		Two resins from the scale-up vendor were tested, BSC-3380-2P-0100 (BSC00) and BSC-3380-2P-0101 (BSC01). No particle breakage was observed for these resins. The permeability of these resins was ~2.3×10^{-10} m^2. Radial and axial pressures during down-flow regeneration of these resins were typically five times higher than the differential pressure indicative of the residual stresses from constrained bed expansion. The resins exhibited radial and axial pressures comparable to the differential pressure when processing simulated LAW. Up-flow LAW introduction in Wave 2 allowed unrestrained bed expansion so there was little residual stress. Three resins from the 100-gallon production batches, 5E-370/641 (MB641), 5J-370/686 (MB686), and a blend of BSC-3380-3-0200 and BSC-3380-3-0201 (BSblend) were tested. No particle breakage was observed for these resins. Regeneration was typically conducted up-flow with radial and axial pressures comparable to the differential pressure (i.e. no residual stresses since the bed underwent free expansion). The single down-flow MB641 regeneration test yielded a permeability of 2.4×10^{-10} m^2 with radial and axial pressures indicative of residual stresses from constrained bed expansion. The permeability of these resins was ~2.7×10^{-10} m^2 when processing LAW down-flow following up-flow LAW introduction. Radial and axial pressures were comparable to the differential pressure following up-flow LAW introduction since the bed was allowed to freely expand following its initial contraction. However, bed pressures were 3 times the differential pressure when down-flow LAW processing immediately followed down-flow regeneration, which again indicates residual stresses from constrained bed expansion.

Table S.1. Test Objective Evaluation

Test Objective	Objective met	Discussion
Estimate the full-scale hydraulic performance of the resins to assist in column operation and design.	Yes	Regeneration solution and simulated LAW was pumped through the test columns at sufficient flow rate to theoretically replicate the differential pressure expected in the full-scale columns. The full-scale hydraulic performance of the resins was thereby estimated as described above.
Compare the hydraulic performance of the candidate RF resins and SL644 resin.	Yes	The SL644 resin was tested alongside the BRF18 development resin. SL644 permeabilities during regeneration and LAW processing were ~1.0×10^{-10} m^2 and ~2.4×10^{-10} m^2, respectively. BRF18 permeability was higher at ~3.5×10^{-10} m^2 and 2.9×10^{-10} m^2 during regeneration and LAW processing, respectively. In contrast to BRF18, significant particle breakage was observed for SL644, resulting in decreasing permeability with increasing cycle number. SL644 radial and axial pressures during regeneration were typically seven times the differential pressure, compared to ten times for BRF18. SL644 exhibited radial and axial pressures comparable to the differential pressure when processing simulated LAW, showing little change in bed volume.
Measure approximate resin chemical performance degradation caused by hydraulic cycling for one chosen resin formulation.	Yes	The BRF15 resin was selected to test for chemical performance degradation caused by hydraulic testing. Batch contacts on the fresh and cycled resins showed that the equilibrium performance of the resin was not impaired by hydraulic cycling.

Test Exceptions

Table S.2 discusses the five test exceptions, provided by Thorson(a)(b)(c)(a)(b) and applied to this test.

(a) MR Thorson. 2004. Test Exception 24590-PTF-TEF-RT-04-00002, Revision 0, RPP-WTP, Richland, WA.

(b) MR Thorson. 2004. Test Exception 24590-PTF-TEF-RT-04-00004, Revision 0, RPP-WTP, Richland, WA.

(c) MR Thorson. 2005. Test Exception 24590-PTF-TEF-RT-05-00002, Revision 0, RPP-WTP, Richland, WA.

Table S.2. Test Exceptions

Test Exception	Discussion
24590-PTF-TEF-RT-04-00002	Resin for testing in Waves 2 and 3 was to be pre-conditioned and pretreated per the protocol P1-RF (WTP document number 097893 *Protocol P1-RF: Spherical Resin Sampling from Containers, Resin Pretreatment, F-factor and Resin Loading to Column*.)
24590-PTF-TEF-RT-04-00004	The scope increased to include more batch-contact tests. These contacts were conducted to assist in selecting resins for hydraulic testing.
24590-PTF-TEF-RT-05-00002	This test exception applied only to Waves 2, 3, and 4. It included revisions to the test column to reflect changes in the WTP full-scale column design and base-line superficial velocity. The test exception also directed PNWD to include a bed fluidization step with simulated LAW before processing simulated LAW. Sparging with air stripped of carbon dioxide was directed so that the resin would be exposed to the same quantity of dissolved oxygen as in the full-scale operating conditions. Finally, the test exception allowed additional or fewer cycles to be performed, as directed by RPP-WTP Research and Technology (R&T) project staff.
24590-PTF-TEF-RT-05-00003	Pretreatment of resins in Waves 2, 3, and 4 may be adjusted to better align it with the pretreatment to be performed under other test scoping statements (specifically A215).
24590-PTF-TEF-RT-05-00006	This test exception directed PNWD to conduct other up-flow and bed fluidization steps (in addition to that described in 24590-PTF-TEF-RT-05-00002) at the direction of RPP-WTP R&T project staff.

Results and Performance Against Success Criteria

Table S.3 discusses the success criteria provided by Thorson.(c)

(d) MR Thorson. 2005. Test Exception 24590-PTF-TEF-RT-05-00003, Revision 0, RPP-WTP, Richland, WA.

(e) MR Thorson. 2005. Test Exception 24590-PTF-TEF-RT-05-00006, Revision 0, RPP-WTP, Richland, WA.

(c) MR Thorson. 2004. *Small Scale Hydraulic Testing of Spherical Resorcinol Formaldehyde Ion Exchange Resin*. 24590-PTF-TSP-RT-04-0002, RPP-WTP project, Richland, WA.

Table S.3. Discussion of Test Success Criteria

Success Criteria	Discussion
Data supporting selection of an RF resin production type most likely to meet WTP requirements.	Testing has successfully generated sufficient bed pressure and permeability data to support RF resin selection.
Data supporting confirmation that the spherical RF resin can be successfully prepared at scale-up proportions (100-gallon production batches).	Results from testing the resin from four 100-gallon production batches were consistent with those from testing the resin from smaller developmental batches.
Data supporting refinement of production specifications based on results of hydraulic testing.	Testing has successfully generated sufficient bed pressure and permeability data to support refining RF resin production conditions.

Quality Requirements

PNWD implemented the RPP-WTP quality requirements in a quality assurance project plan (QAPjP) as approved by the RPP-WTP quality assurance (QA) organization. Testing and analytical activities were conducted in accordance with PNWD's QA project plan, RPP-WTP-QAPjP, which invoked NQA-1-1989 Part I, "Basic and Supplementary Requirements," and NQA-2a-1990, Part 2.7. These quality requirements were implemented through PNWD's Waste Treatment Plant Support Project Quality Assurance Requirements and Description Manual.

PNWD addressed data-verification activities by conducting an independent technical review of the final data report in accordance with Procedure QA-RPP-WTP-604. This review verified that the reported results were traceable, that inferences and conclusions were soundly based, and that the reported work satisfied the test plan objectives.

Research and Technology Test Conditions

The test specification(a) established extensive conditions to verify that the results are valid for RPP-WTP project needs. The conditions are not repeated here because of their extensive nature, but they essentially constitute the test methodology described later in this summary. The conditions, as modified by the test exceptions and test plan,(b) were satisfied.

(a) MR Thorson. 2004. *Small Scale Hydraulic Testing of Spherical Resorcinol Formaldehyde Ion Exchange Resin.* 24590-PTF-TSP-RT-04-0002, RPP-WTP project, Richland, WA.

(b) ST Arm. 2004. *Small Scale Hydraulic Testing of Spherical Resorcinol Formaldehyde Ion Exchange Resins.* TP-RPP-WTP-359, Battelle—Pacific Northwest Division, Richland, WA.

Simulated Waste Use

The tests described by this report used simulated LAW, and the RPP-WTP project has a contractual requirement to compare the results of such testing with those from similar tests using actual LAW. No hydraulic testing of the batches of spherical RF used in these tests with actual waste has been conducted. However, the concentrations of sodium, potassium, cesium, and free hydroxide, the constituents most important to ion exchange performance, were prototypic for AP101 LAW at ~5 M, ~28 g/L, ~6 mg/L, and ~1.9 M, respectively. Viscosity and density are the important properties for hydraulics testing, and Russell et al. (2003) have measured these properties at 3.4 cP and 1.256 g/mL for actual diluted AP101 LAW. Typical viscosity and density values reported in this work are 2.6 cP and 1.2 g/mL, respectively, and so are consistent with the actual waste.

Test Methodology

Testing was performed in what are termed as waves in this report and four waves of testing were completed. Three resins from a development vendor (BRF14, BRF15, and BRF18), two resins from a production scale-up vendor (BSC-3380-2P-0100 and BSC-3380-2P-0101), three resins from 100-gallon production batches (5E-370/641, 5J-370/686 and blended BSC-3380-3-0200 and BSC-3380-3-0201), and SL644 resin underwent hydraulic testing as part of this test. Testing was performed in a 76-mm (nominally 3-inch) diameter stainless steel column containing an ion exchange bed up to 124 mm (4.88 inches) deep. The column was instrumented with diaphragm pressure transducers located on the bottom and on the side near the bottom, a differential pressure transducer, and a thermocouple. A bolted flange attached a transparent column section to the top of the stainless steel section. The height of the plastic section was sufficient to view where the top of the resin bed and column wall intersect, and gradations marked onto the internal surface of the wall enabled bed height measurement.

Hydraulic testing involved subjecting the resins to a number of ion exchange cycles, including simulated AP101 LAW processing, feed displacement with 0.1 M sodium hydroxide, pre-elution rinse with de-mineralized water, elution with 0.5 M nitric acid, post-elution rinse with de-mineralized water, and regeneration with 0.5 M sodium hydroxide. Simulated AP101 LAW processing and regeneration were performed at flow rates sufficient to replicate the bed differential pressure of the full-scale column and were measured by a mass flowmeter. Flow rates used in other steps were scaled from the full-scale with respect to the bed residence time. Resins from the scale-up vendor and 100-gallon batches were subjected to a bed fluidization step with 0.5 M sodium hydroxide and/or simulated AP101 LAW before processing the simulated LAW down-flow. Electronic data from the pressure transducers, flowmeter, and thermocouple were collected and recorded using a data-acquisition system.

Resin particle size analysis was performed on fresh and cycled material using a Microtrac Particle Size Analyzer Model S3000. Fluid densities were determined by weighing known volumes, and viscosities were measured using a Canon-Fenske viscometer.

Batch contacts were performed on the virgin and cycled resin from the development vendor to assess the impact of hydraulic testing on equilibrium chemical performance. The tests were performed in duplicate on each resin using simulated AP101 LAW containing cesium at three concentrations.

Results Summary

Three resins from a development vendor (BRF14, BRF15, and BRF18), two resins from a production scale-up vendor (BSC-3380-2P-0100 and BSC-3380-2P-0101), three resins from 100-gallon production batches (5E-370/641, 5J-370/686 and blended BSC-3380-3-0200 and BSC-3380-3-0201), and SL644 resin were hydraulically characterized in terms of their bed voidage, permeability and bed pressure. Resin fluidization and capacity was characterized for the resins from the scale-up vendor and those from the 100-gallon production batches.

The spherical RF resins exhibited consistent hydraulic performance and permeability. The permeability of the development vendor's RF resins was ~3.2×10^{-10} m^2, while that of the scale-up vendor's RF resins was ~2.1×10^{-10} m^2. The 100-gallon batch RF resin permeability was ~2.7×10^{-10} m^2 following up-flow LAW. The permeability of the 100-gallon production resin batch 5E-370/641 reduced from 2.9×10^{-10} m^2 to 2.0×10^{-10} m^2 when the LAW was introduced down-flow immediately following down-flow regeneration. The lower permeabilities of the scale-up and 100-gallon batch RF resins can be attributed to their smaller particle size. No breakage of the spherical RF resins was observed. Average SL644 permeabilities of 1.0×10^{-10} m^2 and 2.4×10^{-10} m^2 were calculated for the regeneration and simulated LAW processing steps, respectively. However, breakage of the granular SL644 resin particles led to the accumulation of fine material in the bed and decreasing permeabilities with increasing cycle number.

The RF resins exhibited radial and axial pressures higher than expected from considering only the action of the hydraulic drag during down-flow regeneration because the bed retains the stresses induced by its constrained expansion. Bed pressures were proportional to the differential pressure during regeneration, as expected from theory. Similarly, bed pressures were higher than the differential pressure when processing LAW because the bed undergoes initial contraction and then re-expansion. Up-flow LAW introduction to the scale-up and 100-gallon batch RF resins before processing the simulated LAW down-flow appears to relieve the stresses associated with expansion of the bed following its initial contraction in LAW. Bed pressures were, therefore, comparable to the differential pressure.

Radial and axial pressures exerted by the SL644 resin were also higher than the differential pressure, which is again indicative of the stresses induced by the beds constrained expansion. The SL644 bed volume did not significantly change when processing LAW so bed pressures were comparable to the differential pressure, in contrast to the RF resins.

Down-flow regenerated RF ion exchange beds could not be fluidized with simulated AP101 LAW, except where assisted by bubbles entrained in the feed, and the beds behave as plugs adhering to the column walls. Up-flow LAW introduction, without fluidization, could be accomplished, but the observed partial break-up of the bed may potentially lead to fissures in the bed that would have channeled LAW and led to unacceptably early cesium breakthrough. Two methods for fluidizing the beds with simulated AP101 were successfully tested to achieve a level settled bed:

- Relieve the radial pressures by alternately pumping and terminating up-flow simulated LAW introduction while the bed undergoes initial contraction in simulated LAW. The bed can then be fluidized with simulated LAW.
- Eliminate the radial pressures exerted by the bed by performing up-flow regeneration before its fluidization in simulated LAW.

Up-flow regeneration was considered the more practical option for performing in the WTP and was extensively characterized for the 100-gallon production resin batches. The bed height increased as the resin expanded, and the time to attain full expansion was inversely proportionate to the flow rate. The effluent sodium hydroxide concentration was measured in later cycles to develop sodium consumption profiles. Sodium consumption typically tracked the bed expansion profiles, and a capacity of ~1.6 mol/L wet sodium form resin was calculated for the 100-gallon production resin batches. Up-flow and fluidized bed elution were successfully demonstrated in the Wave 4 tests at a range of fluid velocities. An average capacity of 1.8 mol/L wet sodium form resin was calculated for the Wave 4 resins based on nitric acid consumption. The difference between the regeneration and elution capacities is most likely caused by experimental uncertainties.

The density of the bed in the 3-inch column used in these tests appears to be 10% lower than that measured in the 2-cm columns of TSS A225. This difference is most likely because of the 2-cm column being tapped until a constant volume is achieved whereas no such configuring of the bed was attempted in the 3-inch column to be representative of the actual conditions expected in the WTP.

There was no impact of chemical cycling on the equilibrium performance of the development vendor's RF resin, as measured in batch contacts.

Discrepancies and Follow-on Tests

No discrepancies concerning hydraulic performance of the resins were identified.

Acronyms, Abbreviations, and Definitions

A_{IX}	cross-sectional area of the column
ASTM	American Society for Testing and Materials
AV	apparatus volume
BNI	Bechtel National, Inc.
BV	bed volume
cP	centi-poise
C_1	equilibrium cesium-137 concentration in solution
C_{eq}	final (equilibrium) cesium concentration
C_o	initial cesium concentration
Cs_R	equilibrium cesium concentration in the resin
D	Column diameter
D_p	Particle diameter
DI	de-ionized (water)
F_f	differential friction drag force
F_g	differential buoyancy force
F_q	differential hydraulic drag force
F	F-factor—mass of the dried resin divided by the mass of the resin weighed for batch contact testing
g	gravitational acceleration
GEA	gamma energy analysis
HLW	high-level waste
HP	hot persulfate
HT	hydraulic tested

IC	ion chromatography
ICP-AES	inductively coupled plasma-atomic emission spectrometry
ICP-MS	inductively coupled plasma-mass spectrometry
I_{Na}	mass increase of acid-form resin to sodium-form resin
I/O	input/output
K	resin permeability
k’	radial to axial stress ratio
K_d	batch distribution coefficient
LAW	low-activity waste
LEPS	low-energy photon spectroscopy
M_{Rd}	mass of resin dried to constant mass at $50^{o}C$ and under vacuum
M_{Ri}	mass of resin dried to a free-flowing state under ambient conditions
M&TE	measuring and test equipment
P_q	Stress from hydraulic drag
P_a	bed axial stress
P_r	bed radial stress
PNWD	Battelle—Pacific Northwest Division
QA	quality assurance
QAPjP	Quality Assurance Project Plan
QC	quality control
RF	resorcinol formaldehyde
RPL ASO	Radiochemical Processing Laboratory Analytical Service Operations
RPP-WTP	River Protection Project-Waste Treatment Plant
R&T	Research and Technology
SL	SuperLig®

SOW	Statement of Work
SRNL	Savannah River National Laboratory
V_l	volume of the liquid sample
VR	virgin (resin)
V_o	superficial velocity of the fluid
$(V_o)_{IX\ col}$	flow velocity in the full-scale ion exchange column
$(V_o)_{ts}$	flow velocity in the test section
VE Zero	air stripped of carbon dioxide
WTPSP	Waste Treatment Plant Support Project
z	distance
Z	resin bed height
Z_{IX}	bed height in the full-scale ion exchange column
Z_{ts}	bed height in the test section
ε	bed porosity
ε_p	particle porosity
ϕ	internal angle of friction
ρ_l	liquid density
ρ_s	solid skeletal density
μ	viscosity
μ'	coefficient of friction

Contents

Figures

Tables

1.0 Introduction

1.1 Background

Battelle—Pacific Northwest Division (PNWD) is contracted to Bechtel National Inc. (BNI) on the River Protection Project-Waste Treatment Plant (RPP-WTP) project to perform research and development activities. The purpose of the RPP-WTP project is to design, construct, and commission a plant to treat and immobilize high-level waste (HLW) and low-activity waste (LAW) stored in underground storage tanks at the Hanford Site. Unit operations of the LAW treatment process include the separation of cesium-137 by ion exchange from the liquid portion of the waste. SuperLig® 644 (SL644) was selected by the project as the baseline ion exchange resin to perform the cesium-137 separation and is available from IBC Advanced Technologies, Inc., American Fork, Utah. Hassan et al. (2001), Kurath et al. (2000a), Kurath et al. (2000b), Arm et al. (2003a), Fiskum et al. (2003a), and Arm et al. (2003b), for example, have tested this resin and shown that it satisfies the performance criteria delineated by the RPP-WTP project. However, BNI contracted with PNWD to test alternative ion exchange resins and down-selected spherical resorcinol formaldehyde (RF) for scale-up production as a result of work by Fiskum et al. (2004), Burgeson et al. (2004), and Arm and Blanchard (2004). This report describes permeability and hydraulic tests on the spherical RF resins generated from scale-up production tests. Raw data and supporting calculations are available to the RPP-WTP project[a].

1.2 Objectives

The primary objectives of this task were to:

- measure the bed permeability, particle breakage, and axial and radial pressure resulting from chemical cycling in a bench-scale ion exchange system that simulates full-scale operation and compare these results for the RF resin batches produced by different production conditions, and by different vendors
- estimate the full-scale hydraulic performance of the resins to assist in column operation and design
- provide a comparison of the hydraulic performance of the candidate RF resins and SL644 resin
- measure approximate resin chemical performance degradation caused by hydraulic cycling for one chosen resin formulation.

1.3 Purpose

This report documents the testing, results, and analysis associated with the spherical RF hydraulics characterization investigation. The purpose of the investigation was to provide information for:

- selecting an RF resin production type most likely to meet WTP requirements
- confirming that the spherical RF resin can be successfully prepared at scale-up proportions (100-gallon production batches)
- refining production specifications based on results of hydraulic testing.

(a) Beeman, GH. 2006. *Data Reported in WTP-RPT-142 Rev 0*. Letter RPP-WTP-06-672 to MR Thorson.

1.4 Quality Assurance

1.4.1 Application of RPP-WTP Quality Assurance Requirements

PNWD implemented the RPP-WTP quality requirements by performing work in accordance with the PNWD Waste Treatment Plant Support Project quality assurance project plan (QAPjP) approved by the RPP-WTP Quality Assurance (QA) organization. This work was performed to the quality requirements of NQA-1-1989 Part I, Basic and Supplementary Requirements, and NQA-2a-1990, Part 2.7. These quality requirements were implemented through PNWD's *Waste Treatment Plant Support Project (WTPSP) Quality Assurance Requirements and Description Manual*. The analytical requirements were implemented through PNWD's *Conducting Analytical Work in Support of Regulatory Programs* through WTPSP's Statement of Work (WTPSP-SOW-005) with the Radiochemical Processing Laboratory Analytical Service Operations (RPL ASO).

A matrix that cross-references the NQA-1 and 2a requirements with PNWD's procedures for this work is given in the test plan.(a) It includes justification for those requirements not implemented.

1.4.2 Conduct of Experimental and Analytical Work

Experiments that were not method-specific were performed in accordance with PNWD's procedures QA-RPP-WTP-1101 "Scientific Investigations" and QA-RPP-WTP-1201 "Calibration Control System," verifying that sufficient data were taken with properly calibrated measuring and test equipment (M&TE) to obtain quality results.

As specified by Thorson,(b) BNI's QAPjP, PL-24590-QA00001, is not applicable because the work was not performed in support of environmental/regulatory testing, and the data will not be used as such.

The applicable quality control (QC) parameters for chemical analysis of the simulated LAW feedstock are delineated in the test plan(a) describing the analysis. Blank spike and/or laboratory control sample QC failures would result in re-analyzing the sample for the particular analyte for which the spike failed. Matrix spike and/or duplicate analysis QC failures would not result in re-analyzing the sample, but probable reasons for the failure would be discussed in the analytical report to be stored in the project files. A qualitative impact assessment of the failure on the results would be discussed in the report.

Analytical processes were performed in accordance with WTPSP's Statement of Work (WTPSP-SOW-005) with the RPL ASO. Cesium-137 tracer used in the batch contact tests was counted using a gamma energy analysis (GEA) system consisting of a multi-channel analyzer and a suitable detector, such as a high-purity germanium detector. Counting was performed according to the procedure *Gamma Energy Analysis (GEA) and Low Energy Photon Spectroscopy (LEPS)*, PNL-ALO-450, when activity concentrations were required for reporting. The procedure *Routine Research Operations*, RPL-OP-001, was used to control counting when relative activity concentrations in calculating

---

(a) SK Fiskum. 2004. *Column Performance Testing of Variations of Spherical Resorcinol Formaldehyde Resins, Stage 2*. TP-RPP-WTP-368, Battelle—Pacific Northwest Division, Richland, WA.

(b) MR Thorson. 2004. *Small Scale Hydraulic Testing of Spherical Resorcinol Formaldehyde Ion Exchange Resin*. 24590-PTF-TSP-RT-04-0002, RPP-WTP project, Richland, WA.

equilibrium distribution coefficients were required for reporting. Absolute counting efficiency and energy calibration were not required because the analysis was comparative. The GEA instrument was monitored for consistent operation by counting cesium-137 control standards both before and after one day's analysis sequence. The instrument background was counted once each day the system was used.

The hydraulic test apparatus included magnetic flowmeters, thermocouples, diaphragm pressure transducers, and differential pressure transducers. The flowmeters were calibrated by the Colorado Engineering Experiment Station, Inc., Nunn, Colorado, while the pressure transducers and thermocouples were calibrated at the Pacific Northwest National Laboratory.

Additional equipment that was used included a ruler, thermometer, clock, and balances. The thermometer for monitoring the batch-contact temperature, ruler, and timepiece are standard laboratory equipment for use as indicators only. Balances are calibrated annually by a certified contractor, QC Services, Portland, Oregon.

1.4.3 Internal Data Verification and Validation

PNWD addressed internal verification and validation activities by conducting an independent technical review of the final data report in accordance with PNWD's procedure QA-RPP-WTP-604. This review verified that the reported results are traceable, inferences and conclusions are soundly based, and the reported work satisfies the Test Plan objectives. This review procedure is part of PNWD's *WTPSP Quality Assurance Requirements and Description Manual*.

2.0 Test Design and Operation

This section describes 1) the process for preparing simulated AP101 LAW and reagents, 2) the batch-contact procedure, and 3) the ion exchange column test set-up and operation.

2.1 Overview

A number of ion exchange resins underwent hydraulic testing over 2 years as part of this investigation. The resins were tested in several series designated as numbered waves (1-4) and sub-waves. In all cases, Microbeads (Skedsmokorset, Norway) created the seed material used for the spherical RF production. SINTEF((Trondheim, Norway) and Microbeads prepared numerous resin batches under various processing conditions for testing. BNI contracted Boulder Scientific Corporation (BSC, Mead, CO) to prepare spherical RF resin using the Microbeads patent under the supervision of Microbeads personnel.

Different resin lots were prepared under slightly different conditions in an effort to optimize Cs ion exchange capacity and selectivity. Varied production parameters included relative resorcinol-to-formaldehyde mole ratios, curing time, curing temperature, and excess monomer (RF) added beyond the theoretical capacity of the resin sphere. Test Waves 3 and 4 evaluated resin quality from scaled-up production to 100-gallon batches. Table 2-1 summarizes the IDs, manufacturer, lot number, lot size, preparation, and receipt dates for resins assigned to PNWD for each tested resin subdivided according to test wave. Each RF resin was received in the H-form under water. Actual production parameters were confidential and were provided directly to the Research and Technology (R&T) lead from Microbeads.

Hydraulic testing involved subjecting the resins to a number of ion exchange cycles, including simulated Tank 241-AP-101 (AP101) LAW processing, feed displacement, pre-elution rinsing, elution, post-elution rinsing, and regeneration. The tested resins, the number of cycles to which they were subjected, and the flow rates for the simulated LAW processing and regeneration steps were determined in part from the work specified in test scoping statement A225 and in consultation with RPP-WTP project staff. Table 2-1 shows the implemented test strategy.

Existing stocks of spherical RF (BRF18) and SL644 resins were used in the Wave 0 tests performed to primarily verify the approach and equipment and compare the resins. Four spherical RF resins prepared by SINTEF were tested as part of scoping statement A225, and the two most promising resins (BRF14 and BRF15) were then hydraulically tested. In addition, the ion exchange equilibrium performance of the best resin (BRF15) was determined in batch contacts before and after hydraulic testing. Likewise, the most promising two (BSC00 and BSC01) of four resins manufactured by BSC and evaluated as part of test scoping statement A225 were hydraulically tested. Batches of 100 gallons were manufactured and four batches (5E-370/641, 5J-370/686 and blended BSC-3380-3-0200 and BSC-3380-3-0201) were hydraulically tested.

Table 2-1. Hydraulic Testing Strategy

Test wave number	Test description	Identity of tested resin	Initial bed height to diameter ratio(a)	Number of cycles performed	Waste processing and regeneration linear flow rates for each cycle (multipliers of RPP-WTP design basis)(b,c)
0	Shake-down	BRF18(d) SL644(e)	1.61 1.67	3	16, 5, 16
1	Development vendor resins	BRF14(d) BRF15(d)	1.59 1.65	10	Simulated LAW processing: 16, 5, 16, 28, 8, 1, 16, 5, 28, 16 Regeneration: 16, 5, 16, 16, 8, 1, 16, 5, 16, 16
2	Scale-up vendor samples	BSC00(f) BSC01(g)	1.06 1.06	5	Simulated LAW processing: 17, 32, 17, 17, 17 Regeneration: 17, 17, 17, (h)
3	100-gallon batch	5E-370/641(i)	1.19	12	Simulated LAW processing: 1.3, 32, max(j), 17, 17, 17, 17, 17, 32, max(j), 17, 1.3 Regeneration: (k)
4	Subsequent 100-gallon batches	MB686(l) BSblend(m)	1.13 1.13	3	Simulated LAW processing: max(j), 17, max(j)

(a) Initial height measured of bed in fully swollen sodium-form with zero-flow.

(b) For example, the shake-down (Wave 0) tests considered linear flow rates of 16×7.1=114 cm/minute and 5×7.1=36 cm/minute.

(c) The design basis was 7.1 cm/minute in Waves 0 and 1 and 5.85 cm/minute in subsequent waves.

(d) Manufactured by SINTEF in June 2004 in 2-L batches and received by PNWD July 19, 2004.

(e) Manufactured by IBC Advanced Technologies in November 2002 in a 250-gallon batch and received by PNWD July, 2003.

(f) The full resin lot designation is BSC-3380-2P-0100, manufactured by BSC in March, 2005 and received by PNWD March 18, 2005.

(g) The full resin lot designation is BSC-3380-2P-0101, manufactured by BSC in March, 2005 and received by PNWD March 18, 2005.

(h) Regeneration in Cycles 4 and 5 conducted up-flow at various velocities.

(i) Manufactured by Microbeads in May, 2005 and received by PNWD June 6, 2005.

(j) Flow rate set at maximum to maximize pressure drop across bed.

(k) Up-flow at prototypic velocities except Cycle 6 in which the velocity was 17 times the WTP design basis.

(l) The full resin lot designation is 5J-370/686, manufactured by Microbeads in November, 2005 and received by PNWD October 21, 2005.

(m) Equal volumes of lots BSC-3380-3-0200 and BSC-3380-3-0201 were blended for testing. BSC-3380-3-0200 was manufactured by BSC in November, 2005 and received by PNWD December 19, 2005. BSC-3380-3-0201 was manufactured by BSC in May, 2006 and received by PNWD May 12, 2006.

2.2 Simulated AP101 LAW Preparation

Tests were performed using a simulated LAW because using actual waste would have proved unacceptably expensive and impractical from a supply standpoint for the scale of the test.

The LAW currently stored in AP101 was selected as that to simulate and test because the LAW in this tank is scheduled to be processed in the WTP, and in some respects, it is representative of the Envelope A type waste that will constitute the majority of the feed to the WTP. Several gallons of the simulated LAW at a sodium concentration of nominally 5 M were prepared by Noah Technologies Inc. (San Antonio, TX) in two batches under sub-contracts 7526 and 8432. The batches of simulated LAW were analyzed by ion chromatography (IC), inductively coupled plasma-atomic emission spectrometry (ICP-AES), hot persulfate (HP) oxidation, and titration. Table 2-2 compares the actual analyte concentrations with their targets. Only targeted/major analytes are reported. The simulated LAW also included trace constituents as described by Russell et al. (2003).

Cesium was omitted from these batches and added as cesium nitrate by PNWD staff to the concentrations desired for the batch-contact test and are provided later in the report. Cesium concentrations were determined by inductively coupled plasma-mass spectrometry (ICP-MS).

The viscosity and density of the simulated AP101 LAW was determined for the batch processed in each cycle of each wave according to the method outlined in Section 2.7. Table 2-3 shows the average viscosities and densities for each wave.

2.3 Reagent Preparation

All reagents were "reagent grade." Solutions of nominally 0.1 M, 0.5 M, and 1 M sodium hydroxide were prepared by diluting the concentrated 50% sodium hydroxide with de-ionized (DI) water. The solution of 0.5 M nitric acid was prepared by diluting the 68 to 70 wt% nitric acid commercial stock with DI water.

The viscosity and density of the 0.5 M sodium hydroxide was determined for the batch processed down-flow in each cycle of each wave according to the method outlined in Section 2.7. The average viscosities and densities for each wave are provided in Table 2-4.

Table 2-2. Simulated AP101 LAW Composition

Analyte	Analysis Method	Concentration (mg/L)[a,b]		
		Target	Batch 1	Batch 2
Aluminum	ICP-AES[c]	6,990	6,850	6,920
Cesium	ICP-MS	3.39	6.01	5.97[d]
Chromium	ICP-AES	152	160	150
Phosphorus	ICP-AES	384	410	408
Potassium	ICP-AES	27,800	27,800	28,150
Sodium	ICP-AES	115,000	123,000	114,500
Inorganic carbon	HP	5,350	5,400	5,550
Chloride	IC	1,450	1,715	1,170
Hydroxide (free)	Titration	33,000	32,850	30,700
Nitrate	IC	104,000	103,000	105,000
Nitrite	IC	32,500	34,100	32,400
Sulfate	IC	3,580	3,910	3,680

(a) Results have errors likely <15%.

(b) Reported results satisfy the WTP project quality control criteria.

(c) ICP-AES = inductively coupled plasma-atomic emission spectroscopy.

(d) The cesium results are based on the amended formulation used for batch-contact tests and the desired concentration of nominally 6 mg/L was selected to optimize the tests. The simulated LAW used for hydraulic testing contained no added cesium.

Table 2-3. Average Viscosities and Densities for Simulated AP101 LAW

Wave	Viscosity (cP)	Density (g/mL)
0	3.10	1.250
1	3.05	1.240
2	2.56	1.250
3	2.17	1.210
4	2.33	1.230

Table 2-4. Average Viscosities and Densities for 0.5 M Sodium Hydroxide

Wave	Viscosity (cP)	Density (g/mL)
0	Not measured	Not measured
1	1.12	1.010
2	0.96	1.010
3	0.93	1.005
4	Not measured	

2.4 Ion Exchange Column Test Apparatus

The test apparatus was modified before and during testing, and Figure 2-1 provides a process schematic of its final form. A photograph of the apparatus used in waves 0 and 1 is presented in Figure 2-2. The operational philosophy to process reagents at sufficiently high flow rates to simulate full-scale hydraulic behavior facilitated a relatively small-scale apparatus that minimized costs and wastes that would have otherwise been higher in a larger scale test.

The apparatus consisted of a stainless steel ion exchange column sized to accommodate an ion exchange bed nominally 76 mm (3 inches) in diameter and up to 124 mm (4.88 inches) high. The Wave 0 and Wave 1 tests used a sodium-form resin bed volume of nominally 610 mL whereas subsequent tests used a sodium-form resin bed volume of nominally 410 mL. As shown in Figure 2-3, a stainless steel 6-mm (0.25-inch) tube extending to the bed bottom was used in most cycles of Wave 0 and Wave 1 tests to simulate the instrumented dry well planned for the plant columns. Wave 2, 3, and 4 tests replaced the central rod with two 3-mm (0.125-inch) rods located 135° apart on a radius of 21 mm and extending to within 32 mm (1.26 inches) of the bed bottom to simulate the revised WTP design for the dry wells. A bolted flange attached a transparent plastic column section to the top of the stainless steel column. The plastic section was completely flooded to maintain a head of fluid above the resin bed. The height of the plastic section was sufficient to view where the top of the resin bed and column wall intersect, and gradations marked onto the internal surface of the wall enabled bed-height measurement.

The column was instrumented with diaphragm pressure transducers (Honeywell Sensotec Model S) located on the bottom and on the side near the bottom, a differential pressure transducer, and a thermocouple. After Wave 1, a gauge that measured the pressure in the line from the column bottom was added. The measurement from this gauge enabled the fluid pressure just above the screen to be calculated and subtracted from the diaphragm pressure transducer measurements. In this way, only the pressure exerted by the bed was considered for analysis. Note that the negative pressures sometimes measured by these gauges are within their tolerance.

Reagents were pumped up (Wave 2, 3, and 4 testing only) or down through the column from one of two feed lines. The low flow line pumped reagents using a piston pump (Fluid Metering, Inc., Syosset, NY) at rates representative of those expected in the RPP-WTP (relative, scaled with respect to the bed volume). The high-flow line fed reagents using a gear pump (T-series, Tuthill Corporation, Concord, California) at sufficient flow rates to replicate the bed differential pressure arising from the frictional drag expected in a full-scale plant column. The high-flow line was instrumented with a magnetic flow meter (Krohne series IFM5090K). Numerous vent lines were included in the apparatus to minimize entrainment of air bubbles in the feed lines.

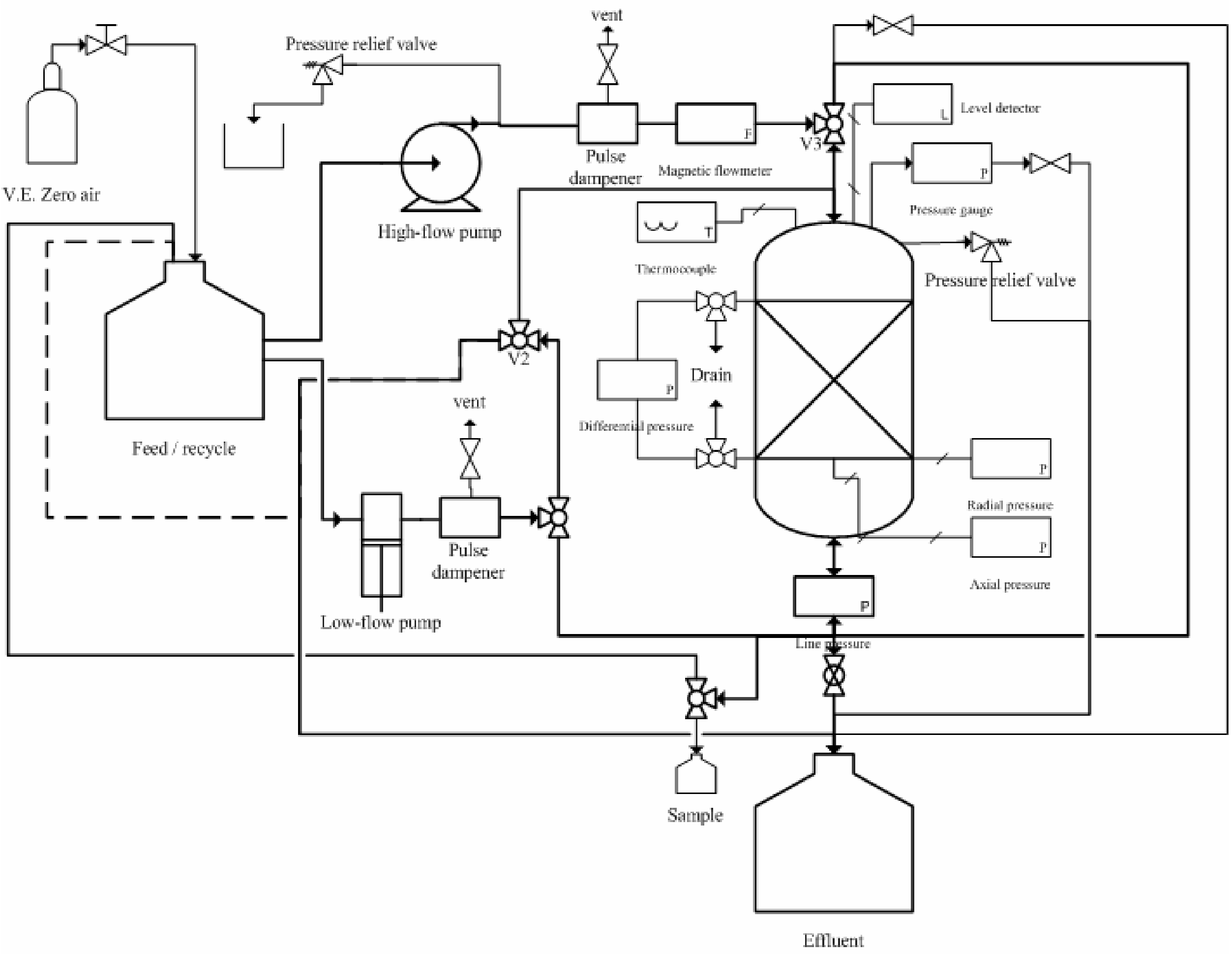

Figure 2-1. Schematic of Resin Hydraulics Test Process

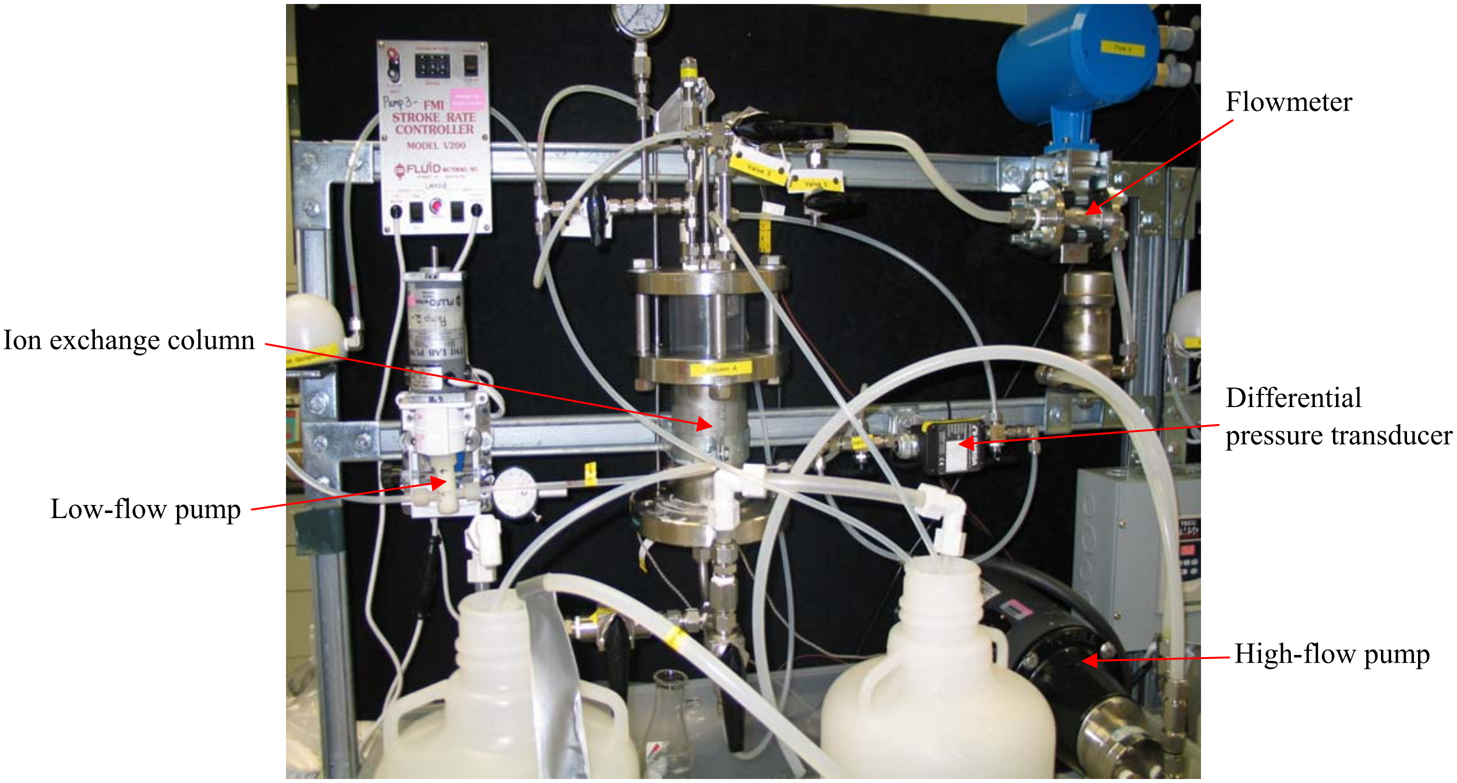

Figure 2-2. Photograph of hydraulics testing apparatus used in waves 0 and 1

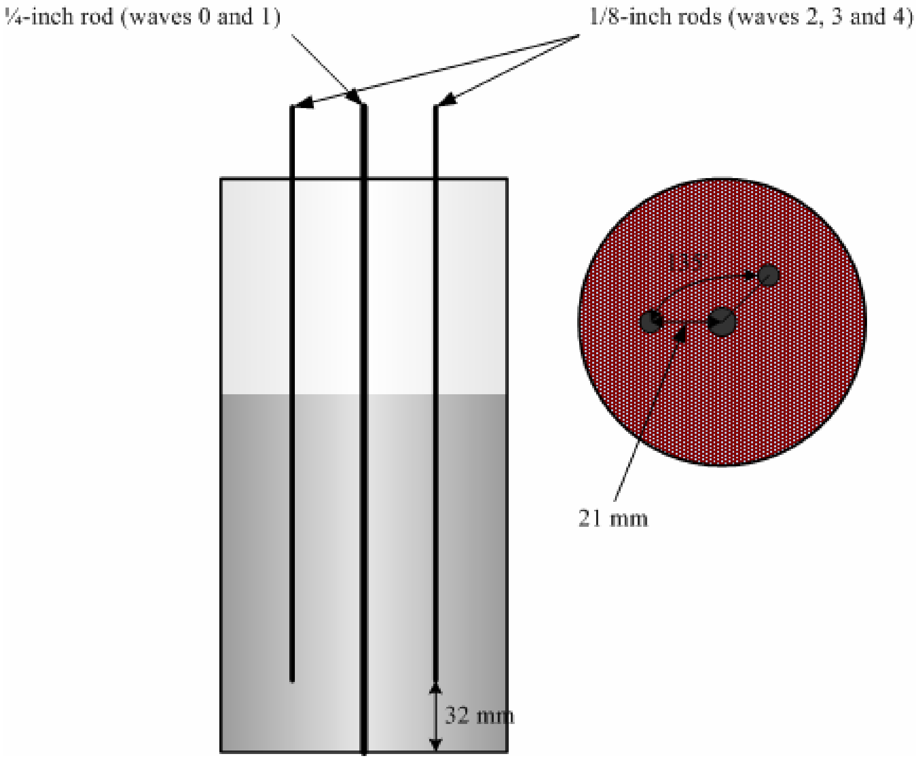

Figure 2-3. Column schematic show simulated thermal wells

2.5 Ion Exchange Column Test Operation

Resin conditioning consisted of contacting the resins with sodium hydroxide so they were loaded into the columns in their fully expanded state. The resins expand from their as-received, acid – form as the protons are exchanged for hydrated sodium ions. Resins for Wave 0 and Wave 1 testing were pre-conditioned by soaking the requisite volume in three bed volumes of 1 M sodium hydroxide for 2 hours according to a procedure approved by BNI. Wave 2, 3, and 4 resins were also soaked in three bed volumes of 1 M sodium hydroxide but left to soak overnight according to standard protocol that was issued by BNI after completing Wave 1 testing. The sodium hydroxide was then decanted and replaced with deionized (DI) water when the slurry was transferred to the column using a pipette.

Following transfer of the Wave 0 and Wave 1 resin to the column, the sodium-form resin was conditioned in a single cycle that consisted of pumping the following reagents down through the bed.

1. Three apparatus volumes (AVs, one AV was equivalent to 810 mL and included the column and feed and effluent lines) of DI water at 3 BV/hour.
2. Six bed volumes (BVs) of 0.5 M nitric acid at 3 BV/hour.
3. Three AVs of DI water at 3 BV/hour.
4. Six BVs of 0.5 M sodium hydroxide solution at 3 BV/hour.

Wave 2 resins were also conditioned in a single cycle that consisted of pumping the following reagents through the bed.

1. Three AVs of DI water down-flow at 3 BV/hour.
2. Six BVs of 0.5 M sodium hydroxide down-flow at 3 BV/hour to raise the the pH of the column contents to avoid precipitation from the LAW when it is introduced in the next step.
3. Simulated AP101 LAW up-flow at a flow rate sufficient to fluidize the bed and expand its volume by 50% for 15 minutes and displace 0.5 M sodium hydroxide from the column. This step was performed to replicate the intended full-scale operation. The difference in density between LAW and 0.5 M sodium hydroxide causes turbulence in the head-space, which then leads to an uneven bed level when the LAW is immediately introduced down-flow.
4. Simulated AP101 LAW down-flow at 4.5 L/minute (17 times the WTP baseline design velocity) for 1 hour. The dissolved oxygen concentration in the simulated AP101 LAW was to be maintained using VE Zero air (air stripped of carbon dioxide) such that the resin consumed the same quantity of oxygen as it would have processing 150 BVs at 3 BV/hour. Assuming that all of the feed dissolved oxygen was consumed by the resin, the recycled feedstock was replenished with dissolved oxygen by sparging for 15 minutes with VE zero air.
5. Three BVs of 0.1 M sodium hydroxide down-flow at 3 BV/hour to displace the simulated LAW from the apparatus.
6. Three BVs of DI water down-flow at 3 BV/hour to displace the 0.1 M sodium hydroxide from the apparatus.
7. Six BVs of 0.5 M nitric acid down-flow at 3 BV/hour to convert the resin to the acid-form.
8. Three AVs of DI water at 3 BV/hour to displace the nitric acid from the apparatus.

The Wave 3 resin was conditioned in two cycles. Cycle 1 consisted of pumping the following reagents through the bed.

1. 0.5 M sodium hydroxide at 0.86 L/minute up-flow to achieve 50% bed expansion for ½ hour. Up-flow regeneration was performed as a precursor to up-flow LAW introduction to avoid generating the high bed pressures that prevented bed fluidization in LAW, as described in section 6.5.
2. 0.5 M sodium hydroxide down-flow at 4.5 L/minute (17 times the WTP baseline design velocity) for 15 minutes to determine the change in bed height resulting from switching to down-flow.
3. 0.5 M sodium hydroxide at 0.75 L/minute up-flow to achieve 50% bed expansion for 15 minutes.
4. Simulated AP101 LAW down-flow at 4.5 L/minute (17 times the WTP baseline design velocity) for 1 hour.
5. Three BVs of 0.1 M sodium hydroxide down-flow at 3 BV/hour.
6. Three BVs of DI water down-flow at 3 BV/hour.
7. Six BVs of 0.5 M nitric acid down-flow at 3 BV/hour.
8. Three AVs of DI water at 3 BV/hour.

Cycle 2 of Wave 3 resin conditioning consisted of pumping the following reagents through the bed.

1. Up-flow 0.5 M sodium hydroxide at various flow rates investigating the onset of resin motion for 2 hours.
2. Up-flow simulated AP101 LAW at 0.12 L/minute (2.5 cm/minute) up-flow for 15 minutes.
3. Simulated AP101 LAW down-flow at 4.5 L/minute (17 times the WTP baseline design velocity) for 1 hour.
4. Three BVs of 0.1 M sodium hydroxide down-flow at 3 BV/hour.
5. Three BVs of DI water down-flow at 3 BV/hour.
6. Six BVs of 0.5 M nitric acid down-flow at 3 BV/hour.
7. Three AVs of DI water at 3 BV/hour.

The Wave 4 resins were conditioned in the same manner as Cycle 2 of Wave 3 resin conditioning except that elution was performed up-flow at various flow rates to investigate fluidization behavior.

The Wave 0 and Wave 1 process cycles were initiated by conducting a hydraulics test with simulated AP101 LAW pumped down through the bed for 1 hour at the prescribed flow rate (defined in Table 2-1). Except for the first AV, which was collected as waste, simulated AP101 LAW was recycled to the feed tank without replacing depleted ions to minimize waste generation. The valve on the recycle line was opened before closing the one on the effluent line to avoid subjecting the bed to a pressure shock. A cycle was then continued by pumping the following reagents down through the bed.

1. Three BVs of 0.1 M sodium hydroxide at 3 BV/hour (feed displacement).
2. Three BVs of DI water at 3 BV/hour (pre-elution rinse).

3. Twelve BVs of 0.5 M nitric acid at 6 BV/hour (elution).
4. Three BVs of DI water at 1.4 BV/hour (post-elution rinse).

The cycle was then completed by performing a hydraulics test with 0.5 M sodium hydroxide regeneration solution pumped at 5.5 L/minute (16.5 times the original WTP baseline velocity of 7.1 cm/minute) down through the bed for 2 hours.

The Wave 2 process cycles (Cycles 1 through 3) commenced by conducting a hydraulics test with 0.5 M sodium hydroxide regeneration solution pumped at 4.5 L/minute (17 times the WTP baseline velocity of 5.85 cm/minute) down through the bed for 2 hours. Regeneration was followed by pumping simulated AP101 LAW up-flow to fluidize the bed for 30 minutes. A hydraulics test was then performed with simulated AP101 LAW at the prescribed flow rate (defined in Table 2-1) for 1 hour with VE Zero air sparging for the first 15 minutes. Feed displacement, pre-elution rinse, elution, and post-elution rinse operations were then performed as described above to complete the cycle. Cycles 4 and 5 of the Wave involved replacing the down-flow regeneration with up-flow or fluidized regeneration.

The Wave 3 process cycles commenced by pumping 0.5 M sodium hydroxide up through the bed at various flow rates to investigate bed behavior for up to 2 hours, except for Cycle 6. Cycle 6 regeneration was performed by pumping 0.5 M sodium hydroxide down through the bed at 4.5 L/minute (17 times the WTP baseline velocity of 5.85 cm/minute) for 2 hours to conduct a hydraulics test. Regeneration was followed by pumping simulated AP101 LAW up-flow at 0.12 L/minute (2.5 cm/minute) for 15 minutes followed by higher flow rates sufficient to achieve a level settled bed. The latter step was not performed for Cycle 6. A hydraulics test was then performed with simulated AP101 LAW at the prescribed flow rate (defined in Table 2-1) for 1 hour with VE Zero air sparging for 15 minutes. Feed displacement, pre-elution rinse, elution, and post-elution rinse operations were then performed as described above to complete a cycle.

The Wave 4 process cycles commenced by pumping 0.5 M sodium hydroxide up through the bed at 0.6 L/minute for up to 2 hours. Regeneration was followed by pumping simulated AP101 LAW up-flow at 0.12 L/minute (2.5 cm/minute) until simulated LAW was observed in the effluent tube, and then the flow rate was increased to 0.2 L/minute for 15 minutes. A hydraulics test was then performed with simulated AP101 LAW at the prescribed flow rate (defined in Table 2-1) for 1 hour with Zero air sparging for 15 minutes. Feed displacement and pre-elution rinse operations were then performed as described above. Elution was performed at various flow rates in up-flow mode to investigate bed behavior for up to 2 hours. The post-elution rinse was performed as described above to complete a cycle.

The bed height and total column pressure were measured every 10 minutes during simulated AP101 LAW processing and regeneration and at the beginning and end of the other processing steps. The resin bed height was measured by counting the gradations in the column wall visible above the bed. Electronic data from the diaphragm, line and differential pressure gauges, flow meters, and thermocouples were collected with IO Tech, Personal Daq/56, and PDQ2 data-acquisition software (Cleveland, OH) installed on a Micron Electronics TransPort TREK 2 computer with an analog input/digital input/output (I/O) board. The data-acquisition system sampled all channels at 1-second intervals, and data were recorded every 10 seconds.

2.6 Determination of Sodium Concentration

Since sodium is consumed by the resin during its regeneration, regeneration performance was assessed in Wave 3 and Wave 4 by determining sodium hydroxide concentrations from the solution conductivity measured using an ATI Orion conductivity meter and probe 012210. A conductivity-sodium hydroxide concentration correlation was determined by measuring the conductivity of three sodium hydroxide solutions of pre-determined concentration. The concentrations were confirmed by measuring the solution density (as described in Section 2.7.2) and then obtaining the concentrations from the correlation provided by Lide (2004).

2.7 Physical Property Testing

2.7.1 Resin Particle Size Analysis

Except for Waves 3 and 4, approximately 10-g samples of resin were extracted from the top of the bed by pipetting approximately equal volumes of damp resin from the column center and the four quadrants. This procedure was repeated for the remaining bed after approximately all but the last 25 mm of resin had been removed. In Waves 3 and 4, all of the resin was removed from the column into a jar that was then homogenized by shaking. A single 10-g sample of resin was then extracted for analysis. Each sample was then analyzed in a Microtrac Particle Size Analyzer Model S3000. Separate samples of the Wave 4 resins were also converted to the sodium form and then immersed in simulated AP101 LAW, 0.1 M sodium hydroxide and 0.5 M sodium hydroxide for 1 week. Particle size analysis was then conducted with the resin suspended in those solutions.

2.7.2 Fluid Viscosity and Density

Samples of simulated LAW and 0.5 M sodium hydroxide regeneration reagent were tested for viscosity and density upon completion of each cycle. Fluid density was determined by filling a tared 50-mL capacity volumetric flask to the 50-mL level and weighing it. Canon-Fenske viscometers (sizes 75, 100 and 150) immersed in a water bath at 25°C were used to determine fluid viscosities. The viscometers were calibrated by the user with two standards.

2.8 Batch-Contact Testing

Batch-contact tests were performed on the cycled or hydraulic-tested (HT) resin and untested or “virgin” resin (VR) from Wave 1 to assess the impact of hydraulic testing on chemical performance. All resin sampling and processing was conducted in accordance with BNI protocol P1-RF, *Spherical Resin Sampling from Containers, Resin Pretreatment, F-Factor, and Resin Loading to Column*. The HT and VR resins were sampled using the coring technique consistent with American Society for Testing and Materials (ASTM) Method 2687. A 15-mL aliquot of the HT resin was converted to the acid-form by contacting it with 10 BVs 0.5 M nitric acid followed by four water rinses. A 10-mL aliquot of the VR resin was pretreated by cycling twice from the acid-form to the sodium-form and back to the acid-form, consistent with the pretreatment protocol. The acid-form resins were dried under nitrogen flow and/or vacuum at room temperature until they were free-flowing.

Batch-contact stock solutions of simulated AP101 LAW were prepared at three cesium concentrations. Aliquots of the 6 µg Cs/mL (4.46E-5 M) simulated AP101 LAW were spiked with additional cesium nitrate to prepare 156 mg Cs/L (1.17E-03 M) and 702 mg Cs/L (5.28E-3 M) stock solutions. A cesium-137 tracer was added to each stock solution to facilitate tracking of cesium-exchange behavior using GEA.

The batch-contact tests were performed in duplicate on each pretreated resin at each of the three cesium concentrations, except the HT resin, which was tested in triplicate at the intermediate cesium concentration. Nominally 0.18 g of pretreated acid-form resin was contacted with 20 mL of simulated LAW in a 35-mL glass vial. The resin mass was determined to an accuracy of ±0.0002 g. The simulated LAW volume was transferred by pipet; the actual contact volume was determined by mass difference and solution density. The targeted phase ratio (liquid volume to exchanger mass) was 100 mL/g. The obtained ratio varied between 100 mL/g and 122 mL/g. Appendix A provides sample-specific volumes and resin masses. The headspace above the simulated LAW was purged with nitrogen gas just before capping. Vials were placed lengthwise in an Eberback Corp. (Ann Arber, MI) reciprocal shaker set to 2.1 cycles per second. Rigorous mixing was observed for all samples. The resin materials were contacted for nominally 46 hours. The temperature was not controlled, but was nominally 22ºC during the contact period. After contact, the samples were filtered through 0.45-µm nylon-membrane syringe filters.

Equilibrium conditions were evaluated as a function of contact time for the VR resin only. Replicate samples were prepared as described above with the 4.46E-5 M cesium contact solution. Duplicate samples were removed at 24-, 46-, and 72-hour contact times.

All solutions were analyzed by GEA to determine the cesium-137 concentration. The cesium-137 tracer concentrations in the un-contacted simulated LAW samples were used to define the initial cesium concentrations (C_o). Final (equilibrium) cesium concentrations (Cs_{eq}) were calculated relative to the cesium-137 tracer recovered in the contacted samples (C_1) according to Equation (2.2):

$$Cs_{Eq} = Cs_0 * \left(\frac{C_1}{C_0}\right) \tag{2.2}$$

where Cs_{Eq} = equilibrium cesium concentration in solution (µg/mL or M)
Cs_0 = initial cesium concentration in solution (µg/mL or M)
C_1 = equilibrium cesium-137 concentration in solution (cpm/mL)
C_0 = initial cesium-137 concentration in solution (cpm/mL).

The equilibrium cesium concentrations in the resins (Cs_R, units of mg cesium per g of dry resin mass) were calculated according to Equation (2.3):

$$\mathrm{Cs_R} = \frac{\mathrm{Cs_0} \times \mathrm{V_l} \times \left(1 - \frac{\mathrm{C_1}}{\mathrm{C_0}}\right)}{\mathrm{M_{Ri}} \times \mathrm{F} \times 1000} \tag{2.3}$$

where V_l = volume of the liquid sample (mL)

M_{Ri} = mass of acid-form ion exchanger dried under ambient conditions to a free-flowing state (g)
F = F-factor
1000 = conversion factor to convert μg to mg.

The cesium batch-distribution coefficient (K_d) values were determined according to the standard formula shown in Equation (2.4).

$$K_d = \frac{(C_0 - C_1)}{C_1} \times \frac{V_1}{M_{Ri} \times F} \qquad (2.4)$$

The F-factor indicates the loss in mass from drying the resin at 50°C under vacuum to constant mass and is defined by the equation

$$F = \frac{M_{Rd}}{M_{Ri}} \qquad (2.5)$$

where M_{Rd} is the mass of resin dried at 50°C under vacuum.

Errors were minimized because cesium tracer was used; samples with low cesium concentrations were counted longer to reduce counting error. Sample count errors were less than 0.5% (1 σ).

To compare batch-contact results with previously reported data, the mass increase of acid-form resin to sodium-form resin (I_{Na}-factor) will need to be incorporated in Equation (2.4). This will effectively increase the resin contact mass and thus decrease the observed K_d. Determining the I_{Na}-factor was beyond the current testing scope.

3.0 Underlying Theory

3.1 Scale-up Basis

This section describes the theory underlying the experimental approach and specifically the basis for pumping at high velocities in the small-scale column to replicate the pressures exerted in the full-scale equipment. The theory is based on Janssen's analysis, which is presented by Nedderman (1992), modified by the addition of fluid drag. The forces exerted on a differential slice of an expanding (i.e. regenerating) resin bed with fluid flow in the downward direction are illustrated in Figure 3-1.

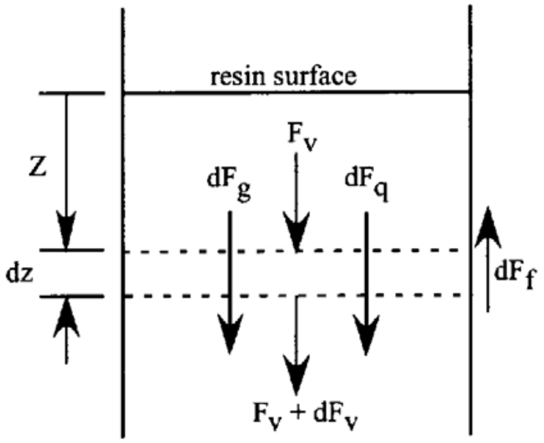

Figure 3-1. Axial Force Balance on Differential Section of Contracting Resin Bed

By the definitions presented by Nedderman (1992), the expanding bed configuration is the 'passive case'. The 'active case' is represented by the contracting bed (i.e. when its being eluted) and the friction forces act in the opposite direction. The differential axial stress in the bed, δF_a, can be expressed in terms of the force balance on a differential "slice" of the bed,

$$\delta F_v = A_{IX}\delta P_a = \delta F_g + \delta F_q - \delta F_f \tag{3.1}$$

where δF_g is the negative buoyancy force = $(\rho_s - \rho_l)(1-\varepsilon_p)(1-\varepsilon)gA_{IX}\delta z$, δF_q is the hydraulic drag force, and δF_f is the friction drag force = $\pm\frac{4\mu'k'}{D}A_{IX}\delta z$, when the sign depends on whether the bed is 'passive' or 'active'.

This yields an expression for the axial stress, in the form

$$\frac{dP_a}{dz} = (\rho_s - \rho_l)(1 - \varepsilon_p)(1 - \varepsilon)g + \frac{dP_q}{dz} \pm 4\frac{\mu'k'}{D}P_a \tag{3.2}$$

where A_{IX} = cross-sectional area of column
P_a = bed axial stress
P_q = stress from hydraulic drag
D = column diameter
g = gravitational acceleration
k' = radial to axial stress ratio
ε_p = particle porosity
ε = bed porosity
μ' = coefficient of friction
ρ_s = solid skeletal density
ρ_l = liquid density

The first term on the right-hand side represents the negative buoyancy force on the particles in the bed, the second term represents the effect of form drag caused by the fluid flowing over the particles in the bed, and the third term represents the friction forces in the bed caused by movement of the particles as the particles slide along the wall or against adjacent particles during contraction of the bed. When the particles are contracting, the net movement is in the downward direction, and the sign of the friction term is negative, as shown in Equation (3.2).

Equation 3.2 is a simple first order differential equation, which can be solved for z = Z (the bed height) by inspection to give:

$$P_a = \pm\frac{D}{4\mu'k'} \times \left[(\rho_s - \rho_l)(1 - \varepsilon)(1 - \varepsilon_p)g + \frac{P_q}{Z}\right] \times \left[\exp\left(\frac{\pm 4\mu'k'Z}{D}\right) - 1\right] \tag{3.3}$$

Since $k' = \frac{P_r}{P_a}$, where P_r is the radial bed pressure,

$$P_r = \pm\frac{D}{4\mu'} \times \left[(\rho_s - \rho_l)(1 - \varepsilon)(1 - \varepsilon_p)g + \frac{P_q}{Z}\right] \times \left[\exp\left(\frac{\pm 4\mu'k'Z}{D}\right) - 1\right] \tag{3.4}$$

The signs are positive for a passive bed and negative for an active bed. Therefore, bed pressure less bed buoyancy is directly proportional to the differential pressure and increases exponentially with respect to the height to diameter ratio. It is important to note at this point that the parameter k' is defined as the radial-to-axial stress ratio in this formulation. This parameter should not be confused with the usual definition for k' as the ratio of an applied force to the normal resultant force in a resin bed, which is normally a constant. For a passive bed, k' is related to the angle of internal friction, ϕ, by the equation,

$$k' = \frac{1 + \sin\phi}{1 - \sin\phi} \tag{3.5}$$

For smooth spheres, Nedderman (1992) provides the angle of internal friction as 20°. For the spherical RF particles, an angle of internal friction of 25° is reasonable and k' is 2.5. For an active bed, k' is given by the inverse of equation 3.5 and for an angle of internal friction of 25° its value is 0.4.

This report compares hydraulic data according to the total axial stress acting on the bed, P_a, to provide a consistent basis. Assuming the bed to be fully swollen, the total stress on the bed is derived from adding the measured differential pressure acting across the bed, P_q, and the product of $(\rho_s - \rho_l)(1-\varepsilon_p)(1-\varepsilon)g$ and bed height. The bed porosity is calculated according to the theory presented in section 3.2. The particle porosity is then calculated from the bed porosity and the measured bed and skeletal densities.

An important assumption in this model is that the time-dependent terms can be ignored in the force balance during the expansion or contraction process. That is, there are no significant inertial effects caused by the change in volume of the particles of the bed. Because the change is relatively gradual in both the expansion and contraction phases, requiring on the order of minutes to hours rather than only seconds, it is reasonable to assume that inertial forces are negligible. The process can be treated in a quasi-steady-state manner using the relationship in Equation (3.3) for the different phases of the process.

The relative magnitude of the friction forces in the different phases of expansion and contraction depend in large part on what sort of motion the particles undergo as a result of the change in volume. In the contraction phase, the particle size decreases, and consequently, the particles tend to fall in toward one another as the overall height of the bed shrinks. Friction forces at the wall tend to hold the bed up in this case, thereby relieving some of the axial stress in the bed. In the expansion phase, the particle size increases, and consequently, the particles tend to push outward against adjacent particles and against the wall. Friction forces at the wall tend to hold the bed down, thereby increasing the axial stress in the bed. The coefficient of friction is material dependent and the test column was manufactured from stainless steel, the same material specified for the actual WTP columns, for this reason.

From a purely pragmatic standpoint, the expansion phase is of the greatest interest because this is the part of the cycle that can be expected to produce the highest stresses in the bed. During the expansion phase, the axial and radial stresses increase until they are sufficient to induce particles to slide upward along the walls of the column and against each other. If the friction forces are strong enough to prevent movement of the particles within the bed, radial stresses will grow until they exceed either the yield stress of the bed material or that of the pipe containing the bed. In the one case, the bed material will undergo fracturing and fragmentation; in the other, the column will swell and possibly burst.

In small-scale testing to determine the effect of stresses caused by expansion of the bed, it is important to produce forces in the test section that are comparable to the forces expected in the full-scale ion exchange column. But because the measurement of interest is the total axial and radial stress in the full-scale ion exchange column, appropriate testing in columns of smaller diameter requires sacrificing some aspects of dimensional similitude in the test conditions as described by Poloski et al (2006). The total buoyancy force will be smaller in the test column than in the full-scale column according to the ratio of the respective column heights. If the flow velocity in the test column is the same magnitude as the velocity in the full-scale column, the fluid drag term will also be smaller than in the full-scale column. In that case, the total axial and radial stress in the test column will be significantly less than what would be obtained in the full-scale column at the same flow rate. This approach to testing in small-scale columns will result in pressure measurements that significantly underestimate the axial and radial stresses in the full-scale column.

The fluid drag term is the only one of the three components of Equation (3.3) that can be adjusted in the testing processes to achieve forces in the small-scale test column that will produce top to bottom axial and radial stress gradients of the same magnitude as in the full-scale column. Scaling the flow rate by the ratio of the bed height of the full-scale column to the test section bed height yields a test section flow velocity that will give fluid drag forces approximately equivalent to those seen in the full-scale column. That is,

$$(V_0)_{ts} = (V_0)_{\mathrm{IX\ col.}} \left(\frac{Z_{IX}}{Z_{ts}} \right) \tag{3.6}$$

where Z_{IX} is the bed height in the full-scale ion exchange column, and Z_{ts} is the bed height in the test section.

The buoyancy force on the bed will be too small by a factor of Z_{IX}/Z_{ts}. Because the particles have a negative buoyancy, this force tends to increase the stress on the bed in the full-scale column. In order for the small-scale column to predict the full-scale bed pressure, the flow drag term should preferably be increased by using slightly more flow to simulate the full pressure component from the negative bed buoyancy in the full-scale column.

3.2 Flow Through Packed Beds

The theory of fluid flow through packed beds is well established and is described in various text books, such as that by Coulson and Richardson (1996). The Reynolds number for flow through the pores of the bed is given by

$$\mathrm{Re} = \frac{V_0 \rho_l D_p}{(1-\varepsilon)\mu} \tag{3.7}$$

For distributions of particle sizes, the appropriate mean diameter is that based on surface area because we are concerned with the frictional losses of fluid flow over the particles. For Re less than about 10, the flow is laminar and is described by a modified form of Darcy's Law:

$$V_o = \frac{K(-P_q)}{\mu Z} \tag{3.8}$$

where K = Permeability (m^2).
Z = Bed height (m)

Reynolds numbers were typically of the order of 10 or somewhat higher in the 3-inch column tests, and it is necessary to consider the inertial component to the flow. For this case, Ergun (1952) derived a generalized equation to describe the flow through packed beds that accounts for both viscous and inertial flow components:

$$\frac{\left(-P_q\right)}{Z} = \frac{150(1-\varepsilon)^2 \mu V_o}{\varepsilon^3 D_p{}^2} + \frac{1.75(1-\varepsilon)\rho_l V_o{}^2}{D_p \varepsilon^3} \tag{3.9}$$

While deviations from the Ergun equation have been noted by Ergun (1952), the model is well-established for describing fluid flow through packed beds. The bed voidage is the only parameter not measured in the tests described in this report and is calculated from Equation (3.9) using the pressure drop measurement and presented as the parameter of interest. The first term on the right side of equation 3.9 represents the contribution from viscous flow to the pressure drop. Considering only the viscous term in comparison to Darcy's Law (equation 3.8) shows that the permeability is related to the bed voidage by the expression:

$$K = \frac{\varepsilon^3 D_p{}^2}{150(1-\varepsilon)^2} \tag{3.10}$$

Therefore, permeabilities are calculated from Equation 3.10 using the bed voidage values calculated from Equation 3.9.

4.0 Wave 0 (Shake-down) Test Results and Discussion

This section describes the following results of the Wave 0 test:

- The transient performance of the resins was analyzed, and SL644 was compared with spherical RF.
- The resin bed voidages were compared.
- Steady-state pressures of the resins were compared during regeneration.
- Steady-state pressures of the resins were compared during processing of LAW.
- Both fresh and cycled acid-form resins were analyzed to determine their particle size distributions.

Wave 0 resins were pre-treated by soaking them in 1 M sodium hydroxide for two hours before loading them into the columns to produce beds with height to diameter ratios of 1.61 and 1.67 for BRF18 and SL644, respectively. Conditioning of the resins in the columns was performed by first converting them to the acid-form by pumping DI water and then 0.5 M nitric acid down-flow through the bed. A wash with DI water and then 0.5 M sodium hydroxide pumped down-flow through the bed converted the resin back to the sodium-form to prepare it for processing simulated LAW in the first cycle. All process operations (simulated LAW processing, 0.1 M sodium hydroxide feed displacement, DI water washes, elution and regeneration) were performed down-flow.

4.1 Transient Performance

The Wave 0 test results were used to understand the transient performance of the resins in analyzing the results from succeeding waves as well as to compare SL644 with spherical RF. Both ion exchange resins expand during regeneration as protons are exchanged for sodium ions at the ion exchange sites, and this is clearly represented in Figure 4-1 and Figure 4-2, which show the transient performance of the resins during first-cycle regeneration. Radial and axial pressures (note 1×10^5 Pa is equal to 14.5 psi) typically increase over the first 30 minutes as a result of the bed expansion over this period. Note that the pressure measurements included both the hydraulic and bed pressures, as described in section 2.4. Higher radial pressures are observed because the bed is constrained by the column walls. It is relatively free to axially expand, although constrained by the bottom screen and fluid pressure above. A peak in the BRF18 radial pressure is perhaps associated with a spontaneous re-arrangement of the bed at some critical pressure leading to partial relief of the radial pressure. Subsequent analyses averaged pressures over the final hour of regeneration to obtain the steady-state values on the basis of these results.

The SL644 bed height remained essentially constant during first-cycle LAW processing, as illustrated in Figure 4-3, as expected, although the small increase is an anomaly that may be due to operator error. In contrast, BRF18 bed height and radial and axial pressures increased over the first 30 minutes of waste processing, as shown in Figure 4-4. This observation is consistent with previous work by Fiskum et al. (2004) showing spherical RF resin to initially contract and then expand upon contact with LAW. The pressures for SL644 decreased over the same period and, indeed, appeared to be continuing to decrease upon completion of LAW processing. Subsequent analyses averaged BRF (and other spherical RF resins) pressures over the final 30 minutes of LAW processing to obtain the steady-state values on the basis of these results.

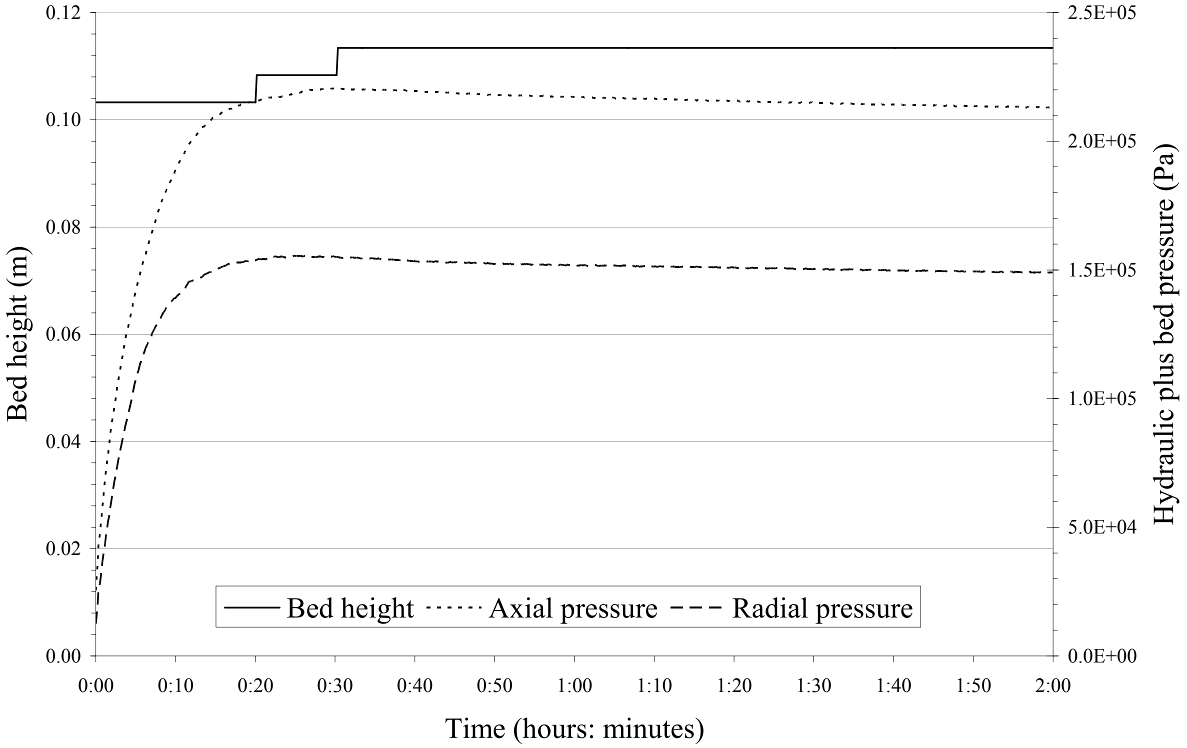

Figure 4-1. SL644 Transient Performance During Cycle 1 Regeneration (fluid velocity of 1.9 cm/s and steady state differential pressure less bed buoyancy of 3.0×10^4 Pa)

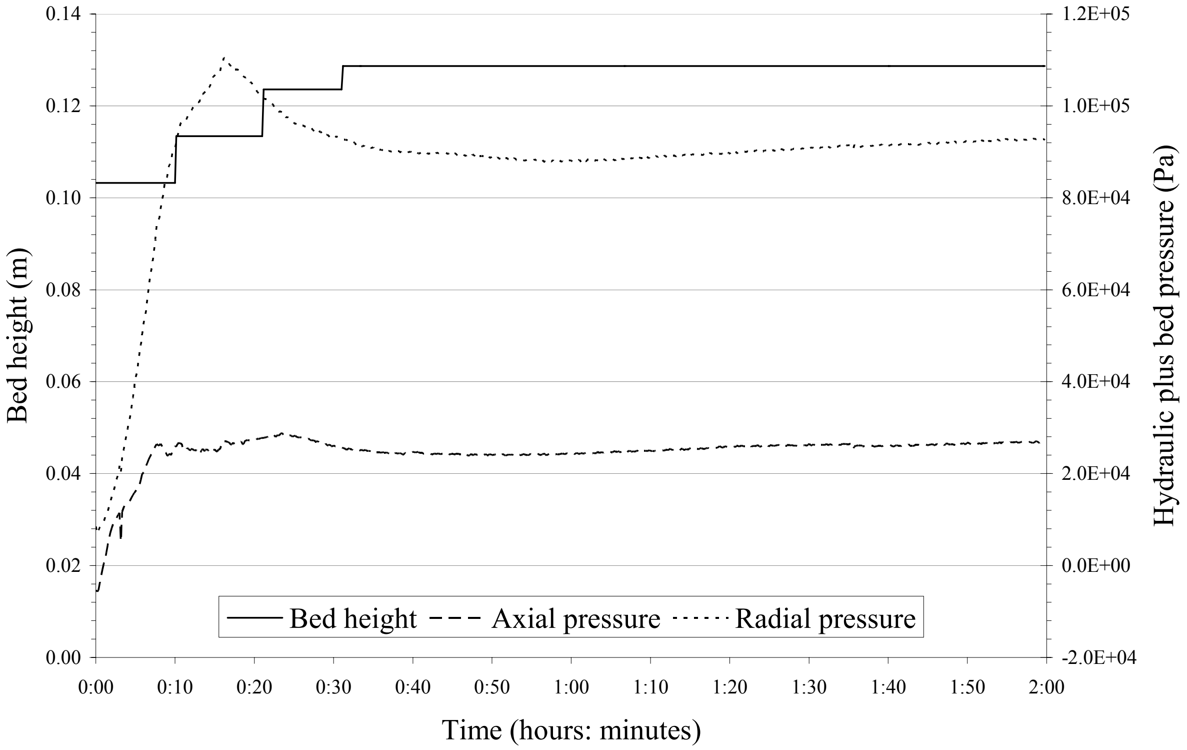

Figure 4-2. BRF18 Transient Performance During Cycle 1 Regeneration (fluid velocity of 1.9 cm/s and steady state differential pressure less bed buoyancy of 0.9×10^4 Pa)

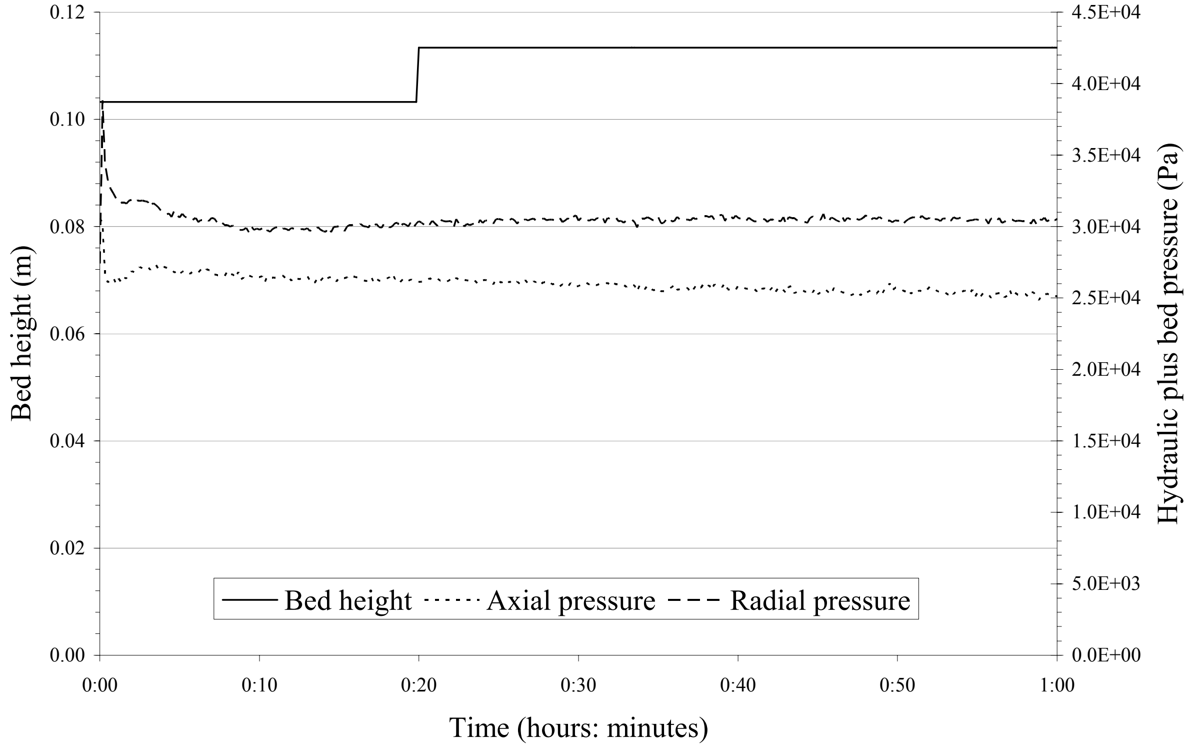

Figure 4-3. SL644 Transient Performance During Cycle 1 LAW Processing (fluid velocity of 1.9 cm/s and steady state differential pressure less bed buoyancy of 2.2×10^4 Pa)

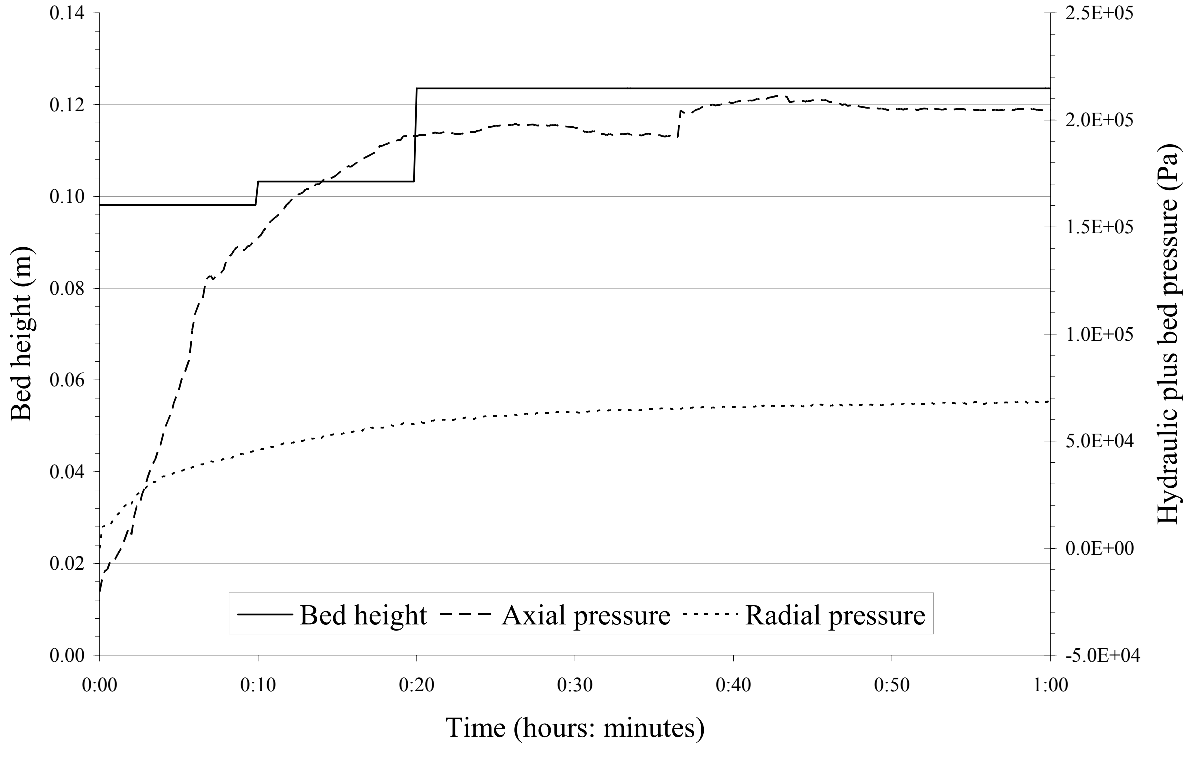

Figure 4-4. BRF18 Transient Performance During Cycle 1 LAW Processing (fluid velocity of 1.9 cm/s and steady state differential pressure less bed buoyancy of 2.2×10^4 Pa)

4.2 Bed Voidage and Permeability

Figure 4-5 compares the bed voidage for SL644 and BRF on the basis of differential pressure less bed buoyancy as defined in section 3.1. BRF18 bed voidage was higher than that of SL644 probably because of the spherical nature of the former, leading to a lower packing density. SL644 porosity would also be lower because of the breakage of resin particles to generate fine material, as described in Section 4.5. Note that regeneration and simulated LAW processing were performed down-flow. The average BRF18 bed voidage was 0.38 and 0.37 during regeneration and LAW processing, respectively. Average SL644 bed voidages of 0.25 and 0.32 were calculated for the regeneration and LAW processing steps, respectively. However, SL644 bed voidage reduced with respect to cycle number, consistent with the breakage of resin particles to generate fine material, as described in Section 4.5. The low bed voidage in the first cycle of SL644 regeneration appears to be anomalous, inconsistent with the trend of reducing bed voidage observed when processing LAW. As described in Section 4.5, the BRF18 did not fracture, and the particle size remained constant. The constant bed voidage observed for regeneration is consistent with this observation while the lower voidage in the third cycle when processing LAW appears to be anomalous because it was not observed for the other spherical RF resins described later. Anomalous results in Wave 0 are probably a result of experimental error introduced as staff gained experience with operating the apparatus. Indeed, Wave 0 was considered the shake-down run and the results from subsequent waves include significantly fewer anomalies.

The permeability of BRF18 resin processing LAW was 2.9×10^{-10} m^2 and that during regeneration was 3.5×10^{-10} m^2. SL644 permeability in LAW decreased from 3.2×10^{-10} m^2 to 1.7×10^{-10} m^2 over the three cycles, reflecting the reduction in bed voidage and particle size. Similarly, the permeability during regeneration reduced from 0.88×10^{-10} m^2 in the first cycle to 0.72×10^{-10} m^2 in the third.

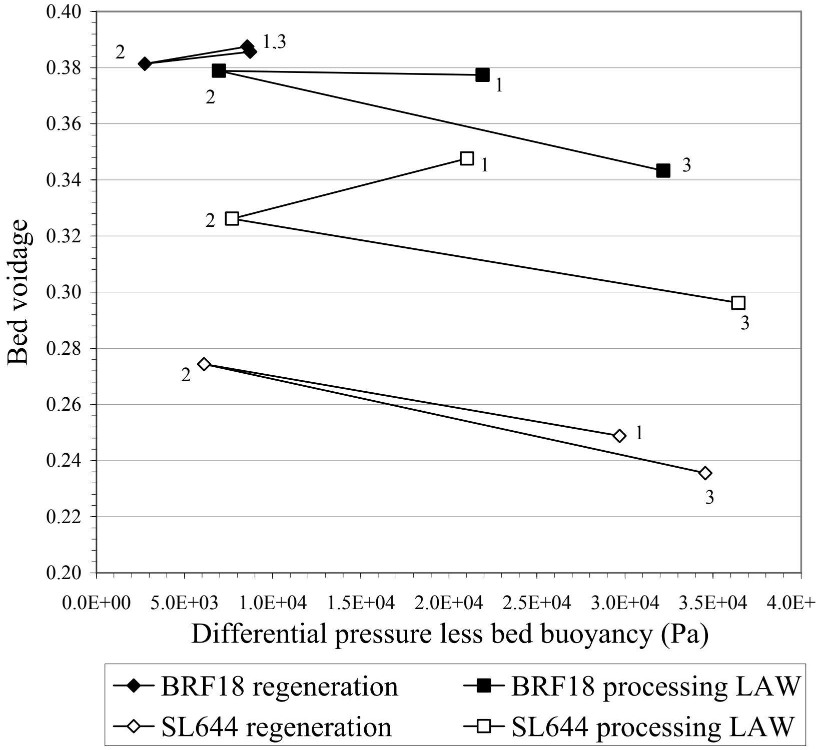

Figure 4-5. Bed Voidage of BRF18 and SL644 (data points labeled with the cycle number)

4.3 Steady-State Pressures in Regeneration

The ratio of radial to axial pressures were approximately three times higher for BRF18 than SL644 during regeneration, as illustrated in Figure 4-6 and Figure 4-7, at the same differential pressure. Note that these pressures also include the fluid pressure as well as the pressure exerted by the bed. In addition to stresses caused by the constrained expansion of the resin, the bed will also exert a force on the screen and wall as a result of the hydraulic drag. Therefore, axial and radial pressures would have been comparable to the differential pressure less bed buoyancy if the bed had totally relaxed following its expansion. That the BRF18 radial and SL644 axial pressures are a factor of ~10 higher than the differential pressure indicates that the stresses introduced from constrained expansion are retained by the bed. SL644 bed pressures were probably higher than for BRF18 for the same flow rate (or cycle) because of the higher differential pressure. In contrast to the BRF18 data, the SL644 exhibit two regions as identified by the broken lines in Figure 4-6. At low differential pressure, the hydraulic drag causes the bed to push out against the column wall and behavior is similar to BRF18. However, at higher differential pressures, the rate of increase in bed pressure decreases because the SL644 particles compress, as observed by Fiskum et al. (2004). The BRF18 beads evidently do not compress at the differential pressures recorded in these tests.

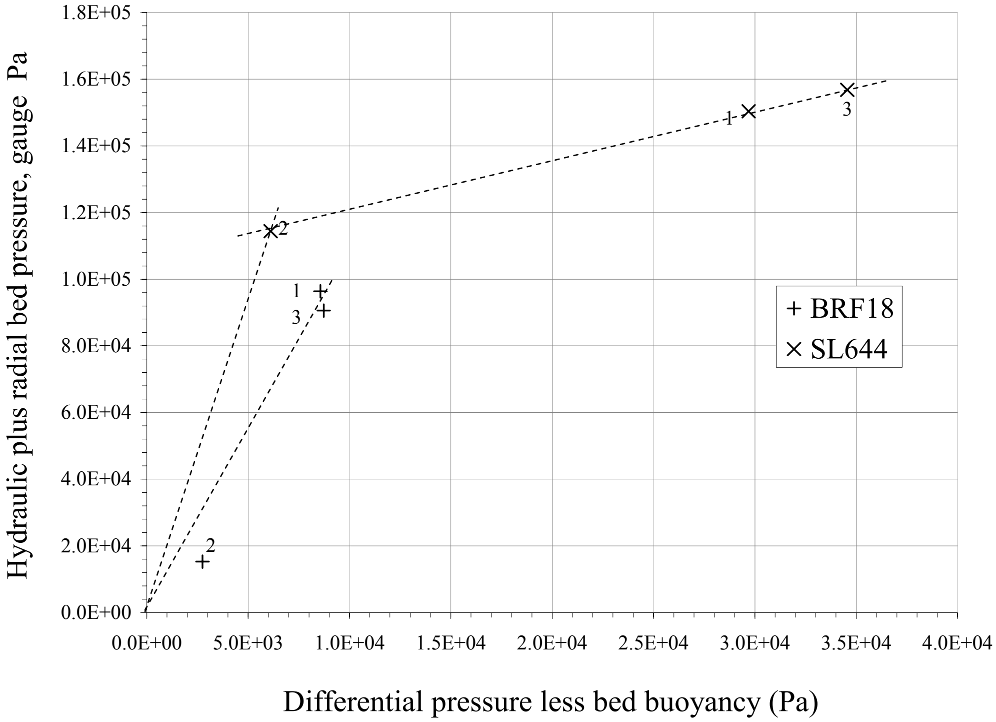

Figure 4-6. Steady-State Radial Pressure During Regeneration of SL644 and BRF18 (height to diameter ratios of relaxed BRF18 and SL644 beds were 1.61 and 1.67, respectively)

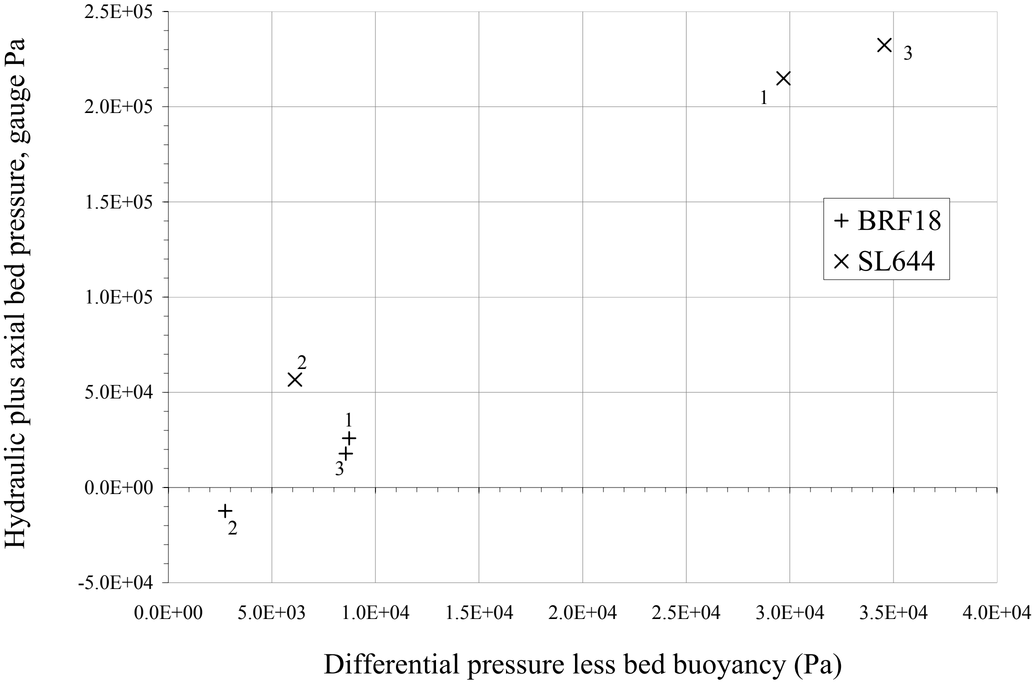

Figure 4-7. Steady-State Axial Pressure During Regeneration of SL644 and BRF18 (height to diameter ratios of relaxed BRF18 and SL644 beds were 1.61 and 1.67, respectively)

4.4 Steady-State Pressures in Processing LAW

In contrast to the results from regeneration, radial and axial pressure ratios were comparable for BRF18 and SL644, as shown in Figure 4-8 and Figure 4-9. SL644 radial and axial pressures were comparable to the differential pressure, presumably because the bed relaxed between terminating regeneration and commencing LAW processing, and there was no significant expansion while processing LAW. SL644 pressures were comparable to the differential pressure, which indicates that only the force transmitted to the bed from the fluid drag across it contributed to its pressure. In contrast, BRF18 pressures were approximately five times higher than the differential pressure during LAW processing. The ratio of radial and axial pressures to bed differential pressure less bed buoyancy was lower in LAW processing than in regeneration. Fiskum et al. (2004) observed the spherical RF resins to initially shrink upon contact with LAW and then expand. Therefore, BRF18 bed re-expansion is again constrained, leading to bed pressures higher than that expected from only that transmitted to the bed by the fluid drag.

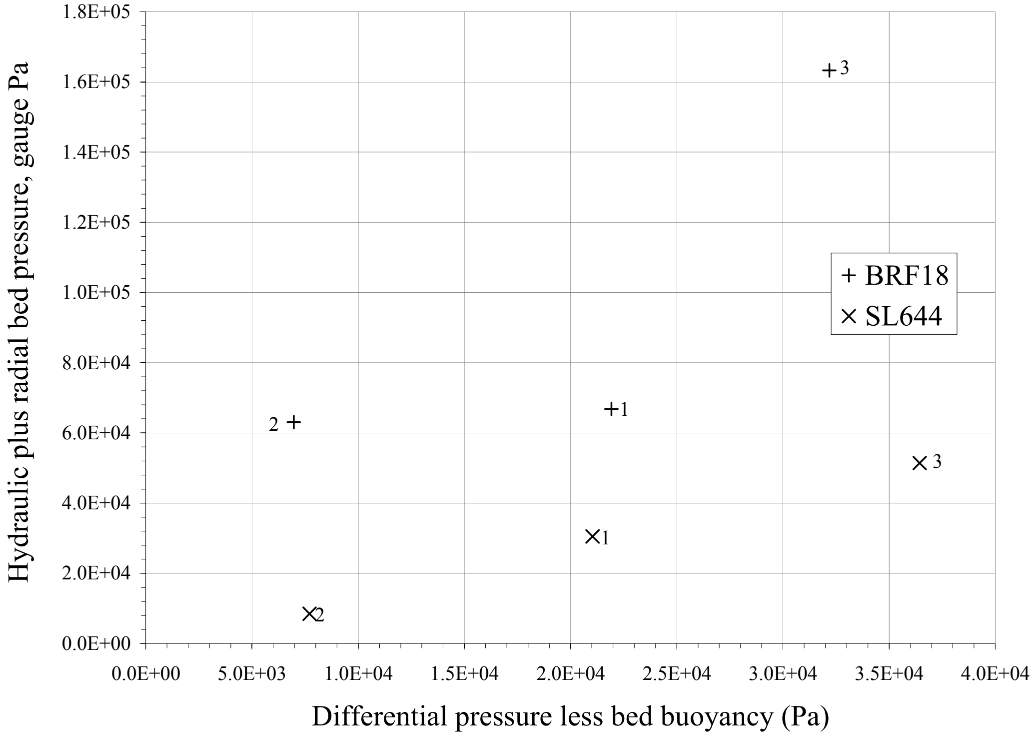

Figure 4-8. Steady-State Radial Pressure During LAW Processing (height to diameter ratios of relaxed BRF18 and SL644 beds were 1.61 and 1.67, respectively)

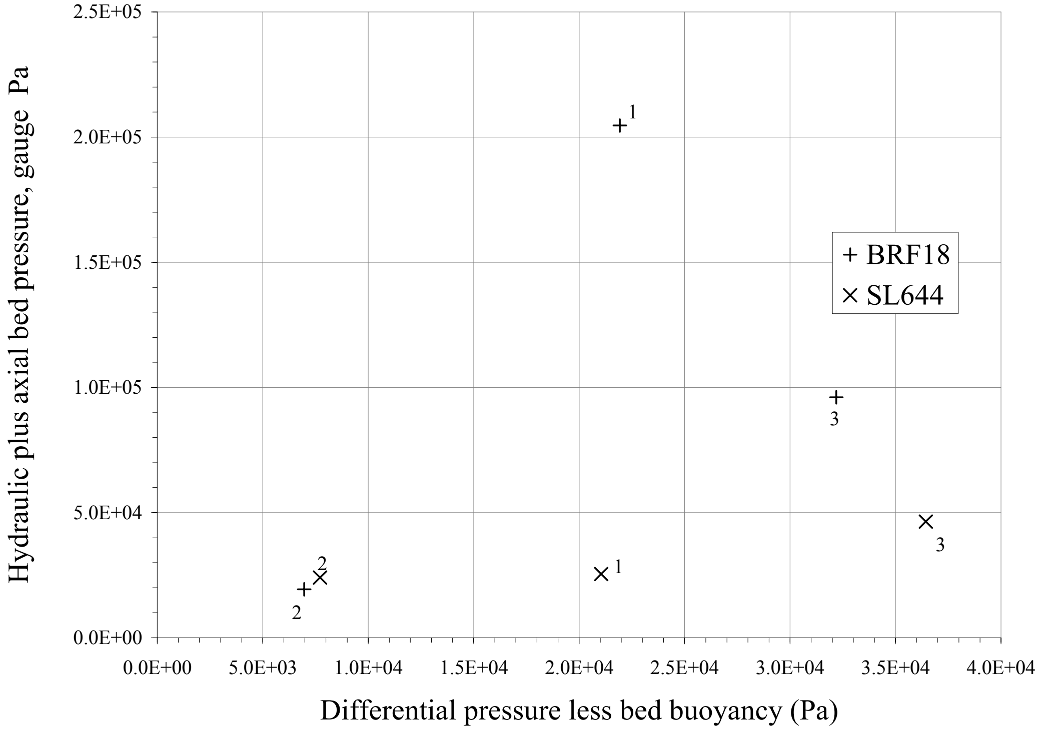

Figure 4-9. Steady-State Axial Pressure During LAW Processing (height to diameter ratios of relaxed BRF18 and SL644 beds were 1.61 and 1.67, respectively)

4.5 Particle Size Distribution

Samples of the fresh and cycled acid-form resins were micrographed and analyzed to determine their particle size distributions. Two samples were extracted from the column of the cycled resin. Samples from the bed top and approximately 25 mm from the bed bottom were extracted from the center and the centers of the four cross-sectional quadrants. Micrographs of the samples of fresh, cycled-top and cycled-bottom resins depicted in Figure 4-10 do not indicate any change in the morphology of the resin with bed depth.

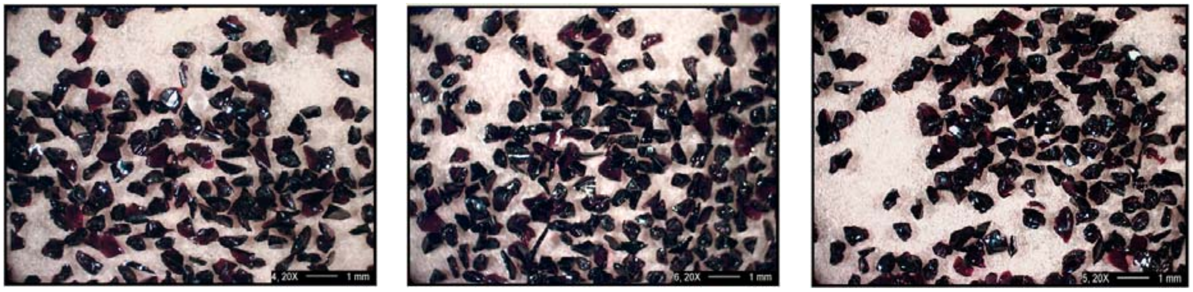

Figure 4-10. Micrographs of (in order left to right) Fresh, Cycled-Bottom, and Cycled-Top SL644

Figure 4-11 compares the fresh and cycled SL644 particle size distributions. A number distribution was selected for presentation to highlight the generation of fine material. Note that the error bands represent twice the standard deviation derived from analyses performed on sub-samples. The fresh resin exhibits a mono-modal size distribution with half of the resin particles of size smaller than 552.3 μm. The samples from the bed top and bottom are bi-modal, which clearly indicates that the fine material is generated by breakage of particles during cycling. The breakage was probably caused by the high osmotic pressures experienced by the particles as they expanded or contracted upon contact with the different process solutions. Half of the resin particles from the bed bottom were smaller than 205 μm whereas half of those from the top were smaller than 419 μm, thereby indicating either that greater breakage occurred at the bottom or the fines migrated to the bed bottom. The generation of finer material explains the increasing pressure drop for the same velocity.

In contrast to the results for SL644, the BRF18 particle mono-modal size distributions compared in Figure 4-12 indicated no significant break-up of this resin. Half of the resin particles in each sample were smaller than approximately 490 μm, and the volumetric mean diameter was 540 μm. The increasing pressure drop observed in succeeding waste processing steps cannot, therefore, be explained by the generation of any finer material as it was for SL644. Note that there is no significant difference in the sizes of the as-received and cycled BRF18 resins. The spherical resins used in the succeeding waves all showed the cycled material having a larger size than as-received, even though both were measured in the acid-form. Therefore, the BRF18 data appears to be anomalous.

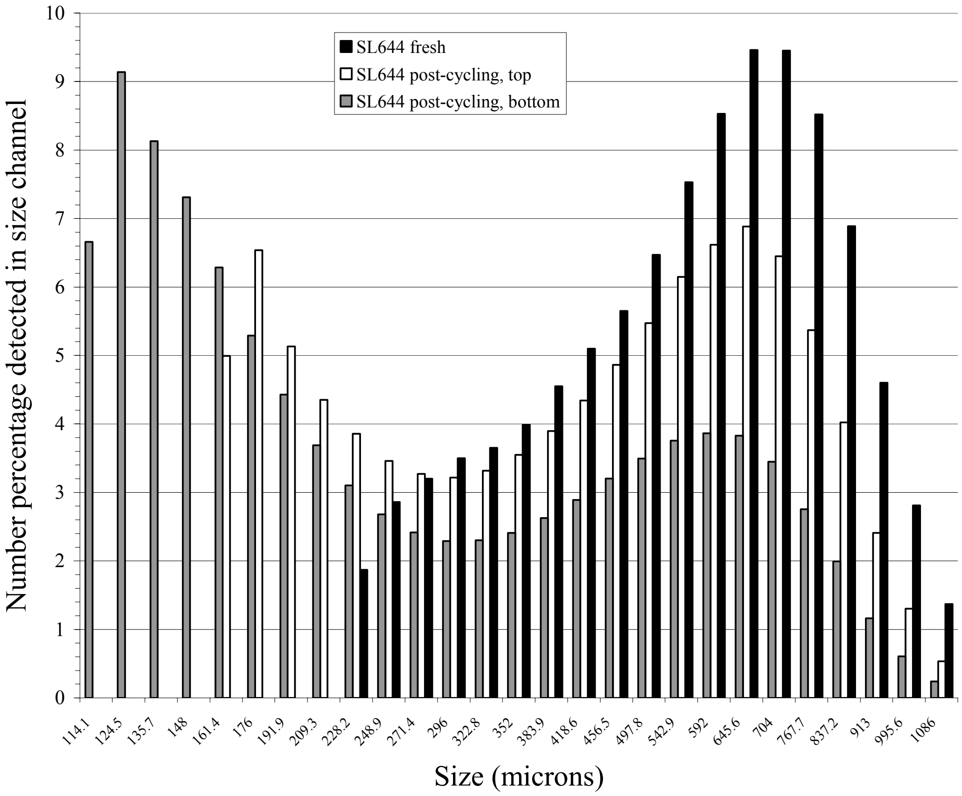

Figure 4-11. Comparison of Fresh and Cycled Acid-Form SL644 Particle Size Distributions

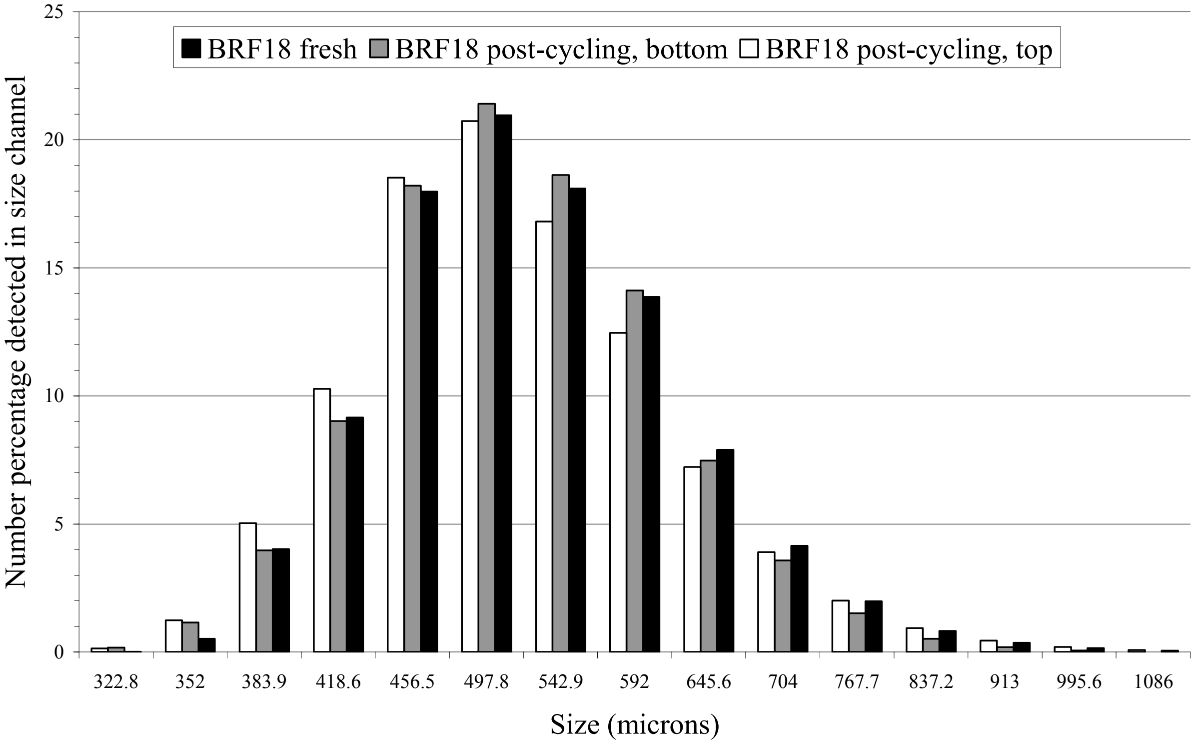

Figure 4-12. Comparison of Fresh and Cycled Acid-Form BRF18 Particle Size Distributions

The conclusions derived from the particle size analysis are confirmed in the micrographs depicted in Figure 4-13, which show the morphology of the fresh and cycled resins to be essentially identical. The cycled resin from the column top is darker than that from the bottom, which Adamson et al. (2006) describe as being caused by oxidation from dissolved oxygen. However, there was apparently no significant impact of resin oxidation after 3 cycles on the resin's hydraulic characteristics.

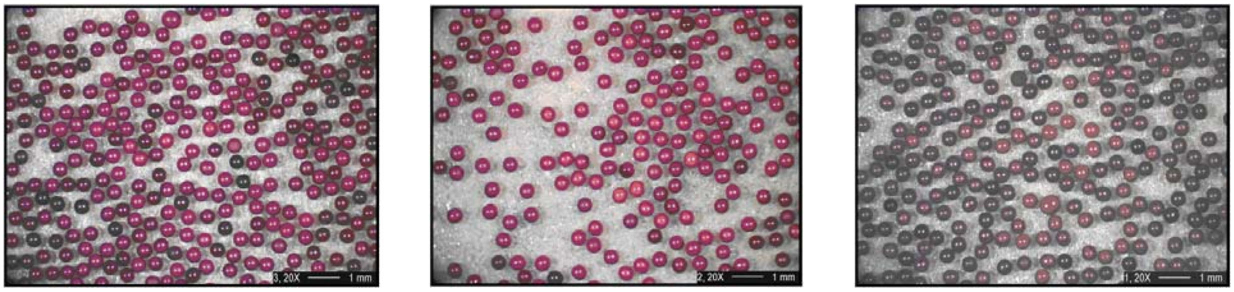

Figure 4-13. Micrographs of (in order left to right) Fresh, Cycled-Bottom, and Cycled-Top BRF18

5.0 Wave 1 (Development Vendor Resins) Results Analysis and Discussion

This section describes the following results obtained from the Wave 1 tests:

- The bed voidages of BRF14 and BRF15 during regeneration and LAW processing
- Steady-state pressures for BRF14 and BRF15 during regeneration
- Steady-state pressures exerted by BRF14 and BRF15 during LAW processing
- Comparison of particle size distributions for the fresh and cycled BRF14 resin.

Wave 1 resins were pre-treated by soaking them in 1 M sodium hydroxide for two hours before loading them into the columns to produce beds with height to diameter ratios of 1.59 and 1.65 for BRF14 and BRF15, respectively. Conditioning of the resins in the columns was performed by first converting them to the acid-form by pumping DI water and then 0.5 M nitric acid down-flow through the bed. A wash with DI water and then 0.5 M sodium hydroxide pumped down-flow through the bed converted the resin back to the sodium-form to prepare it for processing simulated LAW in the first cycle. All process operations (simulated LAW processing, 0.1 M sodium hydroxide feed displacement, DI water washes, elution and regeneration) were performed down-flow.

5.1 Bed Voidage and Permeability

Figure 5-1 and Figure 5-2 show the bed voidage of BRF14 and BRF15 during regeneration as a function of cycle number and differential pressure, respectively. The figures show bed voidage invariant with respect to cycle number, consistent with the BRF18 behavior in the Wave 0 testing. The average bed voidage was 0.38 for both BRF14 and BRF15 and is comparable to that obtained for BRF18. The bed voidage is notably constant, as expected, with respect to bed pressure, indicating little compression arising from the fluid pressure. The reason for the lower bed voidage in Cycle 5 at the lowest flow rate is not known. There was no significant increase in bed differential pressure with increasing cycle number for the same flow rate, consistent with the lack of any particle breakage described in Section 5.4.

There was essentially no variation in bed voidage with respect to cycle number or differential pressure when processing LAW as illustrated in Figure 5-3 and Figure 5-4. The average bed voidage was 0.38 for BRF14 and BRF15. The reason for the lower BRF14 bed voidage at the lowest flow rate is again not known. As for regeneration, there was no significant increase in bed differential pressure with increasing cycle number for the same flow rate.

The derived average permeability was 3.2×10^{-10} m^2 for BRF14 and BRF15 during both regeneration and LAW processing. Note that the bead size in simulated LAW was not measured, and the sodium-form value was assumed. However, the difference is in the permeability in simulated LAW and 0.5 M sodium hydroxide is <1% based on the change in the Wave 4 resin diameters measured in 0.5 M sodium hydroxide and simulated LAW.

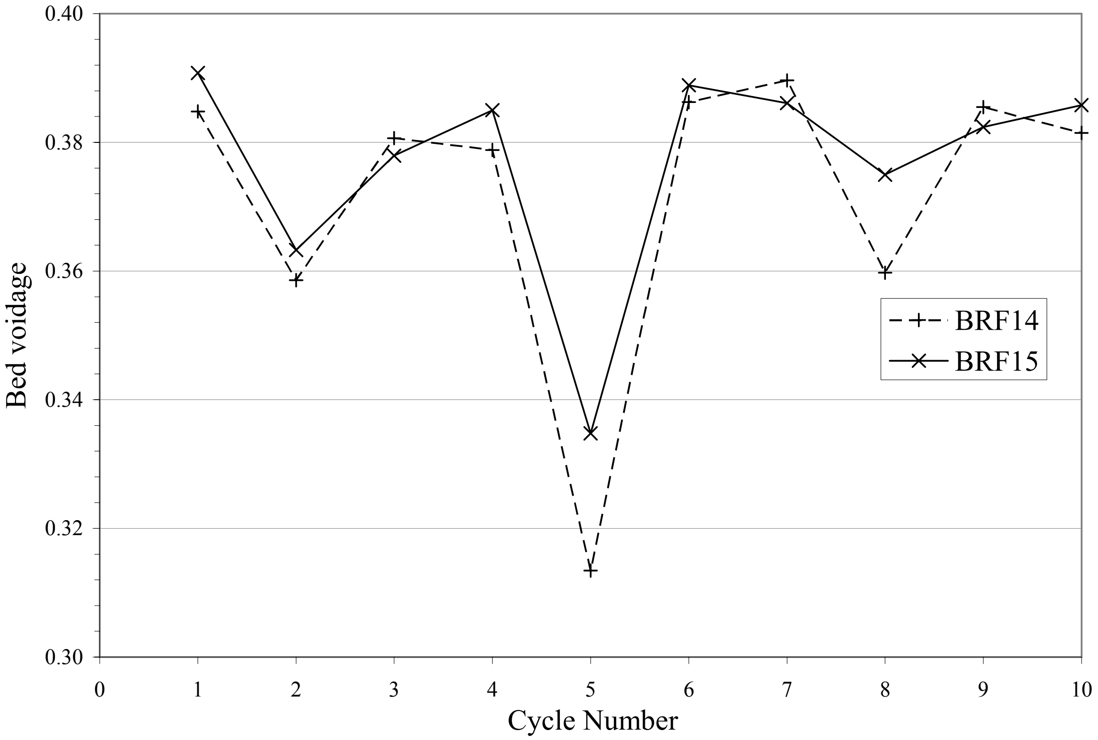

Figure 5-1. BRF14 and BRF15 Bed Voidage During Regeneration as a Function of Cycle Number

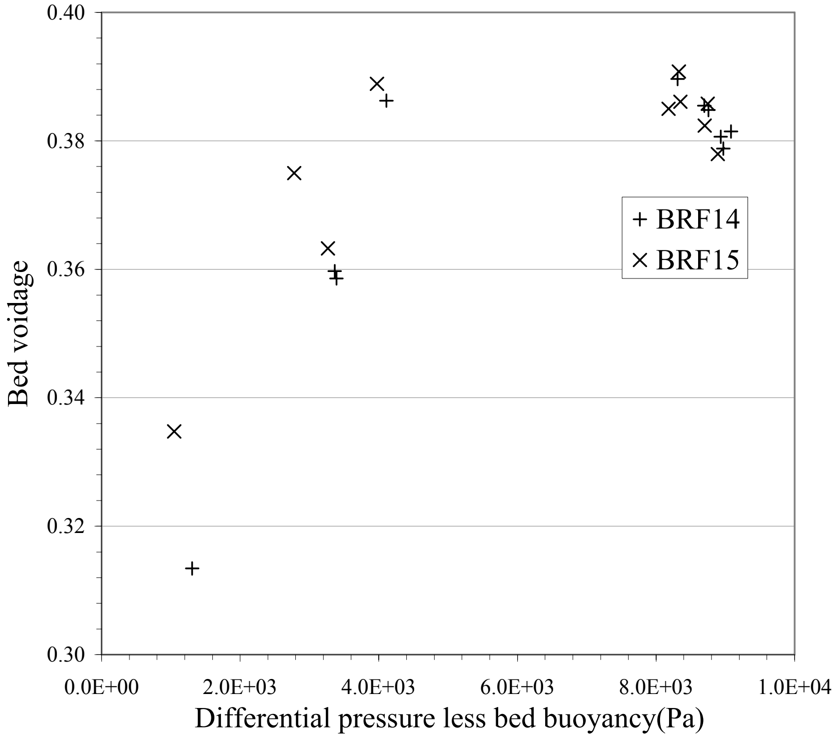

Figure 5-2. BRF14 and BRF15 Bed Voidage During Regeneration as a Function of Differential Pressure

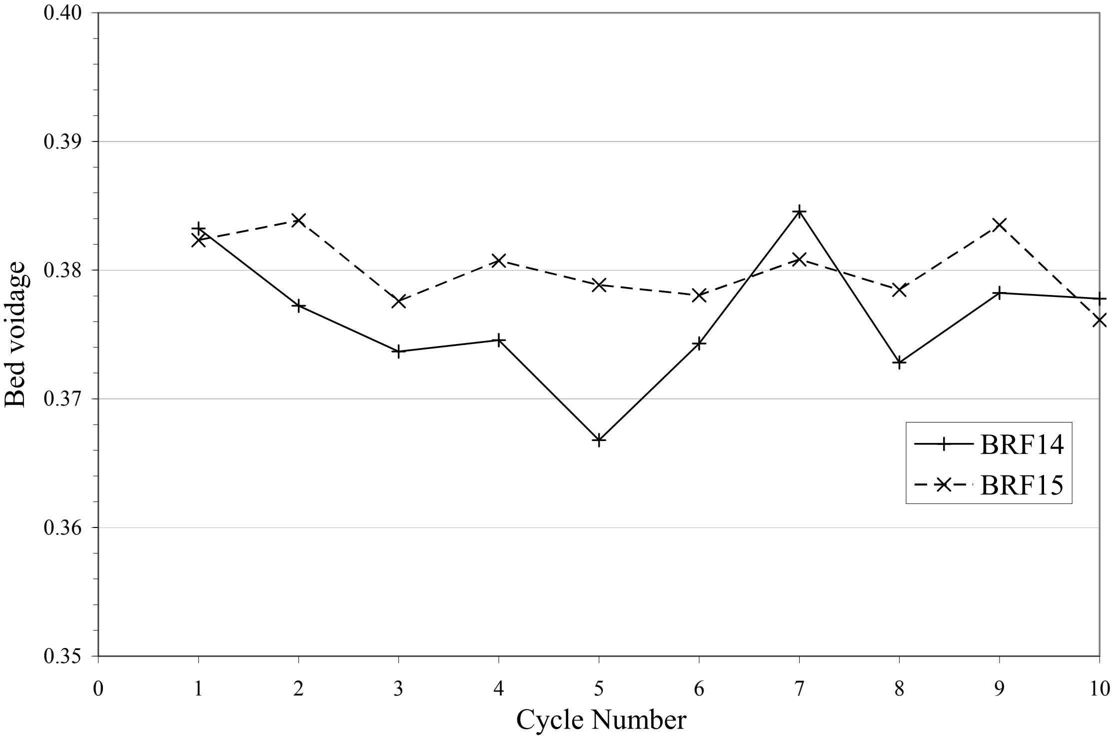

Figure 5-3. BRF14 and BRF15 Bed Voidage During LAW Processing as a Function of Cycle Number

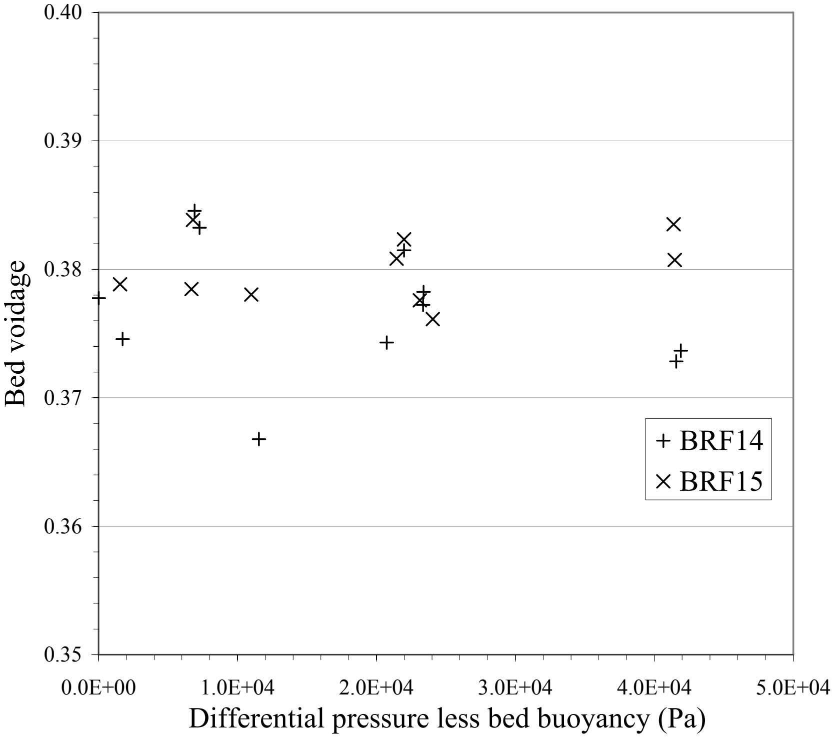

Figure 5-4. BRF14 and BRF15 Bed Voidage During LAW Processing as a Function of Differential Pressure

5.2 Steady-State Regeneration Bed Pressures

Figure 5-5 and Figure 5-6 illustrates steady-state axial and radial pressures, respectively, for BRF14 and BRF15 during regeneration. Axial and radial pressures are approximately 10 and 5 times the differential pressure, respectively, which is comparable to the BRF18 behavior and indicates that the bed retains some of the stress arising during its constrained expansion. Axial pressures appear to be invariant with respect to cycle number and the result from cycle 10 is probably an anomaly. The ratio of radial to axial bed pressure for BRF14 and BRF15 is consistent with that for BRF18 at the same differential pressure less bed buoyancy. The center thermal well rod was removed for Cycles 6, 7, and 8, and then replaced but there was no significant impact on the bed pressures.

Figure 5-5 and Figure 5-6 demonstrate that the axial and radial bed pressures are proportional to the differential pressure less bed buoyancy, as expected from considering equations 3.3 and 3.4. Ignoring the anomaly of BRF15 cycle 3, the axial bed pressure can be correlated with the differential pressure less bed buoyancy in a linear manner with a slope of 4.08 for a mean error of 39%. Similarly, the radial bed pressure can be correlated with the differential pressure less bed buoyancy in a linear manner with a slope of 9.92 for a mean error of 32%. Therefore, the average ratio of radial to axial bed pressures is 2.4 to provide an angle of internal friction of 25^{o}, which is in good agreement with the theory presented in 3.1.

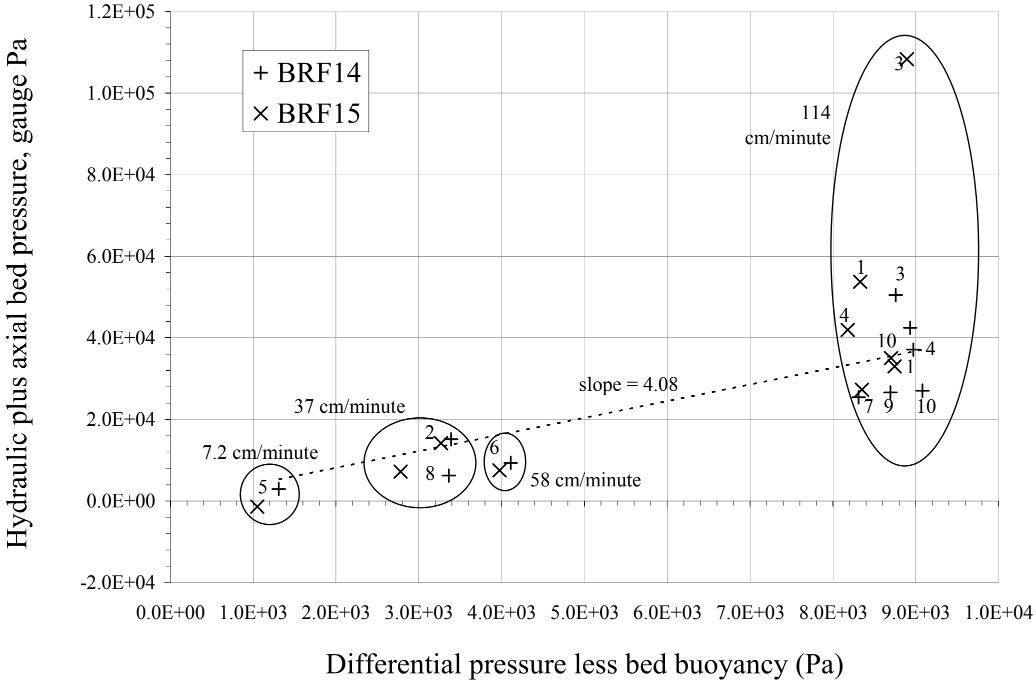

Figure 5-5. Steady-State Axial Pressure for BRF14 and BRF15 Regeneration (height to diameter ratios of relaxed BRF14 and BRF15 beds were 1.59 and 1.65, respectively) (data points labeled with the cycle number)

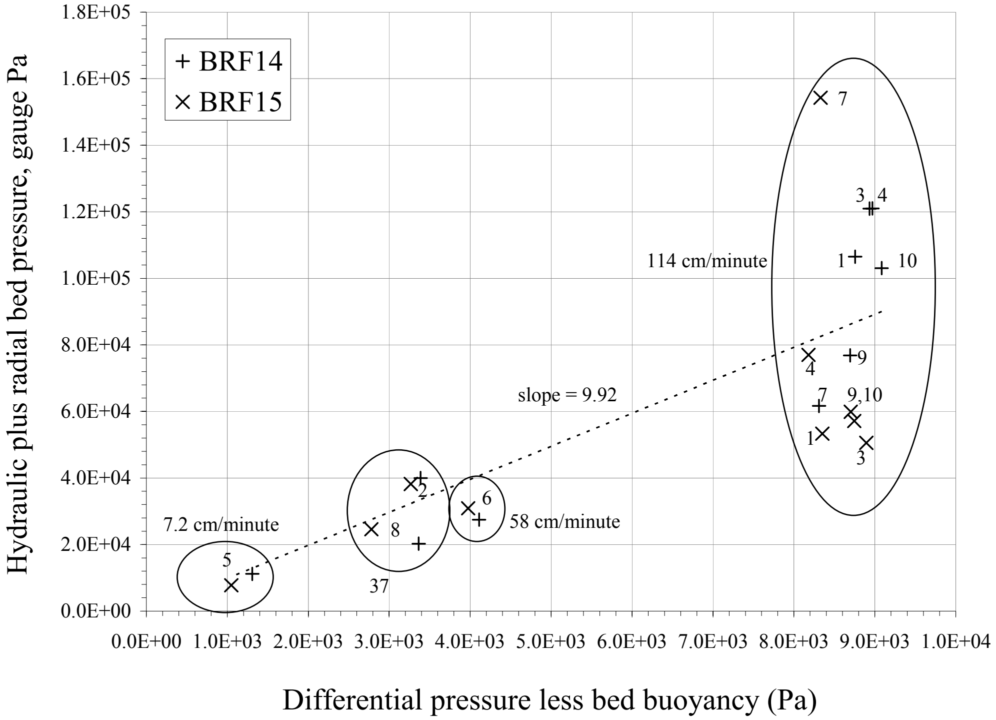

Figure 5-6. Steady-State Radial Pressure for BRF14 and BRF15 Regeneration (height to diameter ratios of relaxed BRF14 and BRF15 beds were 1.59 and 1.65, respectively)

(data points labeled with the cycle number)

5.3 Steady-State Pressures Processing LAW

The axial and radial pressures presented in Figure 5-7 and Figure 5-8) were approximately six times the differential pressure, which is consistent with BRF18. As for regeneration, there appeared to be no significant impact of temporarily removing the thermal well rod in Cycles 6, 7, and 8. The pressures are indicative of residual stresses from the resins' re-expansion following initial contraction in LAW and can be correlated with differential pressure less bed buoyancy in a linear fashion. The slopes of the radial and axial bed pressure correlations are 6.10 and 5.39, respectively, to provide an apparent ratio of 1.13. This ratio should have been the same as that determined for regeneration for the theory presented in section 3.1 to apply since it does not depend on the fluid properties. That the theory appears not to apply for expansion in LAW is probably attributable to the beds not being completely packed. Leva (1959) provides the voidage associated with completely packed spheres as 32%, which compares to 38% measured here. Expansion of the resin in LAW is relatively small compared to that experienced in regeneration and most of the expansion is likely consumed by the additional voidage.

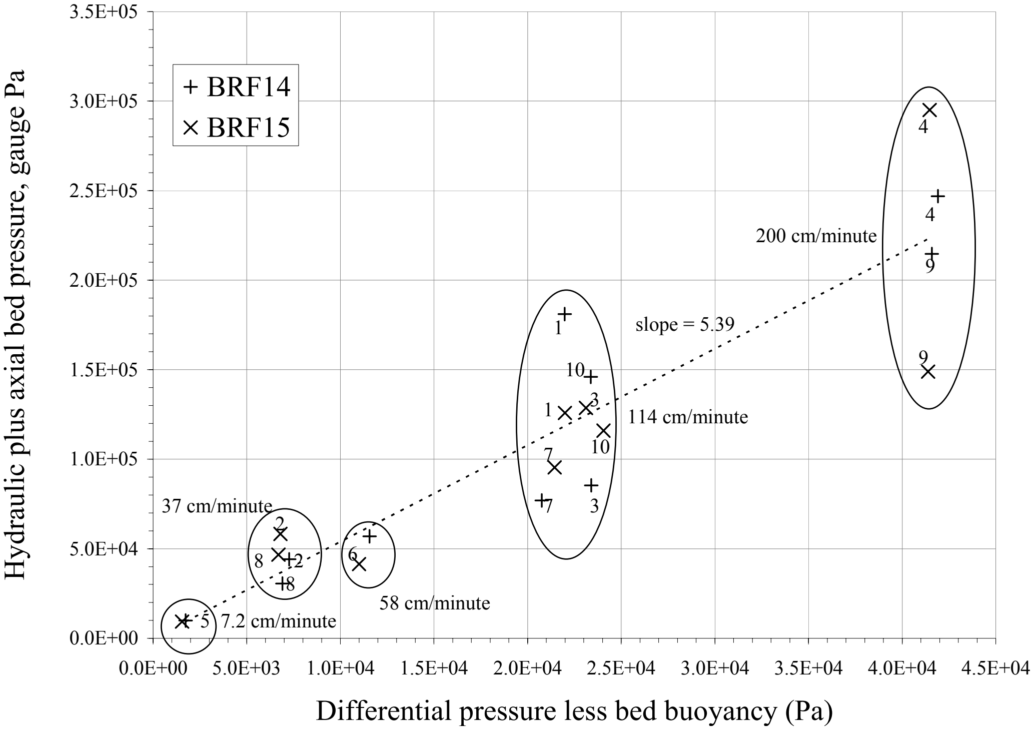

Figure 5-7. Steady-State Axial Pressure for Resin BRF14 and BRF15 Processing LAW (height to diameter ratios of relaxed BRF14 and BRF15 beds were 1.59 and 1.65, respectively) (data points labeled with the cycle number)

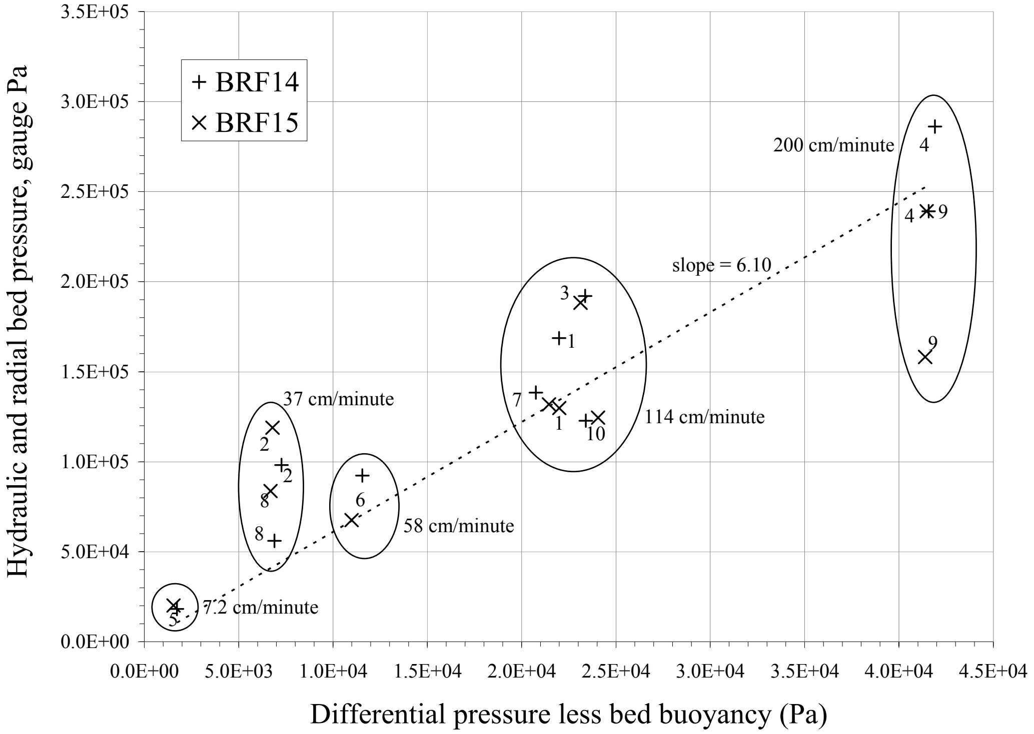

Figure 5-8. Steady-State Radial Pressure for Resin BRF14 and BRF15 Processing LAW (height to diameter ratios of relaxed BRF14 and BRF15 beds were 1.59 and 1.65, respectively) (data points labeled with the cycle number)

5.4 Particle Size Distribution

Figure 5-9 compares the fresh and cycled BRF14 resin particle size distributions and shows that the cycled resin had expanded, which is consistent with the observations of Fiskum (2006)[15]. Fiskum (2006)[14] observed the spherical RF resins never returned to their original as-received size after a single cycle of expansion in sodium hydroxide and contraction in nitric acid. Indeed, that there was no significant variation in bed height or permeability over the 10 cycles indicates this expansion occurred during pretreatment and conditioning. The volumetric mean diameter of the used resins was ~550 μm. Half of the cycled resin particles were smaller than ~490 μm whereas half of the fresh resin particles were smaller than 472 μm. However, the BRF14 resin particles appeared to remain intact given the similar mono-modal distributions and the lack of any very fine material. This observation is consistent with the micrographs in Figure 5-10 and the constant bed permeability.

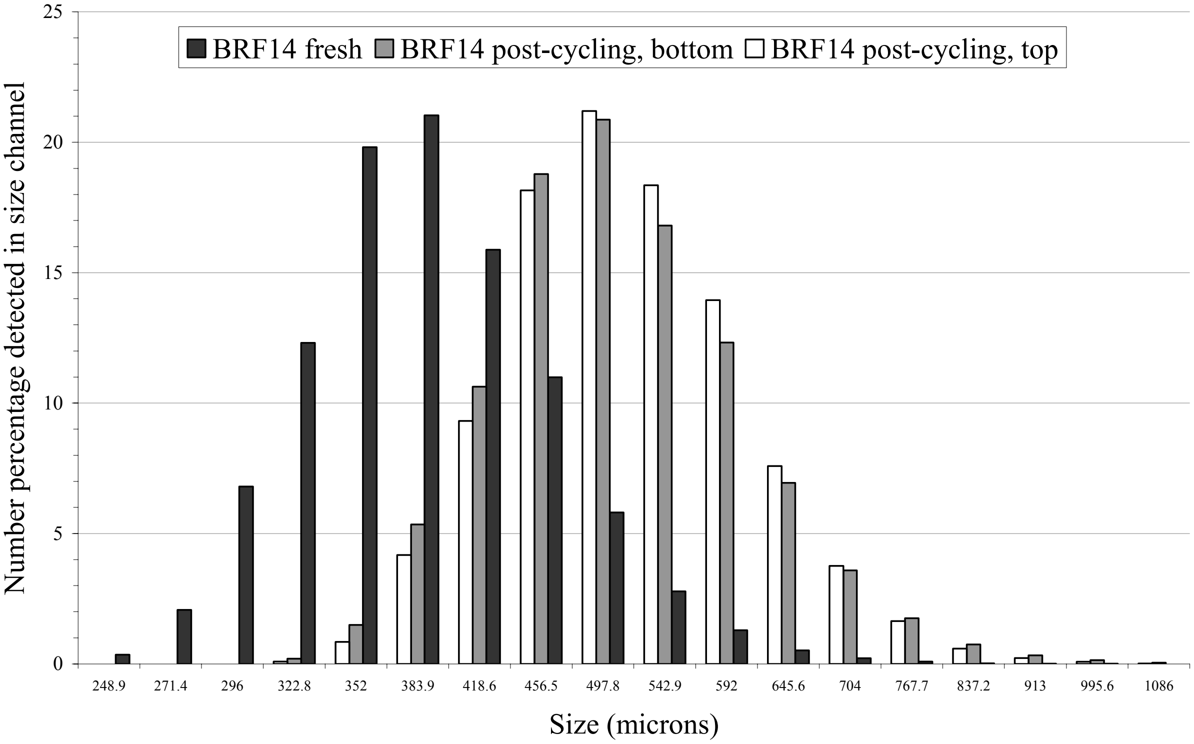

Figure 5-9. Comparison of Fresh and Cycled Acid-Form BRF14 Particle Size Distributions

---

[15] Fiskum, SK, ST Arm, WC Buchmiller, T Trang-Le, JE Martinez, J Matyas, MJ Steele, KK Thomas, DL Blanchard. 2006. *Comparison Testing of Multiple Spherical Resorcinol Formaldehyde Resins for the River Protection Project – Waste Treatment Plant.* WTP-RPT-143 (to be published), Battelle—Pacific Northwest Division, Richland, WA.

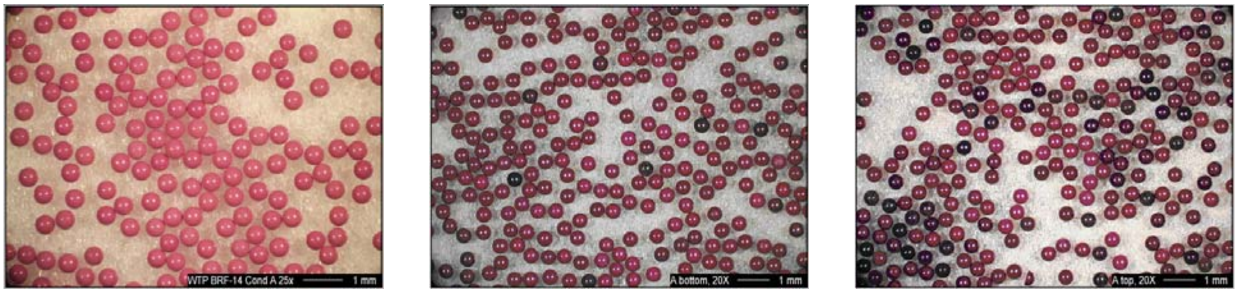

Figure 5-10. Micrographs of (in order left to right) Fresh, Cycled-Bottom and Cycled-Top BRF14

The comparison of the acid-form BRF15 particle size distributions in Figure 5-11 also showed that the cycled resin expanded for the same reasons as BRF14, but the mono-modal distributions indicate that the resin particles remained intact throughout cycling. The volumetric mean diameter of the used resins was ~550 µm. Half of the fresh BRF15 resin particles were smaller than 479 µm compared to 496 µm for the cycled resin. This observation is again consistent with the micrographs in Figure 5-12 and the constant bed permeability noted earlier. Also consistent with the BRF18 resin, the BRF14 and BRF15 resins also became darker and more variable in color as they were oxidized. However, resin oxidation did not appear to significantly affect the resins' hydraulic characteristics after 10 cycles. Section 9.0 also shows the equilibrium performance was not significantly affected by oxidation.

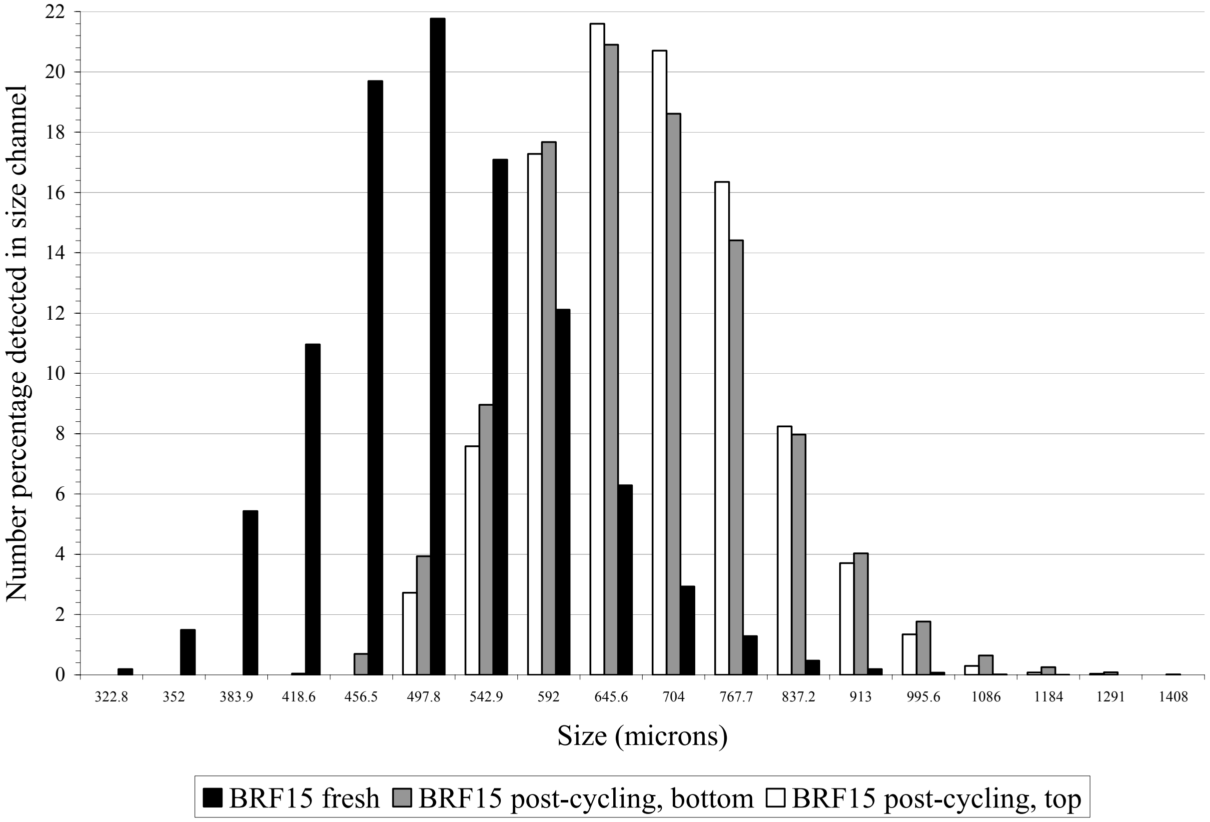

Figure 5-11. Comparison of Fresh and Cycled Acid-Form BRF15 Particle Size Distributions

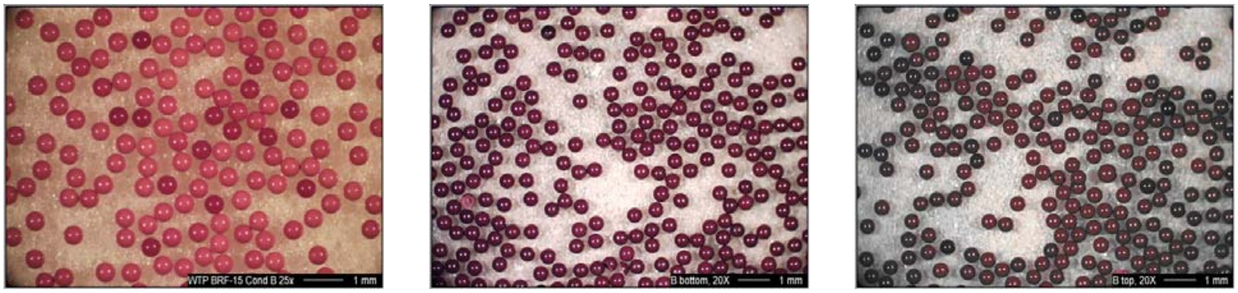

Figure 5-12. Micrographs of (in order left to right) Fresh, Cycled-Bottom, and Cycled-Top BRF15

6.0 Wave 2 (Scale-Up Vendor Samples) Results Analysis and Discussion

This section describes the following results obtained from the Wave 2 testing cycle:

- The bed voidage of resins BSC00 and BSC01 during LAW processing and regeneration
- Steady-state pressures of resins BSC00 and BSC01 during regeneration
- Steady-state pressures of resins BSC00 and BSC01 during LAW processing
- Observations from fluidization steps.

Wave 2 resins were pre-treated by soaking them in 1 M sodium hydroxide overnight before loading them into the columns to produce beds with height to diameter ratios of 1.06 for both resins. Conditioning of the resins in the columns was performed by conducting a complete cycle that included a wash with DI water, conditioning with 0.5 M sodium hydroxide, up-flow simulated LAW introduction, down-flow simulated LAW processing, 0.1 M sodium hydroxide feed displacement, DI water washes and elution. Later cycles repeated the conditioning cycle except that up-flow, or fluidized, regeneration was performed in an effort to resolve operational problems associated with up-flow simulated LAW introduction following down-flow regeneration.

6.1 Bed Voidage and Permeability

Figure 6-1 illustrates the bed voidage of resins BSC00 and BSC01 during processing of LAW and during regeneration. Bed voidage was essentially the same at 0.40 for both resins in regeneration and while processing LAW. Note that the bed voidage during Cycle 4 and 5 regeneration was not calculated because the beds were fluidized. There were no trends of permeability with cycle number, consistent with the absence of fines generation described in Section 6.4.

The derived permeabilities were 2.0×10^{-10} m^2 and 2.3×10^{-10} m^2 for BSC00 during LAW processing and regeneration, respectively. For BSC01 during LAW processing and regeneration, the derived permeabilities were 2.2×10^{-10} m^2 and 1.8×10^{-10} m^2.

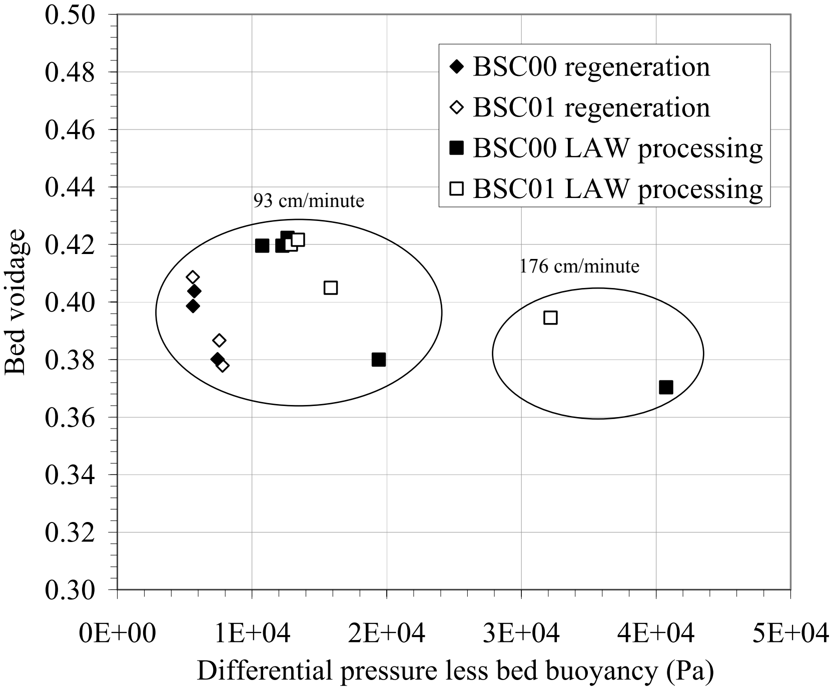

Figure 6-1. Bed Voidage of BSC00 and BSC01 During Regeneration and Processing LAW

6.2 Steady-State Bed Pressures During Regeneration of Wave 2 Resins

Figure 6-2 and Figure 6-3 present the steady-state radial and axial pressures, respectively, for the Wave 2 resins. The figures show that the resins exhibited residual stresses following their expansion because the axial and radial pressures are, respectively, ~3 and ~6 times higher than the differential pressures. Pressures were higher in the first cycle, but the limited data probably preclude drawing technically reasonable conclusions. The Wave 2 resins also exhibited lower ratios of radial to axial bed pressures than those from Wave 1 probably because of the lower bed height in Wave 2. Note that data from the regeneration steps of Cycles 4 and 5 are not reported because the beds were fluidized, and pressures were essentially consistent with the differential pressure.

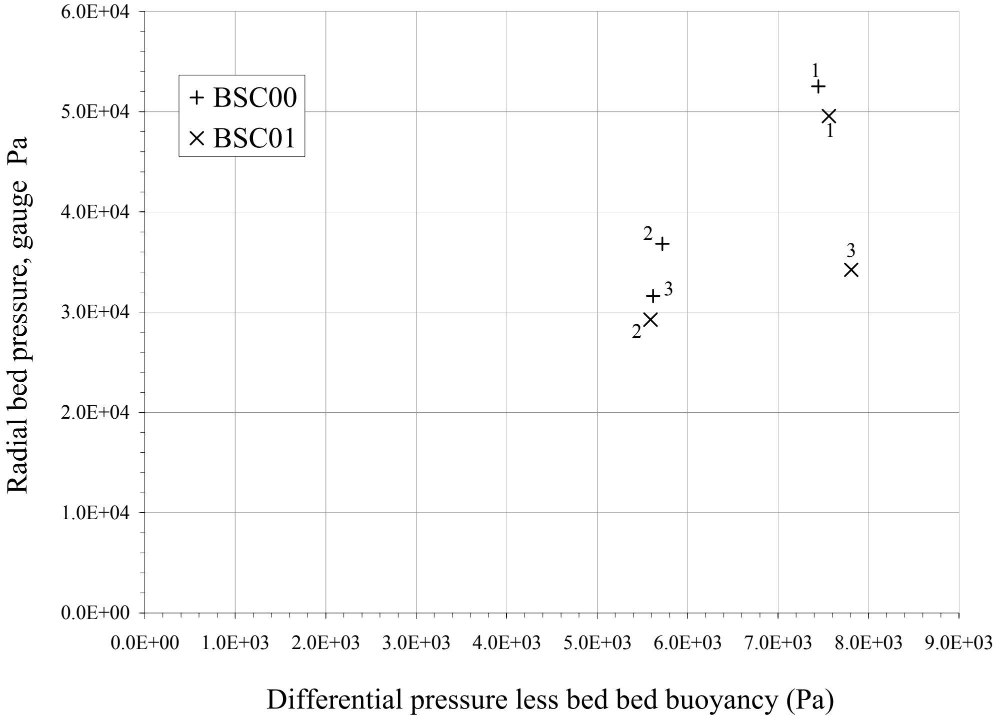

Figure 6-2. Steady-State BSC00 and BSC01 Radial Pressures During Regeneration (at 93 cm/minute, height to diameter ratios of relaxed beds were both 1.06) (data points labeled with the cycle number)

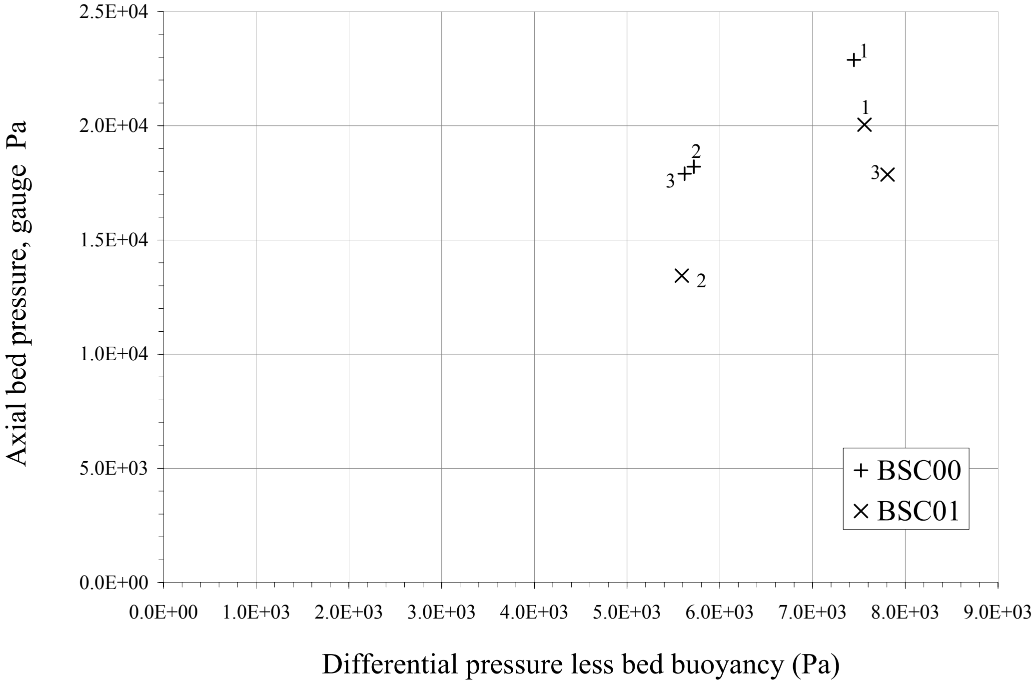

Figure 6-3. Steady-State BSC00 and BSC01 Axial Pressures During Regeneration (at 93 cm/minute, height to diameter ratios of relaxed beds were both 1.06) (data points labeled with the cycle number)

6.3 Steady-State Bed Pressures for Wave 2 Resins Processing LAW

In contrast to the behavior exhibited in regeneration, there appeared to be little residual bed pressure for the resins processing LAW. As illustrated in Figure 6-4 and Figure 6-5, radial and axial pressures for all cycles were comparable to the differential pressure. The bed is simply being pushed down and out by the fluid drag. Therefore, fluidizing the resin before processing simulated LAW appears to relieve the bed stresses residual from initial expansion following contraction in LAW. In addition, there appears to be no adverse impact by fluidized regeneration conducted in Cycles 4 and 5.

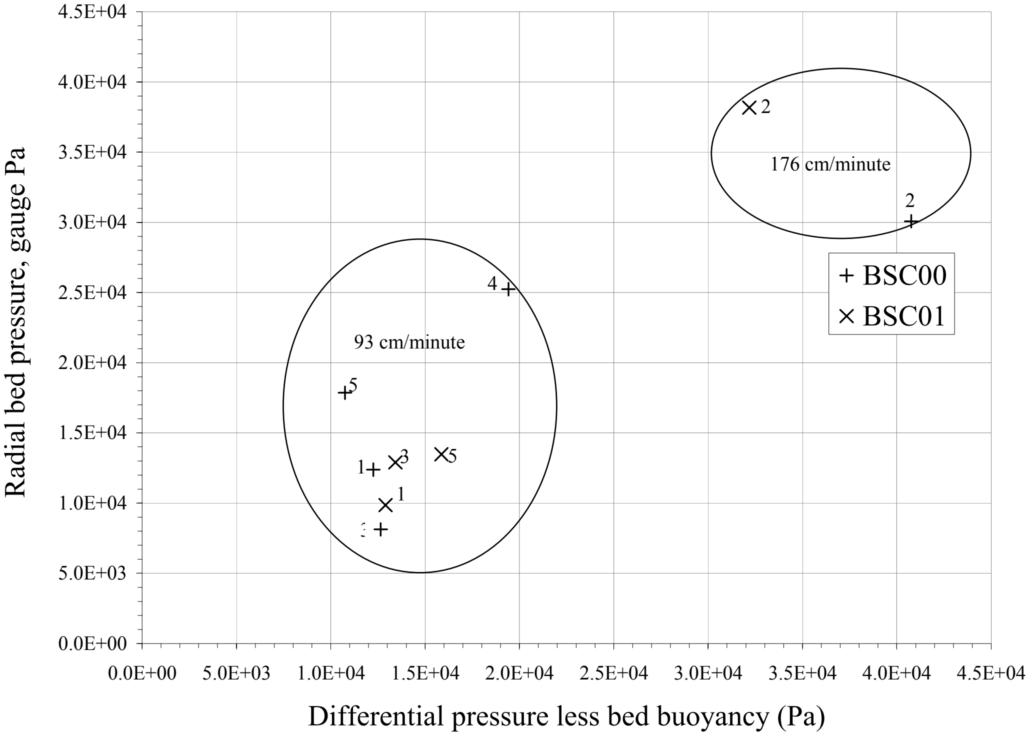

Figure 6-4. Steady-State Radial Pressures for BSC00 and BSC01 Processing LAW (height to diameter ratios of relaxed beds were both 1.06) (data points labeled with the cycle number)

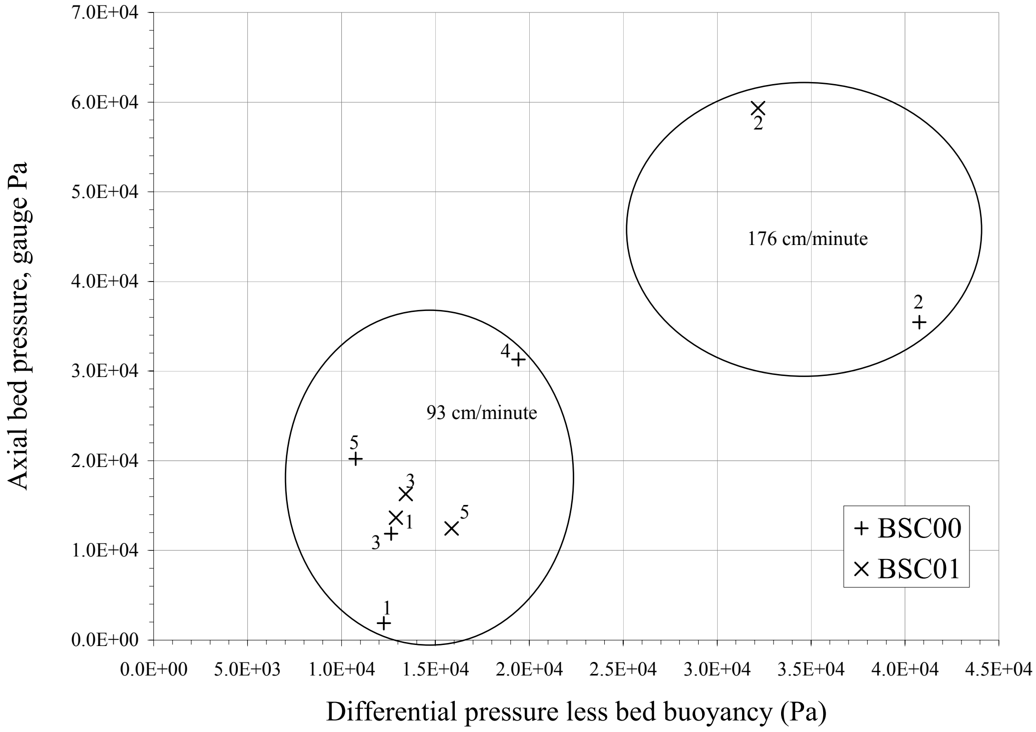

Figure 6-5. Steady-State Axial Pressures for BSC00 and BSC01 Processing LAW (height to diameter ratios of relaxed beds were both 1.06) (data points labeled with the cycle number)

6.4 Particle Size Distribution

Figure 6-6 and Figure 6-7 compare the particle size distributions of fresh and cycled acid-form BSC00 and BSC01 resins, respectively. The resins remained mono-modal and had slightly expanded upon cycling consistent with the Wave 1 observations (section 4.5). There was no generation of fines. Volumetric average particle diameters of the used resin were 420 μm and 400 μm for the BSC00 and BSC01 resins, respectively. The micrographs of the as-received and cycled resins in Figure 6-8 and Figure 6-9 for BSC00 and BSC01, respectively, also do not indicate any fines. Interestingly, broken beads are evident in both as-received and cycled BSC00 micrographs. No broken beads are evident from the BSC01 micrographs, although a few as-received beads are fused together. Both the cycled BSC00 and BSC01 resins are darker and exhibit more color variability than their as-received counterparts. However, resin oxidation did not significantly affect the resins' hydraulic characteristics over 5 cycles, as for the BRF resins, except they appeared more buoyant during up-flow processing, which is consistent with a lower density.

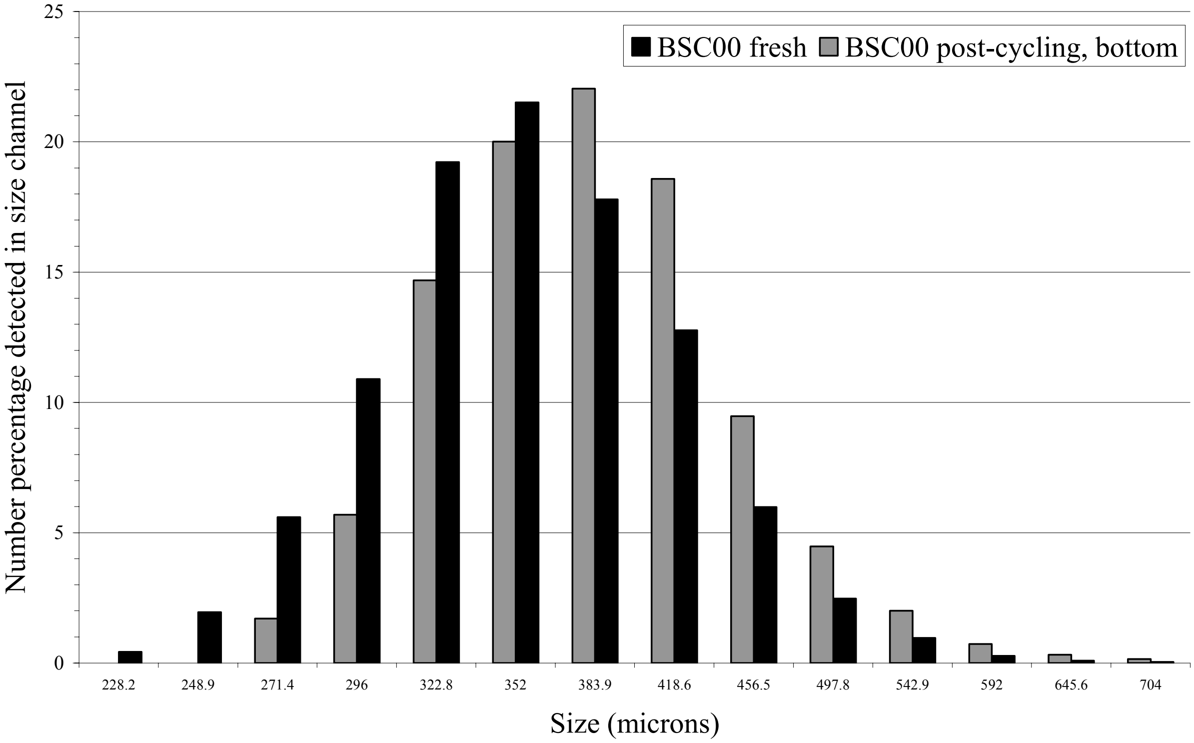

Figure 6-6. Comparison of Fresh and Cycled Acid-Form BSC00 Particle Size Distributions

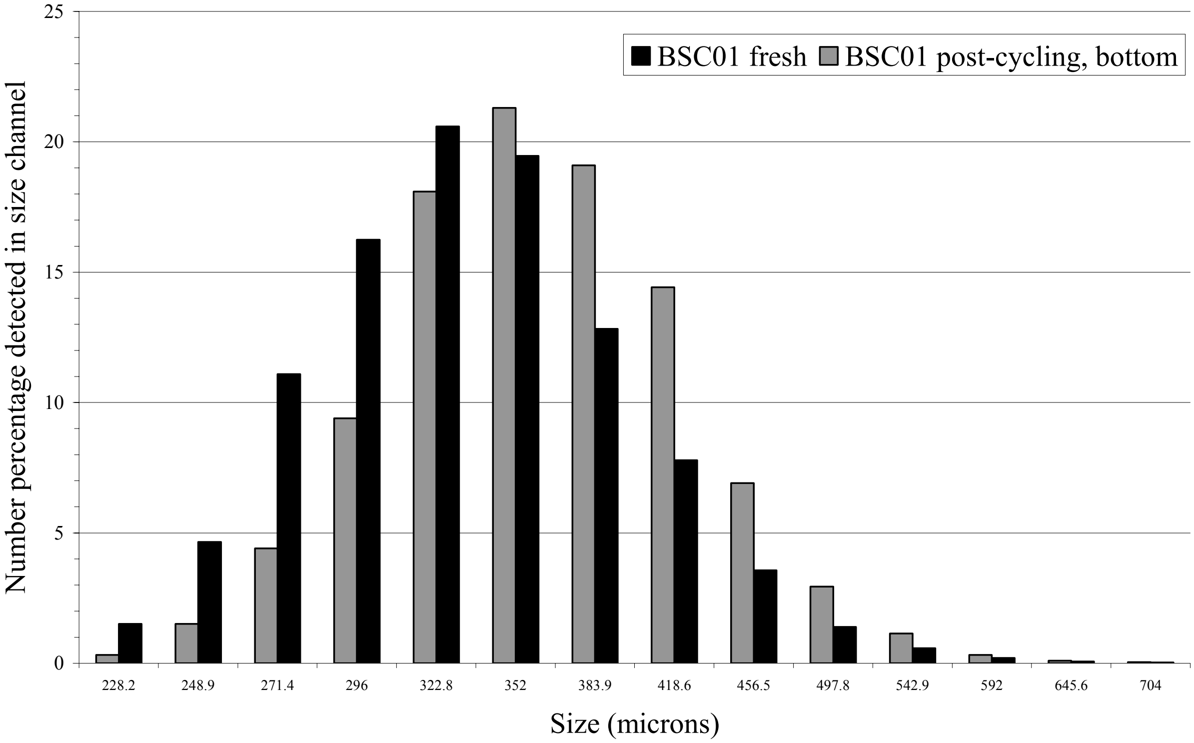

Figure 6-7. Comparison of Fresh and Cycled Acid-Form BSC01 Particle Size Distributions

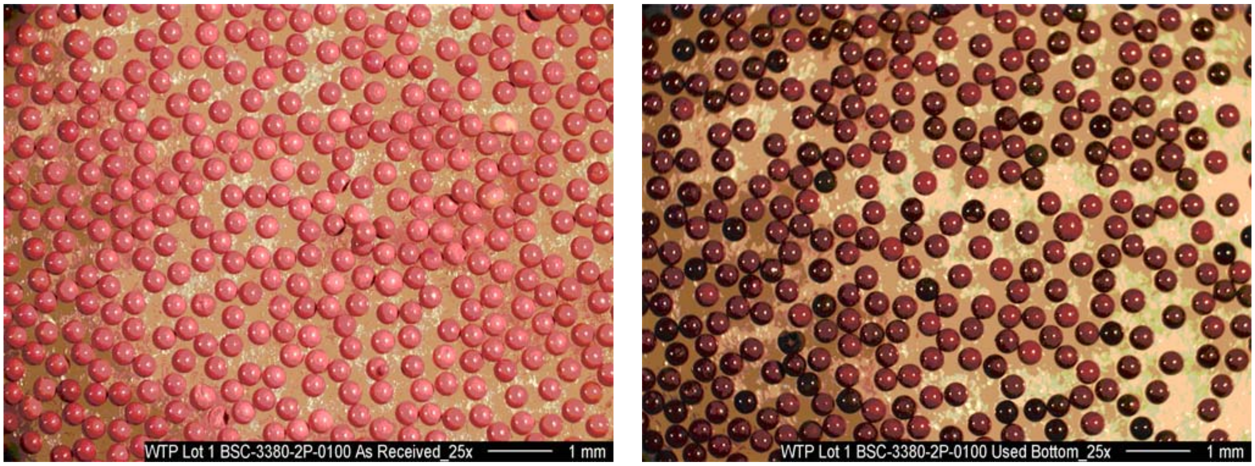

Figure 6-8. Micrographs of Fresh (left) and Cycled-Bottom (right) BSC00

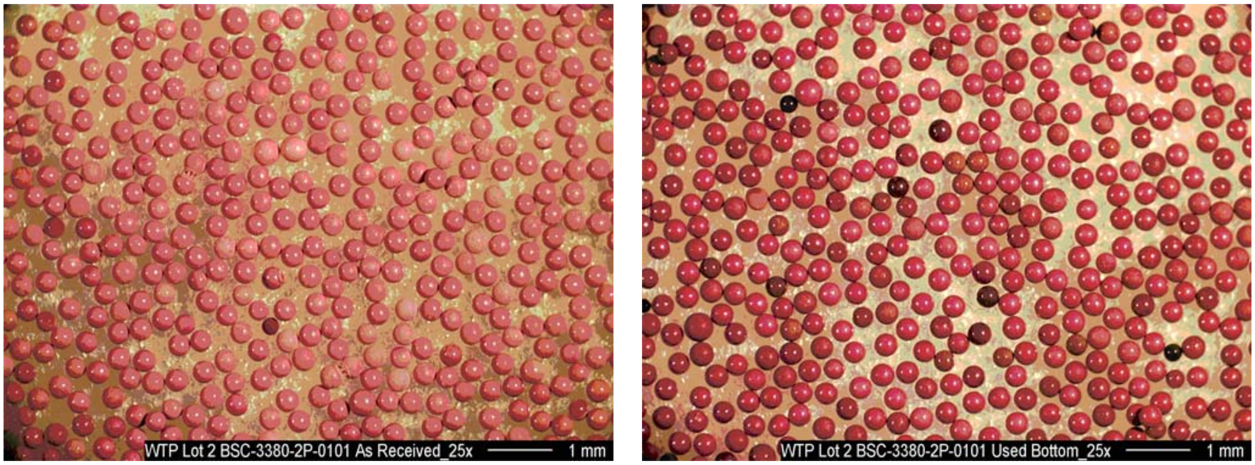

Figure 6-9. Micrographs of Fresh (left) and Cycled-Bottom (right) BSC01

6.5 Observations from Fluidization Steps

This section describes observations on the bed during the fluidization or up-flow steps performed during Wave 2. In the WTP, the ion exchange bed requires fluidization with LAW before processing LAW down-flow to verify that its surface is level. An important factor considered during fluidization testing was whether the bed pressures residual from the bed's expansion in regeneration would be sufficient to prevent its fluidization. Approaches to successful fluidization would then be tested if this proved to be the case.

6.5.1 Conditioning

Both the BSC00 and BSC01 beds were regenerated down-flow at a velocity of 0.44 cm/minute, or 3 BV/hour. At this point, the apparatus was plumbed for up-flow using only the large pump, and, although the bed appeared to be capable of fluidization with simulated LAW, fluidization was abandoned when excessive air bubbles were entrained into the feed. The large pump appeared unable to pump at a sufficiently low rate to achieve fluidization without conveying the resin out of the column.

The apparatus was subsequently re-plumbed for up-flow using only the small pump. The BSC00 resin was regenerated at a velocity of 0.44 cm/minute, or 3 BV/hour, following conditioning, and then successfully fluidized to approximately 50% bed expansion with simulated LAW at a velocity of 3.6 cm/minute.

6.5.2 Cycle 1

Both the BSC00 and BSC01 beds were regenerated down-flow at 100 cm/minute. Subsequent fluidization was unsuccessful with the small pump, and the apparatus was re-plumbed to permit up-flow with the large pump. During simulated LAW introduction, the BSC00 bed initially rose as a plug at a velocity of 31 cm/minute and then held as an elevated plug for 15 minutes at 15.7 cm/minute. Fissures were observed in the side of the bed viewed through the plastic section of column. The BSC01 bed was raised no more than ~1 cm as a plug at 34 cm/minute before excessive line pressure led to abandoning further attempts at fluidization.

6.5.3 Cycle 2

Both the BSC00 and BSC01 beds were again regenerated down-flow at 100 cm/minute. Simulated LAW was pumped down-flow to remove air bubbles in the line before attempting fluidization. However, a large bubble did disturb the bed upon initiating up-flow. The bed elevated to approximately 50% bed expansion at a simulated LAW velocity of 28 cm/minute. However, the surface was poorly defined with numerous fountains of resin recirculating in the headspace. Air bubbles also initially disturbed the BSC01 bed, which was fluidized to achieve 50% bed expansion at a simulated LAW velocity of 21 cm/minute.

6.5.4 Cycle 3

It is likely that fluidization in Cycle 2 only occurred because the beds were disturbed by air bubbles, and the behavior observed in Cycle 1 was the closest to what actually would occur in the WTP. The slow expansion of the spherical RF following its initial contraction in simulated LAW likely leads to radial pressures, in addition to those residual from regeneration, that hold the bed against the walls. Therefore, in Cycle 3, PNWD attempted to use the initial contraction of the beds to fluidize them. Up-flow was initiated and continued for up to 1 minute before it was terminated for up to 2 minutes. The bottom surface of the elevated bed could then rain back down onto the screen. Up-flow could again be initiated and the process repeated so that the radial pressures residual from the beds' regeneration could be relieved.

Both the BSC00 and BSC01 beds were again regenerated down-flow at 100 cm/minute. Simulated LAW was introduced up-flow to the BSC00 bed for 45 seconds at 5.8 cm/minute. The bed was observed to rise approximately 25 mm before the flow was terminated. After 2 minutes, simulated LAW was again introduced up-flow for 40 seconds at 9.6 cm/minute. Flow was stopped for 1 minute and then recommenced for 2 minutes at 9.6 cm/minute and then at 13 cm/minute. A slight eruption from the bed preceded bed fluidization to 50% expansion.

Unfortunately, a bubble again disturbed the BSC01 bed, which was subsequently fluidized at a simulated LAW velocity of 12 cm/minute.

6.5.5 Cycle 4

Cycles 4 and 5 were conducted to investigate up-flow and/or fluidized regeneration followed by up-flow LAW. Up-flow regeneration of BSC00 was successfully conducted at an up-flow velocity of 5.8 cm/minute for 2 hours. Slight activity of the bed surface was observed when the up-flow regeneration of BSC01 was initiated at a velocity of 2.6 cm/minute. The BSC01 bed became fully mobile at an up-flow velocity of 3.6 cm/minute. An area of localized higher velocity (spouting) was observed close to one of the thermowells throughout BSC01 up-flow regeneration. Spouting is thought to be caused by air bubbles becoming trapped beneath the bed support screen, so the solution is diverted around them and channels through the bed. However, this phenomenon was not postulated and tested until Wave 4. The air bubbles are thought to arise either from insufficient flooding of the bottom valve assembly during the previous down-flow elution rinse (air bubbles were sometimes observed to break through the bed during this step) or from becoming entrained in the feed from the pulse dampener. The air bubbles and the spouting phenomena are therefore probably a specific characteristic of the apparatus. Simulated LAW was pumped up-flow at a velocity of 2.7 cm/minute through both beds following regeneration. Neither bed fluidized, as intended, although both rose initially as the 0.5 M sodium hydroxide was displaced from the column. Fountains of recirculating resin were observed in the BSC01 column.

6.5.6 Cycle 5

Up-flow BSC00 regeneration was conducted by gradually increasing the velocity over 2 hours. Table 6-1 provides velocities and observations.

Table 6-1. Cycle 5 Up-flow BSC00 Regeneration

Velocity (cm/minute)	Observations
1.9	Bubbles disturbing bed but otherwise no activity.
2.4	No activity.
5.1	Slight spouting observed.
6.2	Increased spouting.
8.9	Pulsing spout ~8 mm high.
10.2	Spout disappears, wavy bed surface.
19.5	Bed fluidized to 50% expansion.

The spout likely disappeared at a velocity of 10.2 cm/minute because the bed had expanded to a height sufficient that the local area of higher fluid velocity had dissipated over the column cross-section, but it led to a wavy bed surface.

Up-flow BSC01 regeneration was also conducted by gradually increasing the velocity over 2 hours. Table 6-2 provides velocities and observations.

Table 6-2. Cycle 5 Up-Flow BSC01 Regeneration

Velocity (cm/minute)	Observations
5.8	Spout ~8 mm high.
9.6	Fluidized bed with wavy surface with spout.
19.6	Bed fluidized to 50% expansion with wavy bed surface.

Simulated LAW was introduced up-flow into both columns as described for Cycle 4.

6.5.7 Conclusions from Wave 2 Fluidization Testing

Ion exchange beds regenerated down-flow at velocities sufficiently high to reproduce the pressure drop in full-scale columns could not be fluidized with simulated AP101 LAW, except where assisted by bubbles entrained in the feed. The fluid pressure constrained axial expansion of the bed, and the resulting high radial pressures were not relieved upon flow termination such that the beds behaved as plugs adhering to the column walls. Up-flow LAW introduction, without fluidization, could be accomplished, but the observed partial break-up of the bed may potentially lead to fissures in the bed that would have channeled LAW and led to unacceptably early cesium breakthrough. Two methods for up-flow simulated LAW introduction were successfully tested to achieve a level settled bed:

- Relieve the radial pressures by alternately pumping and terminating up-flow simulated LAW while the bed undergoes initial contraction in simulated LAW. The bed can then be fluidized with simulated LAW.
- Eliminate the radial pressures exerted by the bed by performing fluidized regeneration before its fluidization in simulated LAW.

7.0 Wave 3 (100-Gallon Batch) Results Analysis and Discussion

This section describes the following results obtained from the Wave 3 testing cycle:

- The bed voidage of resin 5E-370/641 during processing of LAW
- Steady-state pressures of resin 5E-370/641 during processing of LAW and during regeneration
- Observations from fluidization steps
- Regeneration efficiency.

The Wave 3 resin was pre-treated by soaking it in 1 M sodium hydroxide overnight before loading it into the column to produce a bed with height to diameter ratio of 1.19. Two cycles of in-column resin conditioning were performed. The first conditioning cycle (labeled -1 in the following discussion) included a complete cycle of fluidized conditioning with 0.5 M sodium hydroxide, down-flow simulated LAW processing, 0.1 M sodium hydroxide feed displacement, DI water washes and elution. The second conditioning cycle repeated the first except the simulated LAW was introduced up-flow prior to processing it down-flow. Later cycles repeated the second conditioning cycle.

7.1 Bed Voidage and Permeability

The pertinent data used to calculate the bed voidage and permeability are tabulated in Table 7-1. Note that the two conditioning cycles are designated -1 and 0. Regeneration and simulated LAW introduction was conducted down-flow in cycles -1 and 6 in which the reduction in bed voidage is approximately commensurate with the reduction in bed height.

Table 7-1. Summary of Wave 3 Measurements and Bed Voidage and Permeability

Cycle	Viscosity (cp)	Bed height (cm)	Differential pressure ($\times10^4$ Pa)	Superficial velocity (cm/s)	Voidage (%)	Permeability ($\times10^{-10}$ m^2)
-1	2.53	8.3	1.52	1.56	0.38	2.03
0	2.53	8.7	1.22	1.54	0.41	2.61
1	2.53	8.8	0.92	0.12	0.41	2.63
2	2.53	8.8	2.40	2.91	0.41	2.75
3	2.16	8.7	4.20	5.42	0.41	2.76
4	2.16	8.8	1.02	1.54	0.41	2.80
5	2.05	9.0	0.89	1.55	0.42	3.13
6	2.17	8.3	1.43	1.56	0.38	2.02
7	2.12	9.0	0.94	1.56	0.42	3.10
8	2.25	8.8	1.08	1.55	0.41	2.77
9	2.01	9.0	1.81	2.93	0.42	3.04
10	2.10	8.7	4.01	5.79	0.42	3.08
11	2.03	9.0	0.93	1.55	0.42	2.98
12	1.99	8.9	0.08	0.12	0.40	2.56

Figure 7-1 illustrates that the bed voidage initially appeared to rise before attaining a steady value of 0.42 in simulated AP101 LAW. Note that the initial resin conditioning cycles are represented by negative numbers. The bed voidage in Cycle -1 and 6 (that included down-flow regeneration and no up-flow simulated LAW introduction) was ~12% lower than experienced in other cycles at 0.38 probably because of bed compression. Evidence for bed compression comes from the bed height, which was ~7 mm lower in Cycle 6 (compared to an overall height of 85 mm in Cycle 6) than in other cycles. The higher bed pressures described later also indicate bed compression. The lower bed voidage in Cycle 6 is also consistent with the values reported for the BRF resins, which also experienced down-flow regeneration and no up-flow simulated LAW introduction. Bed compression probably arises from the resin undergoing constrained expansion following initial contraction upon simulated LAW introduction. Resin 5E-370/641 bed voidage is consistent with the value of 0.41 reported for the scale-up vendor's resins (Wave 2), which experienced up-flow simulated LAW introduction and some up-flow regeneration.

Also illustrated in Figure 7-1 are the bed voidage calculated from the data of Adamson et al. (2006) from their 12-inch and 24-inch diameter columns. Bed voidage averaged 0.41 and 0.43 in the 12-inch and 24-inch diameter columns, respectively, and was consistent with that obtained in the 3-inch column. Note that simulated LAW introduction was conducted up-flow for all cycles except on the first cycle (-2 and -1 in the 12-inch and 24-inch column tests, respectively) and cycle 6 in the 24-inch column test when these operations were conducted down-flow. Notably lower bed voidage was observed in cycle 6, consistent with the observation in the 3-inch column.

The permeability of resin 5E-370/641 processing LAW was 2.9×10^{-10} m^2 based on a bed voidage of 0.42 and a bead area mean diameter of 453 μm measured by Adamson et al. (2006).

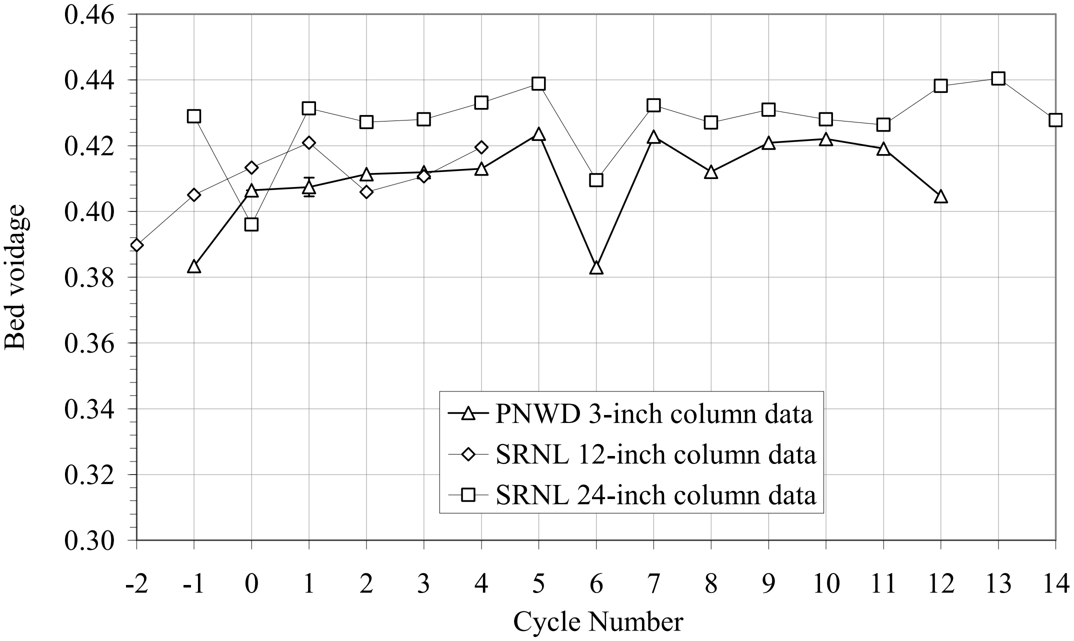

Figure 7-1. Bed Voidage of RF Resin 5E-370/641 as a Function of Cycle Number

(Savannah River National Laboratory [SRNL] column data derived from data supplied by Adamson, personal communication, April 2006)

Figure 7-2 presents the bed voidage as a function of the differential pressure across the bed. The lower bed voidage of the first (cycle -1) and 6th cycles is notable as well as the higher differential pressure compared to other cycles that processed simulated LAW at the same flow rate (Cycles 4, 5, 7, 8, and 11). Greater bed compression is again probably responsible for this observation as a result of not fluidizing the bed prior to processing the simulated LAW.

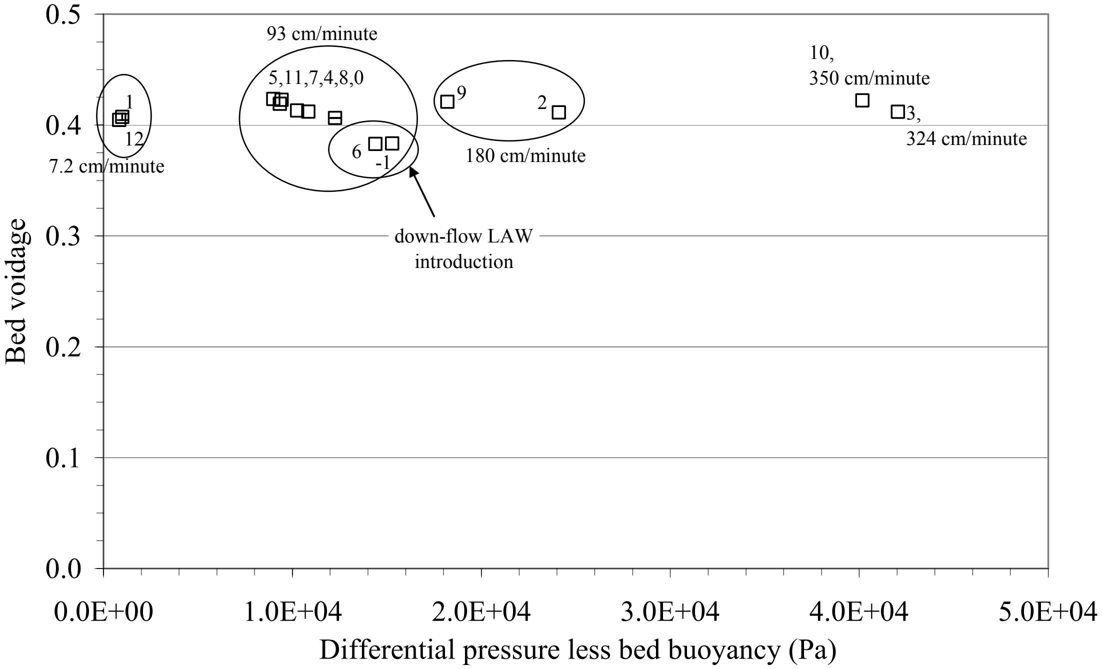

Figure 7-2. Bed Voidage of RF Resin 5E-370/641 as a Function of Bed Differential Pressure (data points labeled with the cycle number and velocity)

7.2 Steady-State Bed Pressures for the Wave 3 Resin Processing LAW

Figure 7-3 presents the steady-state radial bed pressures for resin 5E-370/641 processing LAW. Except for Cycle 6 and -1, the radial pressures are comparable to the differential pressure less bed buoyancy (up to 5×10^4 Pa), indicating that up-flow LAW introduction was effective in relieving radial stresses in the bed arising from its expansion during regeneration and in LAW. The fluid pushes the resin bed down, which then appears to produce a radial force component against the wall. This behavior is consistent with that observed for the Wave 2 resins. The higher radial pressure experienced in Cycles -1 and 6 is probably a result of residual stresses caused by the bed's expansion following its initial contraction upon down-flow introduction of the simulated LAW.

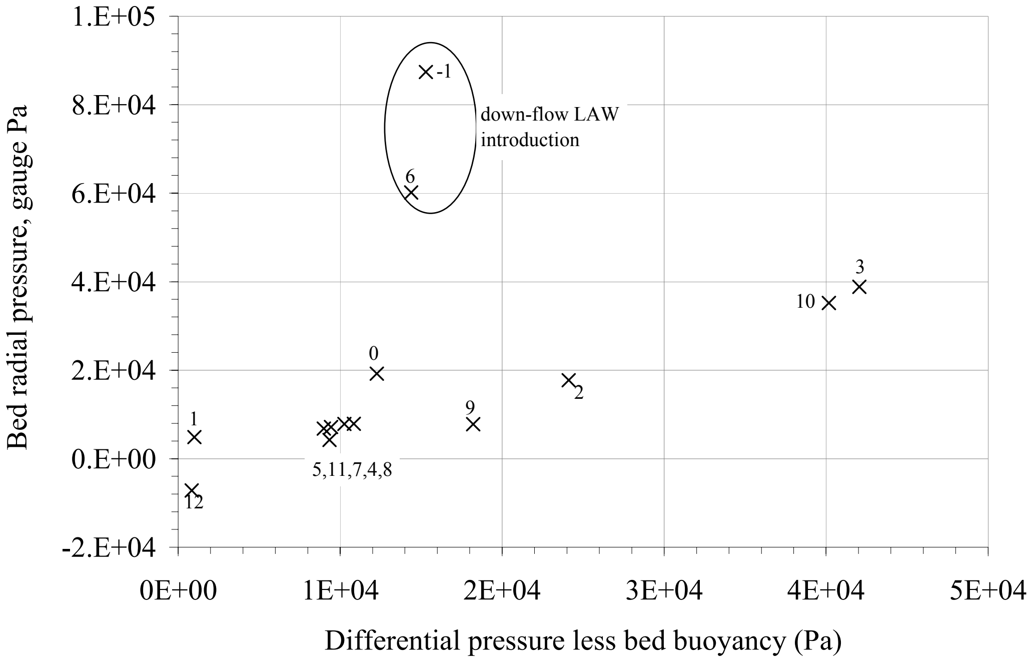

Figure 7-3. Steady-State Radial Pressures for Resin 5E-370/641 Processing LAW (height to diameter ratio of relaxed bed was 1.19) (data points labeled with the cycle number)

The steady-state axial pressures illustrated in Figure 7-4 are also consistent with those observed for the Wave 2 resins in that the pressures are somewhat higher than the differential pressure less bed buoyancy. The axial pressures arise from the fluid drag across the bed.

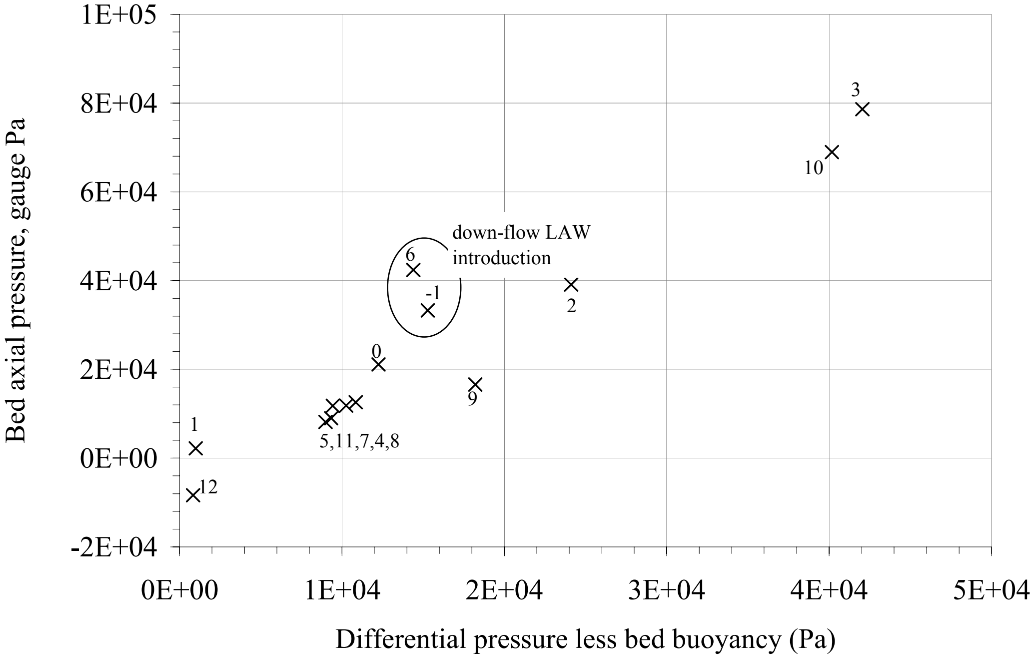

Figure 7-4. Steady-State Axial Pressures for Resin 5E-370/641 Processing LAW (height to diameter ratios of relaxed bed was 1.19) (data points labeled with the cycle number)

7.3 Particle Size Distribution

Figure 7-5 compares the particle size distributions of as-received and cycled acid-form 5E-370/641 resin. The resin remained mono-modal with no generation of fines, though the cycled resin is larger consistent with the Wave 1 observations (section 4.5). As for Wave 1 and shown in Table 7-1, there was no significant variation in bed height or permeability during those cycles in which the simulated LAW was introduced up-flow and so the bead diameter apparently remained constant. Volumetric mean particle diameters were 424 μm and 389 μm for the acid-form cycled and as-received resins, respectively, reflecting the slight expansion of the resin through cycling. Volumetric average particle diameters of the sodium-form pre-cycled and post-cycled resins were 456 μm, indicating that overall expansion occurred upon pretreatment.

There is no evidence that any of the beads broke during process cycling, as shown in the micrographs in Figure 7-6. The micrographs show the cycled resin to be significantly darker and of greater color variability, as observed previously for the spherical RF resin. However, resin oxidation did not significantly affect the resins' hydraulic characteristics over 14 cycles, as noted before, except they appeared more buoyant during up-flow processing, which is consistent with a lower density.

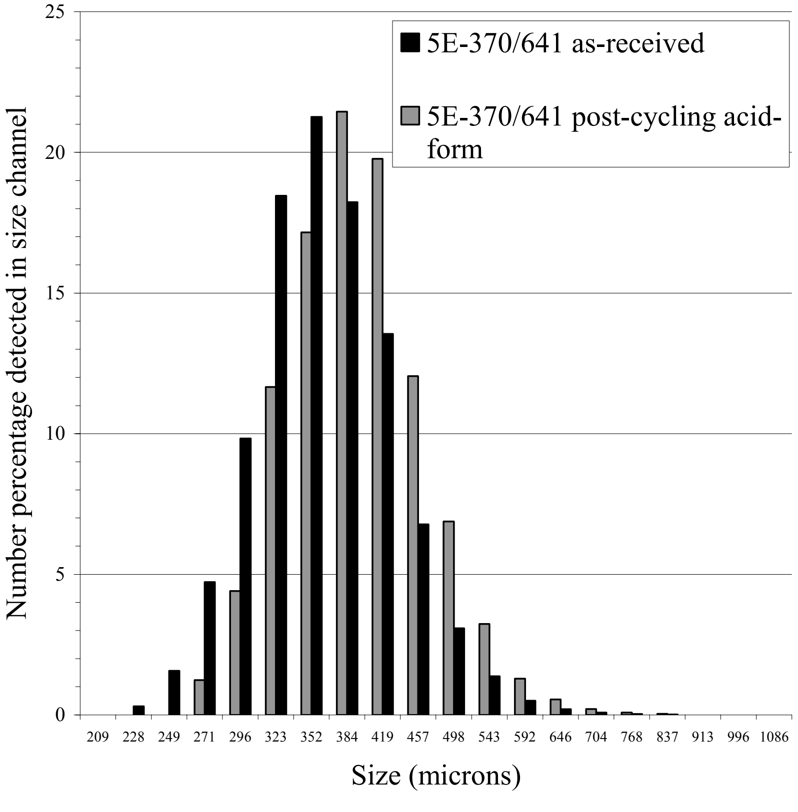

Figure 7-5. Comparison of As-Received and Cycled Acid-Form 5E-370/641 Particle Size Distributions

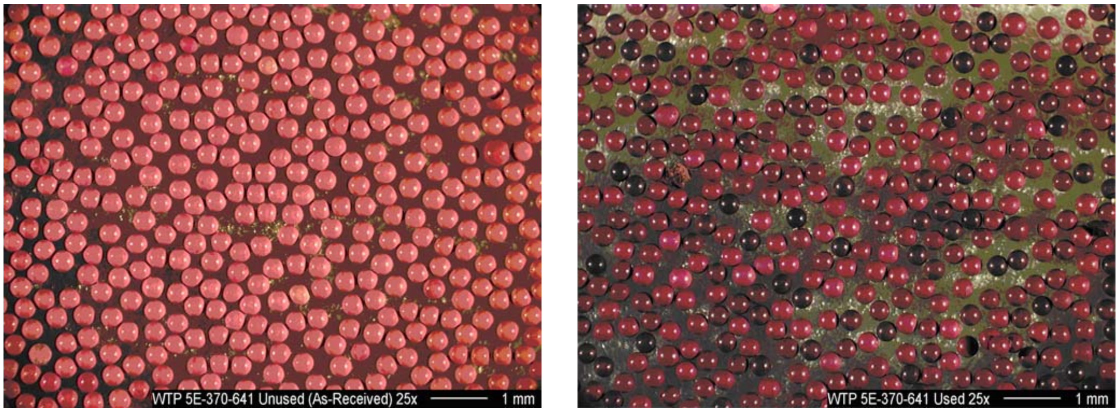

Figure 7-6. Micrographs of As-Received and Cycled Acid-Form 5E-370/641 Resin

7.4 Results and Observations from Up-flow Regeneration and Simulated LAW Introduction

7.4.1 Up-flow Regeneration

The regeneration steps of each cycle were used to investigate various scenarios for regenerating the resin. The variation in bed height and bed behavior with respect to flow rate was measured in the early cycles, and the results are depicted in Figure 7-7 with bed height expressed as percentage bed expansion referenced to the final, settled height. Figure 7-7 indicates that the resin bed initially expanded at a velocity of 4.8 cm/minute. The fluid velocity could not be increased above 19 cm/minute to avoid the fluidized resin bed reaching the column discharge port. Resin motion was observed at velocities above 1.9 cm/minute. Spouts, or regions of higher fluid velocity indicative of solution channeling, were observed at velocities below 12 cm/minute, and the bed was typically ~5 mm higher at the spout. Note that in Cycle 1, the flow rate was gradually increased and then reduced, and Figure 7-7 exhibits a hysteresis effect with lower bed heights on initial expansion that is probably associated with spouting, as shown in Section 8.4.1.

The bed height was also investigated as a function of process time at a constant flow rate, and Figure 7-8 presents the results where bed expansion is expressed as a percentage of the final settled height. The low starting height is due to the smaller acid-form diameter of the resin. Also shown is the profile for Cycle 6, for which regeneration was conducted down-flow at 94 cm/minute. For a quiescent bed and once-through processing, the height should provide a measure of the degree to which the resin has been regenerated. However, there are most likely transient phenomena affecting the height that are manifested as a result of fluidizing resin that is also expanding. Recycling the sodium hydroxide also introduces mass transfer effects because the bulk concentration is also changing throughout the process.

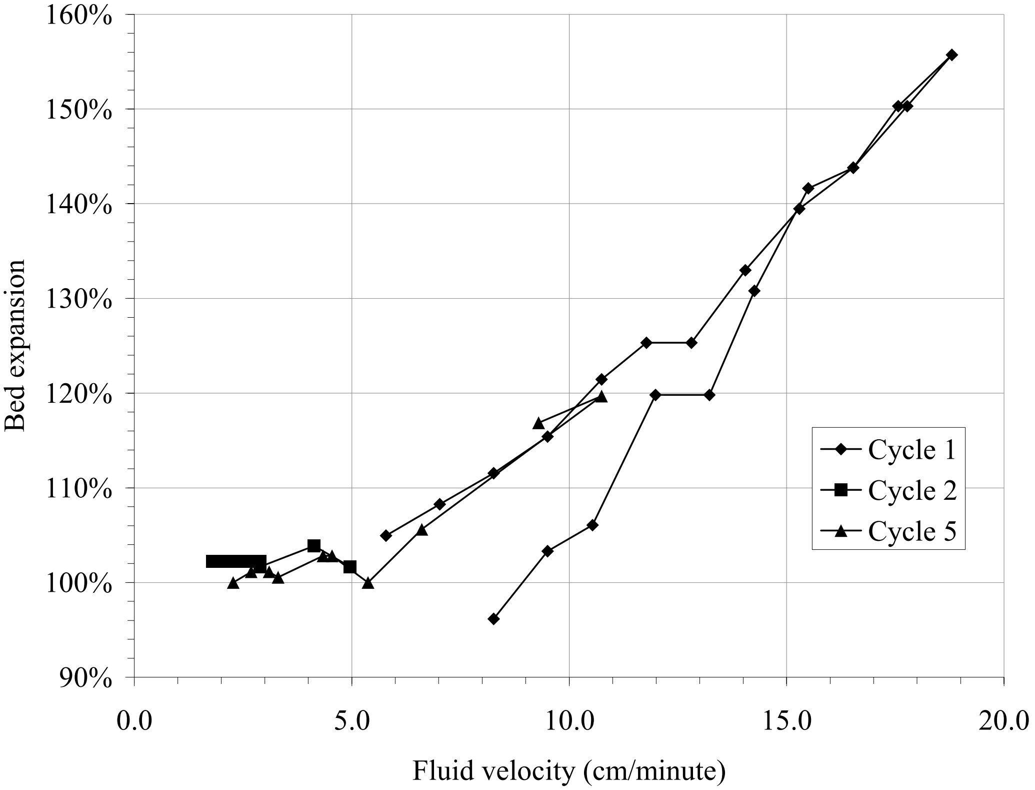

Figure 7-7. Variation of Bed Height with Fluid Velocity During Up-Flow Regeneration

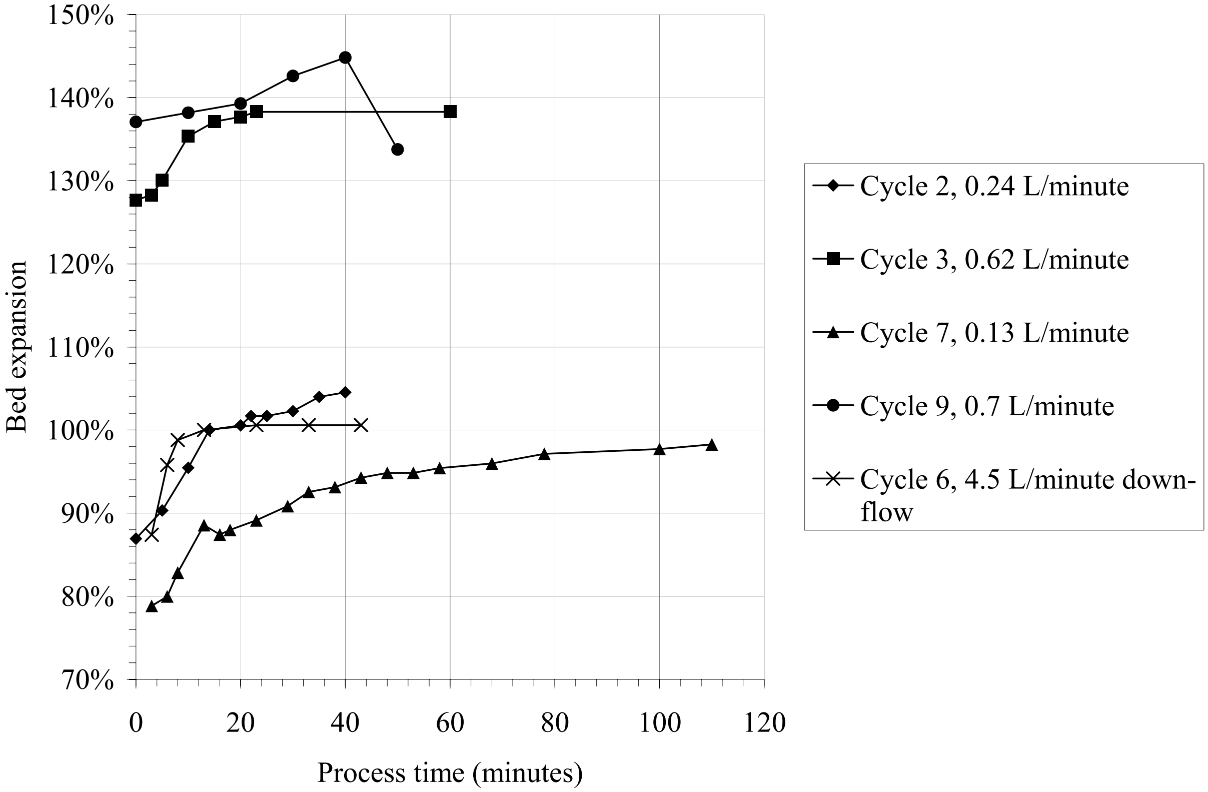

Figure 7-8. Variation of Bed Height with Process Time During Regeneration

Notwithstanding the caveats described above, some qualitative conclusions may be drawn from the results in Figure 7-8. The effects of fluidization dynamics on bed height are minimized in Cycle 7 because at 2.7 cm/minute, the bed was quiescent, as indicated in Figure 7-7. At this velocity, the bed appears to require approximately 120 minutes to attain its full height or, by extension, become fully regenerated. Scaling on the basis of velocity, the bed height should have become steady at approximately 65 minutes in Cycle 2, and though data are only available up to 40 minutes, this extrapolation appears not unreasonable. For Cycle 3, the bed height should have steadied at 24 minutes, which is consistent with the experimental result, and 22 minutes in Cycle 9, which is inconsistent. However, the bed height in Cycle 9 was unsteady throughout the data-collection period, and the bed surface was observed wavy, which may have indicated sodium hydroxide channeling through the bed and inefficient contact between solution and resin. For down-flow regeneration at 94 cm/minute, the bed height should have steadied after only 4 minutes, but actually required 13 minutes. This discrepancy was probably caused by the fluid flow constraining the bed's expansion (manifesting the high axial and radial bed pressures). Indeed, the bed height was approximately 5 mm lower upon concluding down-flow regeneration than observed upon terminating up-flow regeneration.

The sodium hydroxide concentration in the effluent was measured in later cycles using the conductivity probe. The volume of sodium hydroxide recycled was consistently 2.03 L for these cycles to provide a consistent basis for analysis. For analysis purposes, the influent concentration was calculated assuming the feed carboy to be perfectly mixed, and sodium consumption was calculated from the effluent and influent concentration difference. Figure 7-9 compares the sodium consumption and bed expansion profiles from Cycles 10 (performed at 2.1 cm/minute) and 12 (performed at 15 cm/minute, for the first 10 minutes and then 2.1 cm/minute). In Cycle 10, bed expansion appears to track sodium consumption, approaching their asymptotic values after 120 minutes. The change from 15 cm/minute to 2.1 cm/minute in Cycle 12 is distinctive from the change in bed expansion and rate of sodium consumption. Cycles 9 and 11 were also conducted at 15 cm/minute, and these results are presented in Figure 7-10. Sodium consumption was reproducible, attaining asymptotic values after 18 minutes, approximately in proportion to the result from Cycle 10 on the basis of flow rate. However, Cycle 11 bed expansion was significantly lower than in Cycles 9 or 12 and appeared to be increasing when regeneration was terminated. The reason for this observation is currently unknown.

The capacity of the resin was calculated to be 1.55 mol/L based on the total number of moles of sodium consumed by the resin from the results of Cycles 9 through 12.

7.4.2 Up-flow Simulated AP101 LAW Introduction

Up-flow simulated AP101 introduction was generally performed at a velocity of 2.5 cm/minute. In the conditioning cycles and Cycles 1 through 3, the bed rose as a plug sufficiently high that pumping was terminated to allow the plug to break up and settle. Plug break-up then occurred at decreasing heights for each successive cycle until the entire operation could be accomplished without interruption. A small spout could be observed once the plug had settled, but this was sometimes sufficient to lead to an uneven level when flow was terminated. Alternatively, an even bed level could be consistently achieved by fluidizing the bed at velocities greater than 4.2 cm/minute. Therefore, the best simulated LAW introduction procedure was to initially feed at a velocity of 2.5 cm/minute until the simulated LAW had displaced the 0.5 M sodium hydroxide when the bed was fluidized at 4.2 cm/minute.

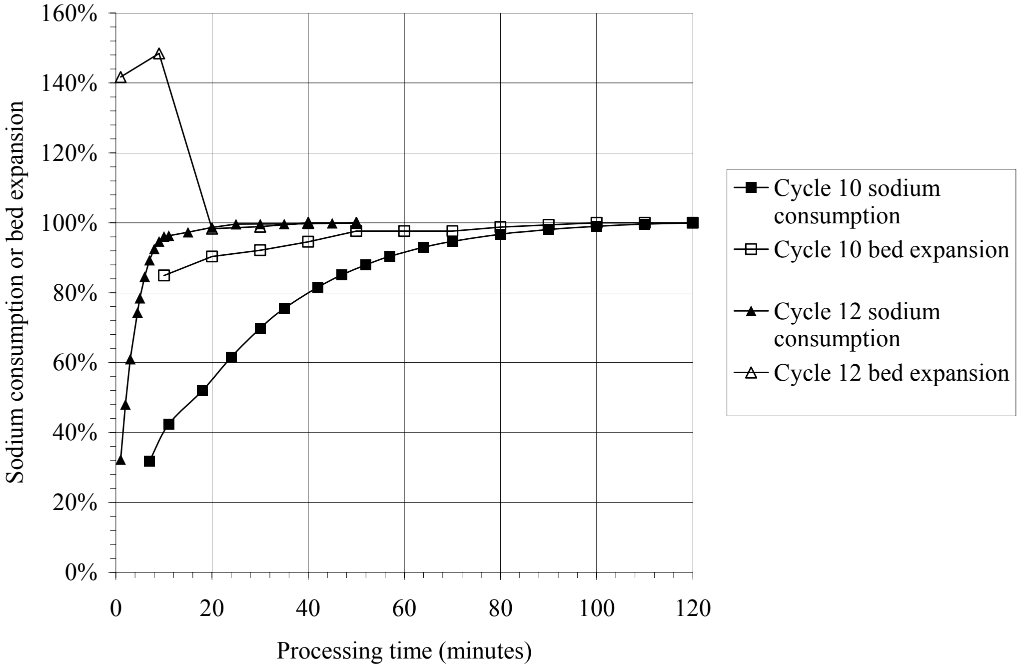

Figure 7-9. Sodium Hydroxide and Bed Expansion Profiles in Cycles 10 (2.1 cm/minute) and 12 (15 cm/minute for first 10 minutes and then 2.1 cm/minute)

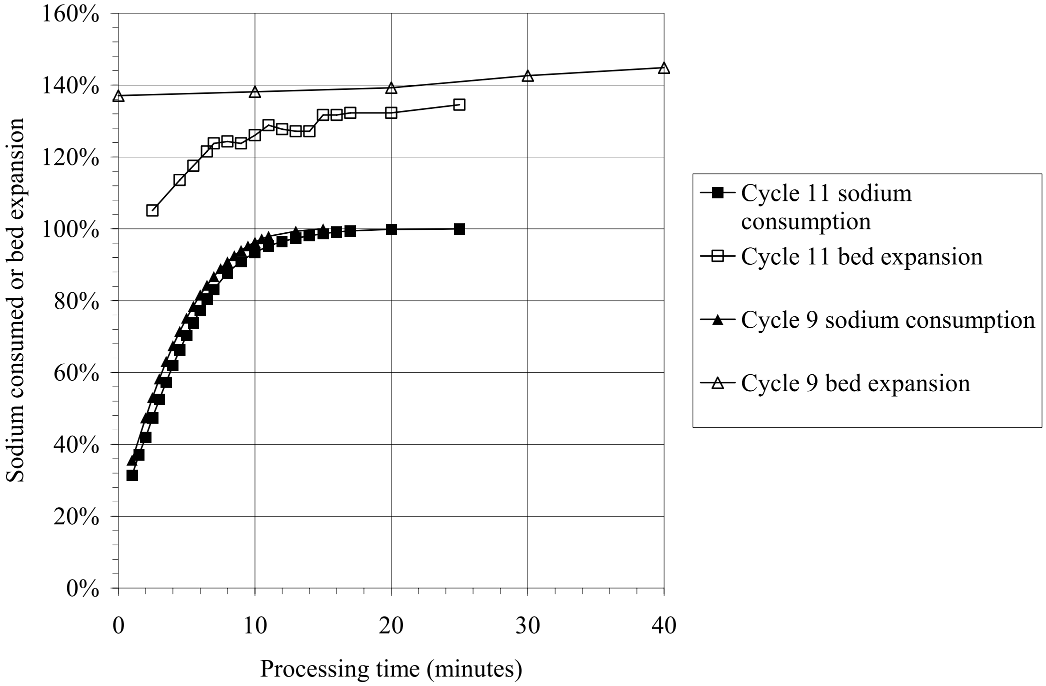

Figure 7-10. Sodium Hydroxide and Bed Expansion Profiles in Cycles 9 and 11 (15 cm/minute)

Two fluid interfaces, caused by a density difference, were observed during up-flow simulated AP101 LAW introduction. The first was always observed above the bed and defined the interface between the 0.5 M sodium hydroxide (density of ~1.01 g/mL) resident in the column from the preceding regeneration and a low-density simulated LAW fluid. The low-density simulated LAW had a density of ~1.1 g/mL, compared to a simulated AP101 LAW density of ~1.2 g/mL, which may be indicative of a lower sodium or potassium concentration. The second interface was most dramatically observed in the early cycles when the flow was terminated to allow the resin plug to break up and settle. This interface always coincided with the top surface of the plug before its break-up. The fluid below this interface had a density consistent with simulated AP101 LAW. This phenomenon cannot be adequately explained at present but may be at least partly associated with back-mixing of sodium hydroxide and simulated LAW or depletion of potassium by ion exchange.

8.0 Wave 4 (Subsequent 100-Gallon Batches) Results Analysis and Discussion

This section describes the following results obtained from the Wave 4 testing cycle:

- The bed voidage of resin 5J-370/686 (MB686) and blend of resins BSC-3380-3-0200 and BSC-3380-3-0201 (BSblend) during processing of LAW
- Steady-state pressures of resin 5J-370/686 and blend of resins BSC-3380-3-0200 and BSC-3380-3-0201 during processing of LAW
- Observations from fluidization steps
- Regeneration and elution efficiency.

Wave 4 resins were pre-treated by soaking them in 1 M sodium hydroxide overnight before loading them into the columns to produce beds with height to diameter ratios of 1.13 for both resins. No in-column conditioning was designated. A complete ion exchange cycle included upflow regeneration (conditioning in cycle 1) with 0.5 M sodium hydroxide, up-flow simulated LAW introduction, down-flow simulated LAW processing, 0.1 M sodium hydroxide feed displacement, DI water washes and up-flow elution.

8.1 Bed Voidage and Permeability

Figure 8-1 and Figure 8-2 illustrate that the bed voidage remained essentially constant through the four cycles and with respect to bed differential pressure with average values of 0.41 for both MB686 and the BSblend resins, which is broadly consistent with the results from Waves 2 and 3. The permeability of the resins processing LAW was 2.5×10^{-10} m^2 based on a bed voidage of 0.41 and a bead area mean diameter of 441 μm and 444 μm for the MB686 and BSblend resins, respectively.

8.2 Steady-State Bed Pressures for the Wave 4 Resins Processing LAW

Figure 8-3 and Figure 8-4 presents the steady-state radial and axial bed pressures for resins MB686 and BSblend processing LAW. In similar manner to Wave 3, the pressures are somewhat higher than the differential pressure less bed buoyancy, indicating that up-flow LAW introduction was effective in relieving any radial stresses in the bed arising from its expansion during regeneration and in LAW. The fluid pushes the resin bed down, which then appears to produce axial and radial force components against the wall.

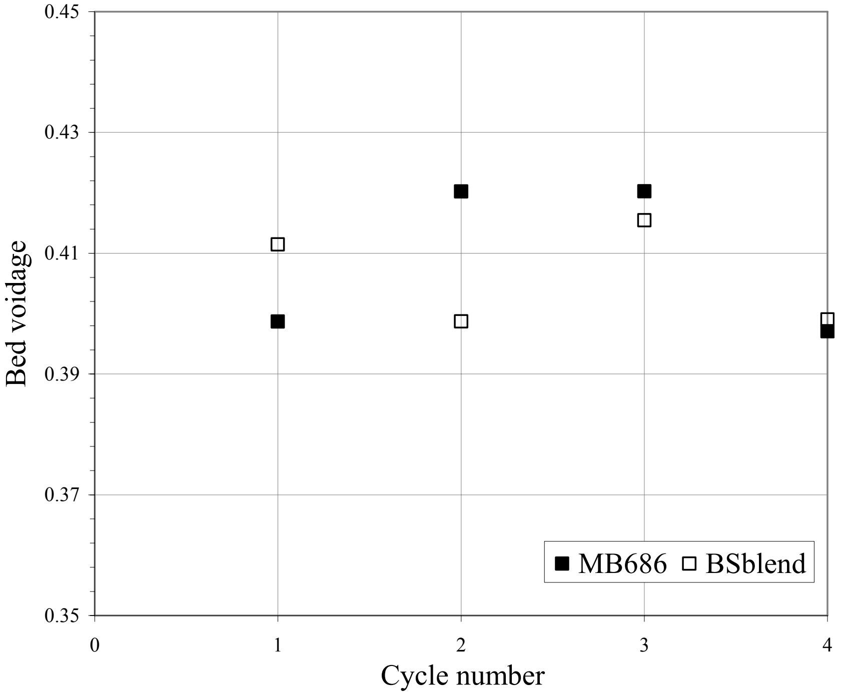

Figure 8-1. Bed Voidage of RF Resins MB686 and BSblend as a Function of Cycle Number

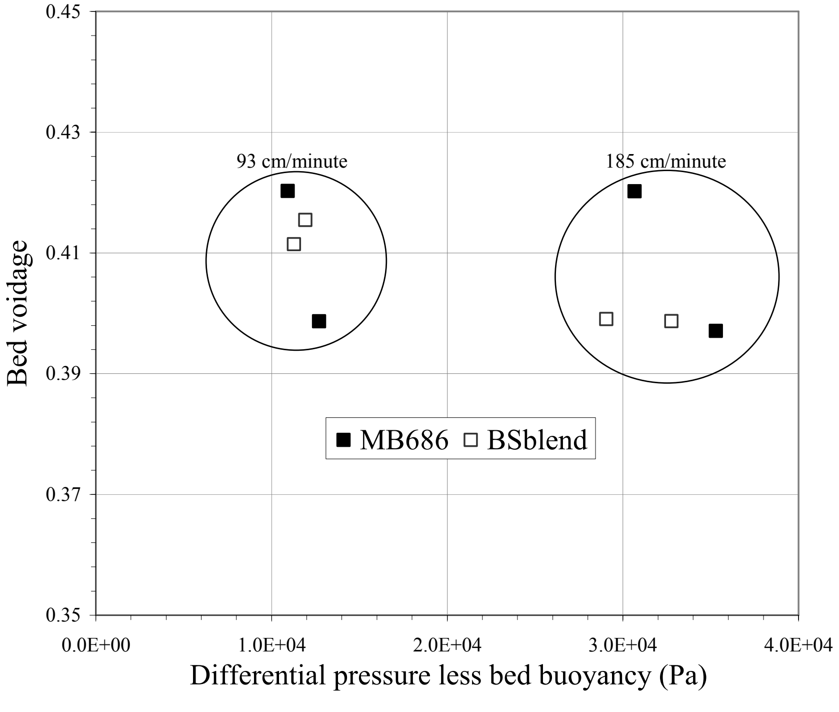

Figure 8-2. Bed Voidage of RF Resins MB686 and BSblend as a Function of Bed Differential Pressure

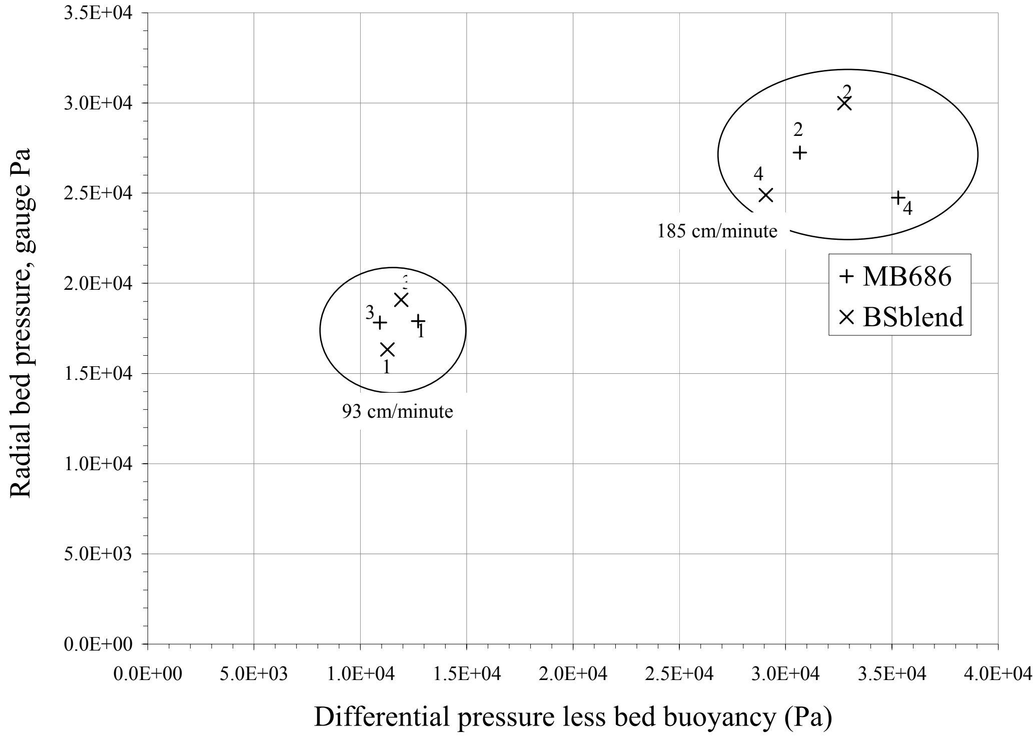

Figure 8-3. Steady-State Radial Pressures for Resins MB686 and BSblend Processing LAW (height to diameter ratios of relaxed beds were both 1.13) (data points labeled with the cycle number)

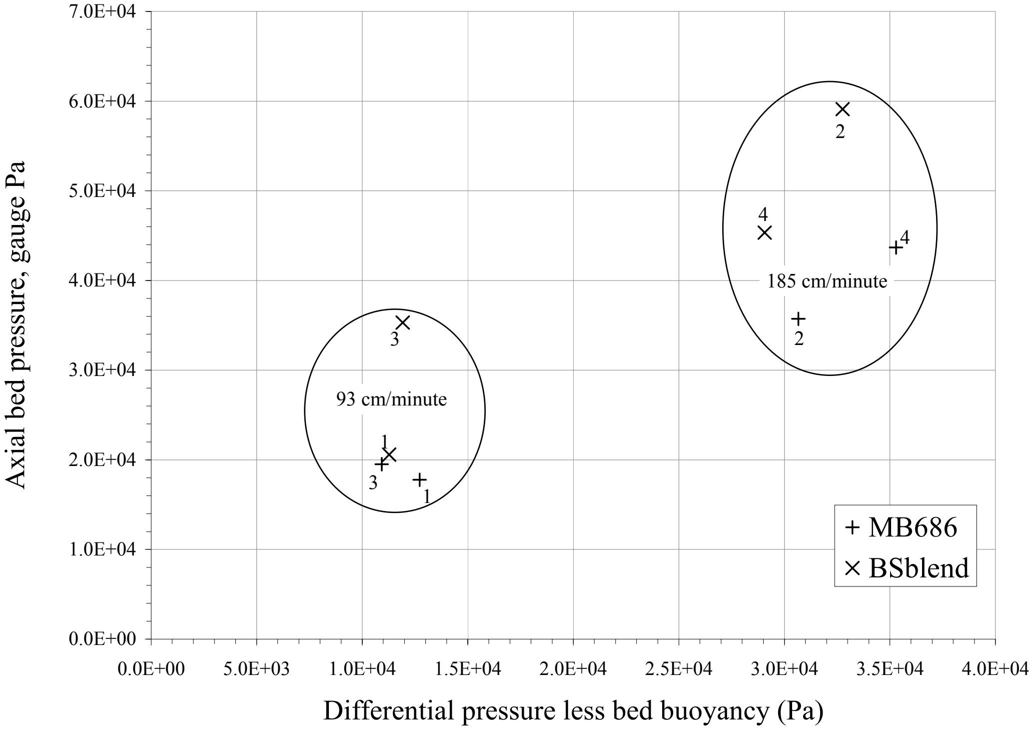

Figure 8-4. Steady-State Axial Pressures for resins MB686 and BSblend processing LAW (height to diameter ratios of relaxed beds were both 1.13) (data points labeled with the cycle number)

8.3 Resin Bed Characterization

8.3.1 Particle Size Distribution

Figure 8-5 and Figure 8-6 compare the particle size distributions of as-received and cycled acid-form MB686 and BSblend resins, respectively. The resin remained mono-modal with no generation of fines. The cycled resin is larger than the as-received consistent with the observations from previous waves in that there was no significant variation in bed height and the bed voidage. Volumetric mean particle diameters were 393 µm and 420 µm for the acid form as-received and cycled MB686 resins, respectively, reflecting the slight expansion of the resin on the first cycle. The acid-form BSblend resin volumetric mean particle diameters were 389 µm and 419 µm as-received and cycled, respectively, which show a similar slight expansion of the resin.

The cycled resins were converted to the sodium form by soaking samples in 1 M sodium hydroxide, decanting the supernatant solution and then rinsing with DI water. Supernatant DI water was decanted, and then the requisite contact solution was added. The resins remained in contact with the solutions for approximately 1 week before the particle size analysis was performed. There appeared to be little change in the mean volume diameter of the cycled MB686 sodium-form resin with respect to the composition of the alkaline contact solution, as shown in Table 8-1. However, a small increase in the area mean diameter is apparent with increasing sodium hydroxide concentration. The insignificant variation of sodium-form bead diameter with contact solution is consistent with the insignificant bed height variation observed for the resin in 0.5M and 0.1M sodium hydroxide and simulated LAW.

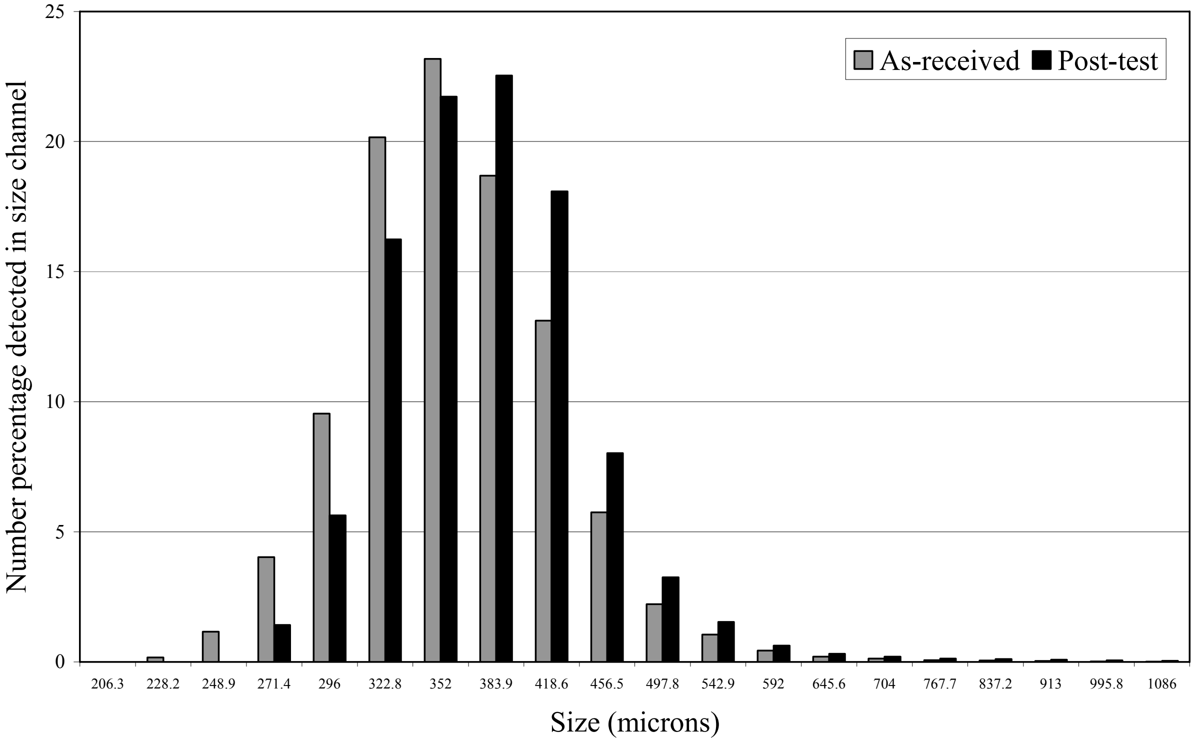

Figure 8-5. Comparison of As-Received and Cycled Acid-Form MB686 Particle Size Distributions

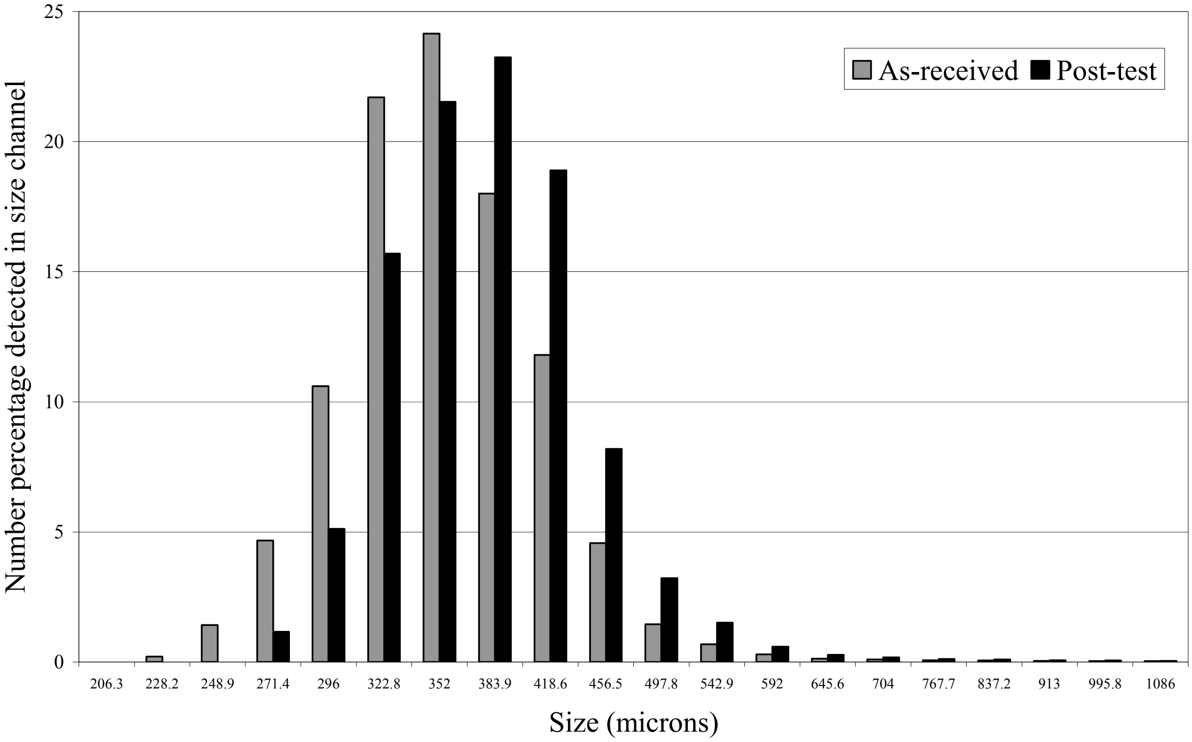

Figure 8-6. Comparison of As-Received and Cycled Acid-Form BSblend Particle Size Distributions

Table 8-1. Particle Size Measurements for Cycled MB686 and BSblend Resins in Various Matrices

Resin (cycled)	Matrix					
	0.1 M sodium hydroxide		0.5 M sodium hydroxide		Simulated LAW	
	Mean diameter (μm)					
	Volume	Area	Volume	Area	Volume	Area
MB686	455	437	456	439	455	441
BSblend	Not measured		Not measured		470	444

8.3.2 Microscopic Analysis

There is no evidence that any of the beads broke during process cycling, as shown in the micrographs in Figure 8-7 and Figure 8-8 for the BSblend and MB686 resins, respectively. The micrographs show both cycled resins to be significantly darker than their as-received counterparts, as observed previously for the spherical RF resins. However, resin oxidation did not significantly affect the resins' hydraulic characteristics over 4 cycles, as noted before, except they appeared more buoyant during up-flow processing, which is consistent with a lower density.

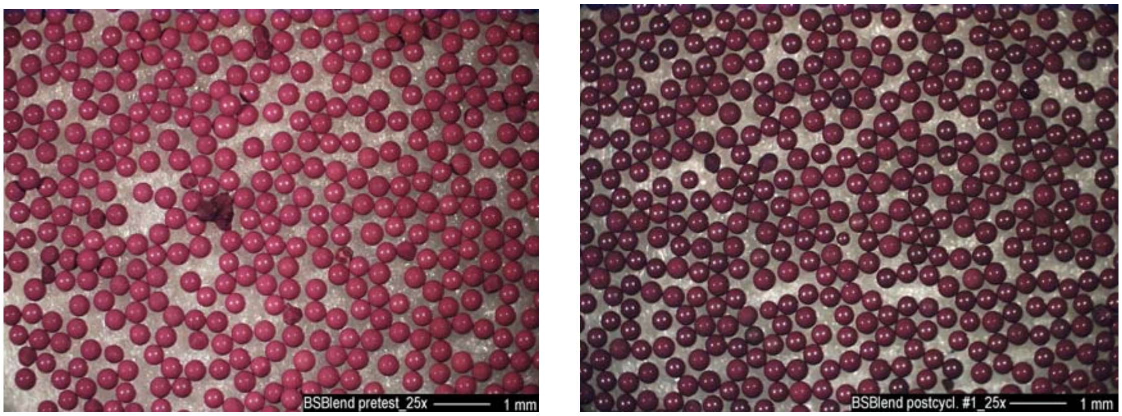

Figure 8-7. Micrographs of As-Received and Cycled Acid-Form BSblend Resin

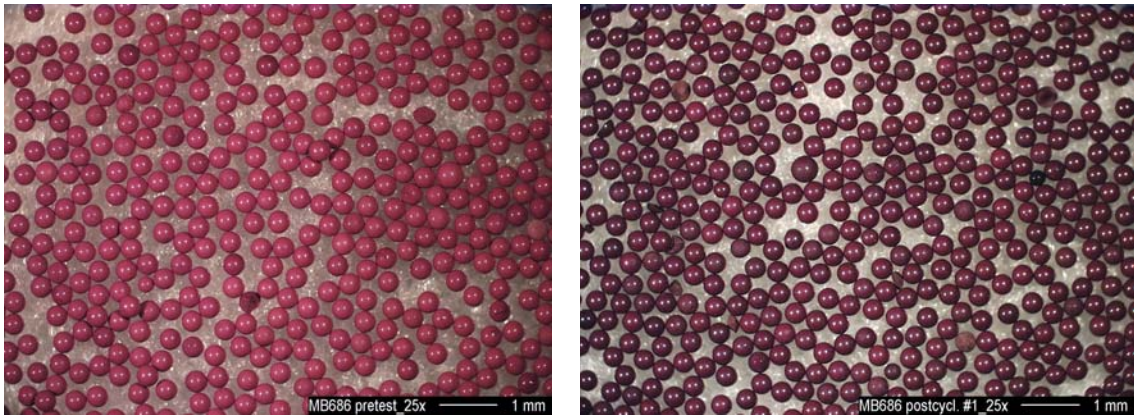

Figure 8-8. Micrographs of As-Received and Cycled Acid-Form MB686 Resin

8.3.3 Bed Density

The bed density in each column was determined by extracting the beds into graduated cylinders (of diameter 2 cm) and then drying a fraction of each bed to obtain the dry weight of resin. The column bed density was calculated from multiplying the graduated cylinder bed density by the ratio of graduated cylinder to column bed volumes. Table 8-2 provides a summary of the results and compares them to values measured and calculated by Fiskum et al. (2006)[15] from 2-cm columns.

Acid-form MB686 and BSblend graduated cylinder bed densities were 370 kg/m^3 and 410 kg/m^3, respectively, which are consistent with the values measured in 2-cm diameter glass columns[16]. In contrast, the acid-form MB686 and BSblend 3-inch column bed densities were calculated at 330 kg/m^{3}and 370 kg/m^3, respectively, which convert to 330 kg/m^{3}and 370 kg/m^3, respectively, in the sodium form in sodium hydroxide. That the bed density was lower in the 3-inch column is surprising because the column walls would be expected to hold the particles up by friction and so create a lower density in the 2-

---

[16] Fiskum, SK, ST Arm, WC Buchmiller, T Trang-Le, JE Martinez, J Matyas, MJ Steele, KK Thomas, DL Blanchard. 2006. *Comparison Testing of Multiple Spherical Resorcinol Formaldehyde Resins for the River Protection Project – Waste Treatment Plant*. WTP-RPT-143 (to be published), Battelle—Pacific Northwest Division, Richland, WA.

cm column. The difference is probably caused by the filled graduated cylinder being tapped until the bed achieved a constant volume whereas the column was never tapped. Clearly, even the simulated LAW pumped down-flow at high velocity was insufficient to configure the bed into its lowest volume because the voidage in the beds after up-flow simulated LAW was introduced was ~0.41 compared to 0.38 with no up-flow step. Acid form bed densities in simulated LAW and 0.5M sodium hydroxide were also lower by 10%. The 3-inch column bed density of the acid form MB686 resin was 270 kg/m^3 in simulated LAW and 0.5M sodium hydroxide compared to 300 kg/m^3 in the 2-cm column. Similarly, the 3-inch column bed densities of the acid form BSblend resin were 290 kg/m^3 in simulated LAW and 300 kg/m^3 in 0.5M sodium hydroxide compared to 340 kg/m^3 in the 2-cm column.

Table 8-2. Comparison of Wave 4 Bed Densities

Resin	Condition	Bed density (kg/m^3)$^{(1)}$	
		3-inch column	2-cm column
MB686	Acid form in water	331	366
	Sodium form in sodium hydroxide	325	Not measured
	Acid form in LAW	270	298
	Acid form in 0.5M sodium hydroxide	267	298
BSblend	Acid form in water	368	422
	Sodium form in sodium hydroxide	367	Not measured
	Acid form in LAW	294	338
	Acid form in 0.5M sodium hydroxide	300	341
1. Bed densities are accurate to two significant figures.			

8.4 Results and Observations from Up-flow Regeneration, Simulated LAW Introduction, and Elution

8.4.1 Up-flow Regeneration

Fluidized regeneration was characterized by measuring the bed height as a function of fluid velocity. Figure 8-9 illustrates the BSblend resin bed expansion as a function of fluid velocity in Cycles 3 and 4. This comparison clearly illustrates the impact of air bubbles trapped beneath the bed support screen, causing spouting. Spouting was observed at all velocities except the highest value in Cycle 3. In contrast, spouting was not observed in Cycle 4 except towards the end of the test at the highest velocity, coincident with air bubbles being observed in the feed tube. The spouting bed of Cycle 3 was consistently smaller at the same velocity because a portion of the fluid flow channeled through the bed to cause the spout. Also note that the bed contracted upon transitioning to the highest velocity in Cycle 4 when the air bubbles and spout were observed. A fluid velocity of 17.5 cm/minute was sufficient to achieve 50% bed expansion before the spout was manifested. A further reduction in velocity reduced the bed volume to a value below that observed earlier in the cycle when no spouting was observed. For example, a fluid velocity of 8.5 cm/minute was sufficient to achieve 20% bed expansion before the spout, but 13 cm/minute was required to achieve the same bed expansion afterward.

Figure 8-9 also illustrates the MB686 bed expansion in Cycle 4, for which no spouting was observed. The Cycle 4 MB686 and BSblend profiles are broadly consistent, indicating similar fluidization characteristics for the two resins.

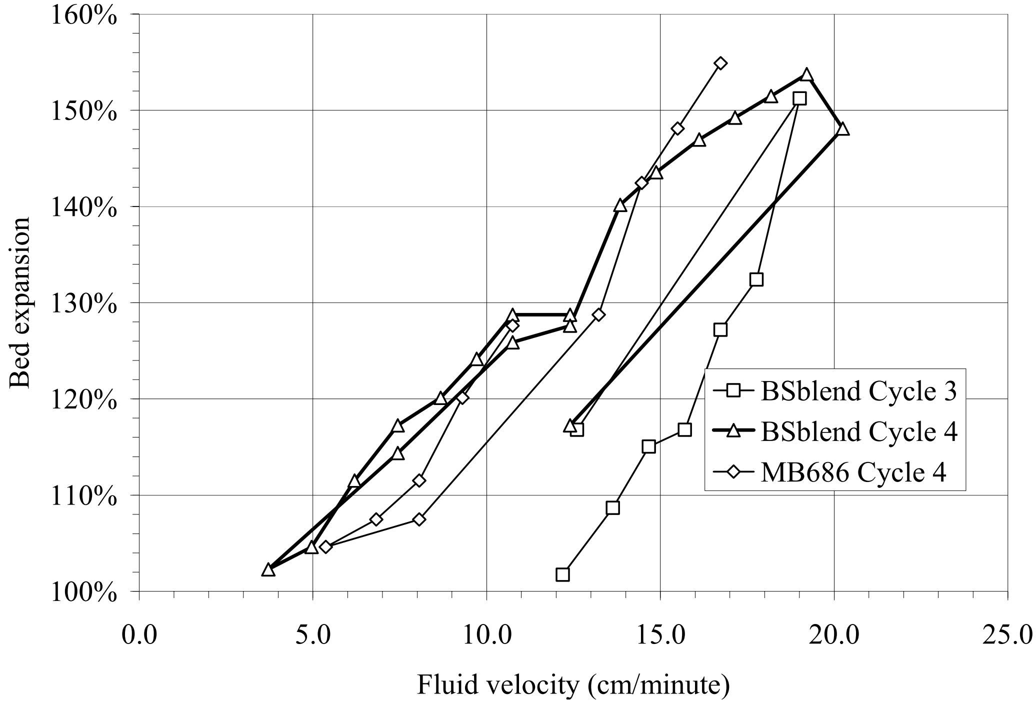

Figure 8-9. Fluidized Regeneration Characterization

MB686 regeneration effluent conductivity was measured in the same manner used in Wave 3 to determine the sodium hydroxide concentration. The effluent sodium hydroxide profiles are presented in Figure 8-10 for Cycles 2 through 4 (the resin was loaded into the column in the sodium form in Cycle 1). The volume of 0.5 M sodium hydroxide feed was adjusted to target a final concentration of 0.1 M. Cycle 2 used a volume of 2.1 L whereas Cycles 3 and 4 used 1.9 L. The profiles are broadly consistent with 95% equilibrium sodium hydroxide concentration achieved after 28 minutes in Cycles 2 and 3 and 22 minutes in Cycle 4. Regeneration appeared faster in Wave 3 with Cycles 9 and 11 requiring approximately 10 minutes to achieve 95% equilibrium sodium hydroxide concentration using 2 L of 0.5 M sodium hydroxide solution. This can be at least partially explained by the higher velocity used in Wave 3 (15 cm/minute) compared to 13 cm/minute used in Wave 4, providing faster mass transfer. In addition, the Wave 4 resins appeared to have a higher capacity than the Wave 3 resin and so may have required longer to become saturated. The MB686 and BSblend resins had average sodium capacities of 1.72 mol/L (wet sodium-form resin bed) and 1.84 mol/L, respectively, compared to 1.55 mol/L for the 5E-370/641 resin used in Wave 3.

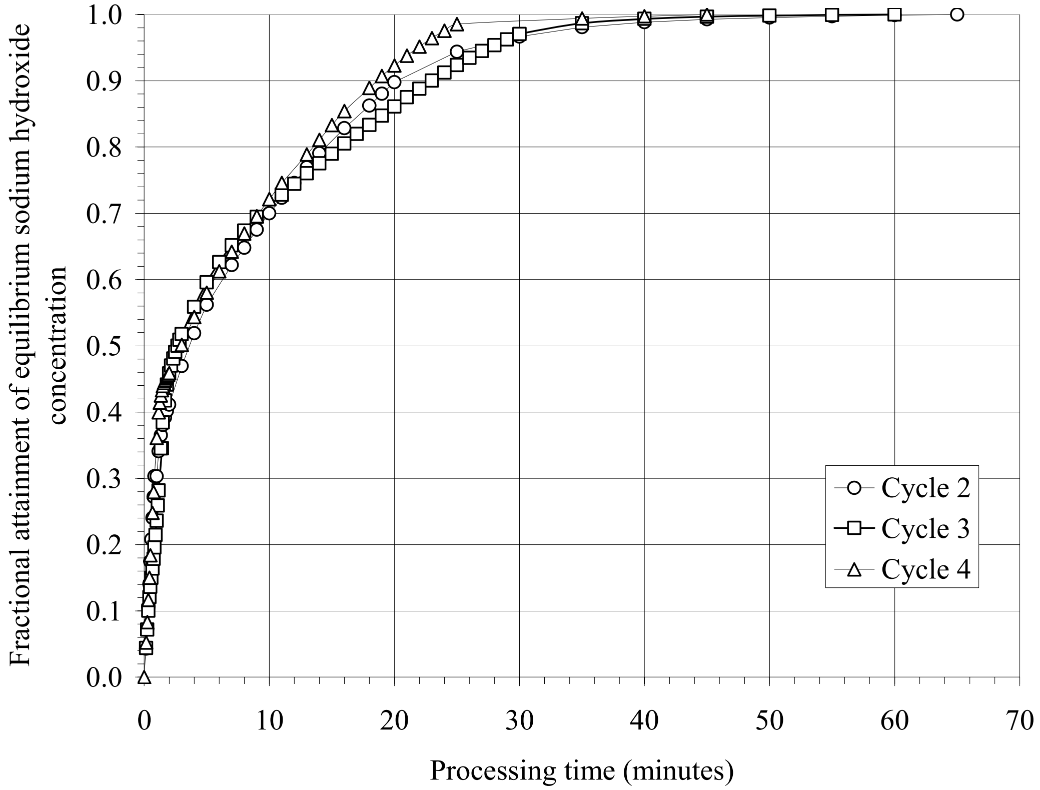

Figure 8-10. MB686 Regeneration Effluent Sodium Hydroxide Profiles

8.4.2 Up-flow Simulated LAW Introduction

Up-flow simulated LAW was introduced in a similar manner to that in Wave 3. Simulated LAW was first introduced at 2.5 cm/minute until the sodium hydroxide solution from regeneration had been displaced when the velocity was increased to 4.2 cm/minute to fluidize the beds. As observed in Wave 3, up-flow at the lowest velocity had to be suspended while the resin settled after rising as a plug. While the BSblend resin settled reasonably quickly, the MB686 resin tended to remain suspended, particularly at the fluid interface coincident with the bed's top surface. This interface, ostensibly between high and low density simulated LAW, had significant structural strength because attempts to break it using simulated LAW down-flow at 2.5 cm/minute failed. Instead, simulated LAW was pumped down-flow to displace the interface through the column bottom and so settle the bed before fluidizing it at 4.2 cm/minute.

8.4.3 Up-flow Elution

Fluidized elution was characterized in the same manner for fluidized regeneration by varying the velocity and measuring the bed height. Spouting, caused by bubbles entrained in the feed becoming trapped beneath the support screen and leading to fluid channeling through the bed, presented an operational issue as it was during regeneration. The best results were obtained from the last cycle for the BSblend resin, and they are presented in Figure 8-11 with the results from Cycle 3. No spouting was observed throughout Cycle 4 elution, and this is consistent with the lack of any hysteresis in the bed-expansion/fluid-velocity profile. A velocity of 10 cm/minute provided 50% bed expansion. Spouting was initially observed in Cycle 3, and the results shown in Figure 8-11 indicate that significantly higher velocities were required to achieve the same bed expansion than found in Cycle 4. For example, 50% bed expansion was achieved at 10 cm/minute in Cycle 4 with no spouting, but 15 cm/minute was required in Cycle 3 with the spout. Clearly, the spout indicates that a portion of the fluid channels through the bed at high velocity so that most of the bed actually experiences a lower velocity than what would be calculated by dividing the flow rate by the column cross-sectional area. An attempt was made to eliminate the spout in Cycle 3 by pumping nitric acid down-flow at high velocity (~190 cm/minute) to drive any trapped bubbles out through the column bottom. This appeared to be at least partially successful because subsequent bed expansion data illustrated in Figure 8-11 are more consistent with the results from Cycle 4, and no spouting was observed.

Acid concentrations were determined for the feed and effluents in Cycles 3 and 4 to derive resin capacities. MB686 capacities were 1.86 and 1.65 mol/L sodium-form resin in Cycles 3 and 4 in contact with nitric acid of final concentrations 0.077 M and 0.11 M, respectively, which are consistent with the capacities calculated from the regeneration step. The BSblend capacity calculated for Cycle 4 was also consistent with the regeneration value at 1.65 mol/L with the resin in contact with nitric acid of final concentration 0.066 M. However, the Cycle 3 value was higher at 1.94 mol/L with the resin in contact with nitric acid of final concentration 0.11 M. Nonetheless the average capacity calculated for these resins of 1.8 mol/L was consistent with the overall average calculated from regeneration.

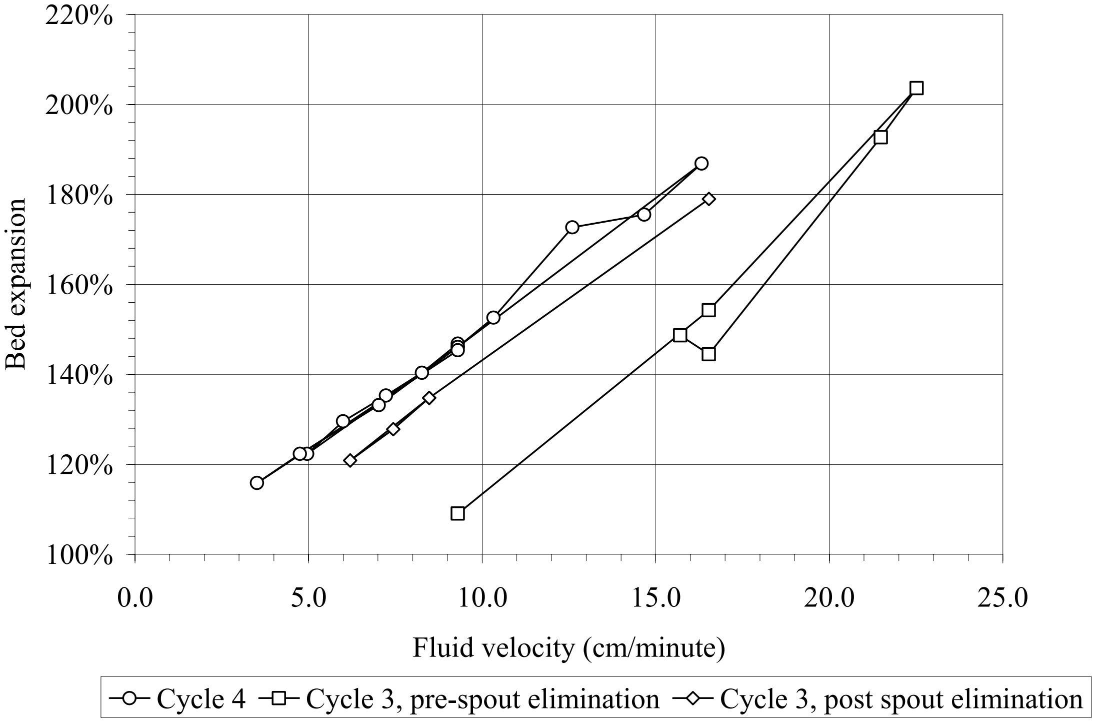

Figure 8-11. Fluidized BSblend Elution Characterization

9.0 Batch-Contact Testing

The following sections discuss the batch-contact equilibrium verification, equilibrium-distribution coefficient determinations, and isotherms for the as-received and cycled BRF14 resins from Wave 1 (section 2.1). Batch-contact details are provided in Appendix A.

9.1 Equilibrium Test

Batch-contact equilibrium, evaluated with the as-received (VR) pretreated resin at the low cesium concentration, was obtained within 24 hours. The average cesium distribution (K_d) results for each contact time (24, 46, and 72 hours) were 582, 564, and 570, respectively, with 2% relative percent differences of the duplicates. The overall average K_d equaled 572 mL/g with a relative standard deviation of 2%. There were no measurable differences in K_d values over the 3 days contacted. Therefore, attainment of the equilibrium condition is assumed at the 46-hour contact time for the remaining batch-contact tests.

The equilibrium results were consistent with those reported by Brown et al. (1995) where cesium equilibrium conditions were established with RF resin in 20 hours and Fiskum et al. (2003b) where cesium equilibrium was shown to be obtained within 24 hours.

9.2 Batch-Contact Comparison of Virgin and Hydraulic-Tested Resins

There was no discernable difference in the equilibrium cesium distribution (K_d values) as a function of the cesium concentration for the HT and VR resins. Table 9-1 summarizes the cesium K_d results. Figure 9-1 presents the same data for clarity of comparison.

Table 9-1. Distribution Coefficients for Virgin and Hydraulic-Tested Resins

Virgin Resin				Hydraulic-Tested Resin			
Equilibrium Cs Concentration		K_d	RPD(1)	Equilibrium Cs Concentration		K_d	RPD(1) or RSD(2)
mg Cs/L	mg Cs/g	mL/g		mg Cs/L	mg Cs/g	mL/g	
0.864	0.505	584	2.2	1.03	0.588	570	0.88
0.917	0.523	572		1.03	0.584	565	
38.5	12.7	331	1.6	44.7	13.7	306	1.3
39.9	13.0	326		41.3	12.9	312	
				41.3	12.9	314	
258.0	48.0	186	0.94	263.0	46.5	177	1.4
268.0	49.5	184		274.0	47.7	174	

1. RPD is the relative percent difference (between two values)
2. RSD is the relative standard deviation (between more than two values)

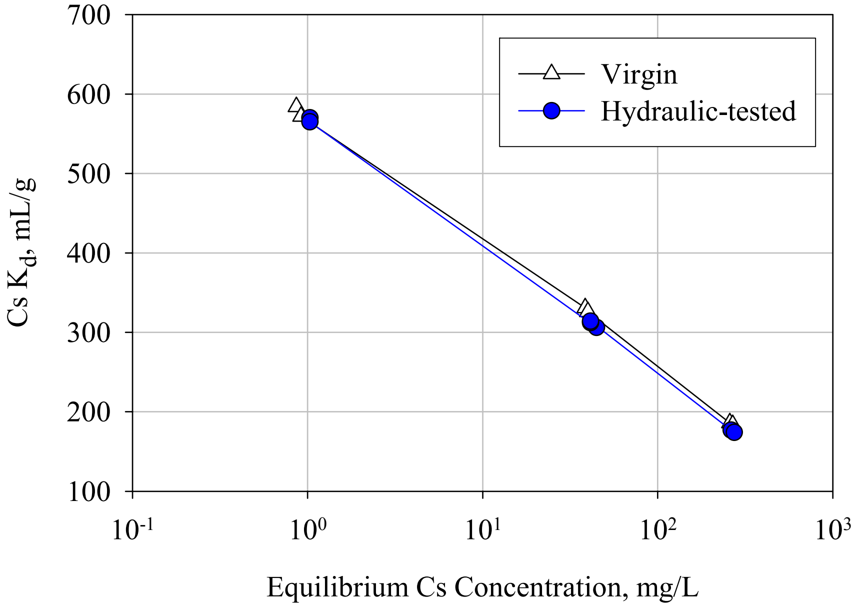

Figure 9-1. Batch Distribution Coefficients as a Function of Cesium Concentration in Simulated AP101 LAW

9.3 Isotherms

The equilibrium cesium concentrations in the supernates were calculated according to Equation (2.2), and the cesium concentrations in the resins were calculated according to Equation (2.1). Table 9-1 provides the calculated equilibrium concentrations.

Figure 9-2 presents the isotherms represented by these values. The equilibrium cesium concentrations in the resins are represented in two manners, concentration expressed as mg/g (left axis) and concentration expressed as mmoles/g (right axis). All resin masses were based on the acid-form resin. To correct for the sodium-form resin mass, the mass increase factor (I_{Na}) on conversion to the sodium form would need to be incorporated. Application of this correction is expected to decrease the reported values.

The equilibrium cesium loading condition followed the Langmuir adsorption equation, which is the basis of the best-fit curves shown in Figure 9-2. The total cesium capacity for the given matrix (simulated AP101 LAW) can be estimated from the isotherm where the curve levels off at a given cesium concentration in the resin. It appeared that the resin had not reached the cesium-capacity limit; the isotherm curves did not level off appreciably and appeared, instead, to continue to climb past the experimental limit of 700 mg/L initial cesium concentration.

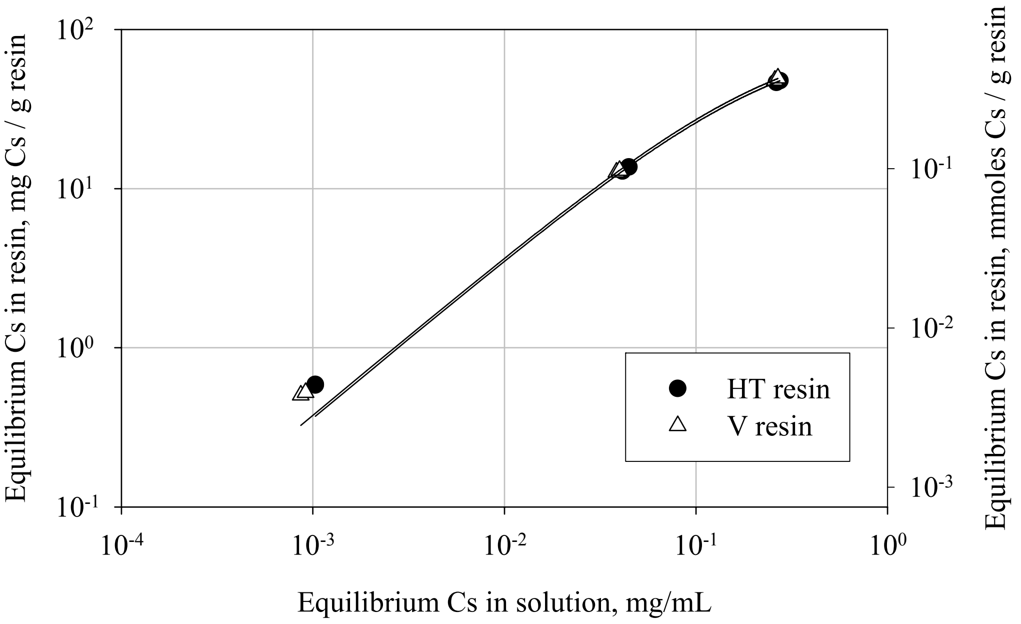

Figure 9-2. Cesium Isotherms for Virgin and Hydraulic-Tested BRF14 Resin

Based on comparison of the equilibrium isotherms and distribution coefficients, there appears to be no significant reduction in chemical performance of the BRF15 resin after 10 cycles. Extrapolating this conclusion to the other spherical RF batches appears reasonable since Fiskum et al. (2006)[17] report a 9% reduction in column performance after 17 cycles for resin 5E-370/641.

---

[17] Fiskum, SK, ST Arm, WC Buchmiller, T Trang-Le, JE Martinez, J Matyas, MJ Steele, KK Thomas, DL Blanchard. 2006. *Comparison Testing of Multiple Spherical Resorcinol Formaldehyde Resins for the River Protection Project – Waste Treatment Plant.* WTP-RPT-143 (to be published), Battelle—Pacific Northwest Division, Richland, WA.

10.0 Conclusions

The laboratory scale hydraulic testing of spherical RF ion exchange resins as described in this report leads to the following conclusions.

- The spherical RF resins experienced no significant deterioration in their hydraulic characteristics as they were cycled. One resin produced in a 100-gallon batch (5E-370/641) and representative of that expected for the WTP, experienced 14 cycles and exhibited no significant change in bed voidage.
- Bed voidage and permeability of the spherical RF resins depended upon the processing conditions. The development vendor's resins (BRF14, BRF15, and BRF18) were processed with down-flow regeneration and simulated LAW processing, leading to a bed voidage of ~0.38 and permeability of $\sim 3.2 \times 10^{-10}$ m^2. The scale-up (BSC00 and BSC01) and 100-gallon batches (5E-370/641, 5J-370/686, BSC-3380-3-0200 and BSC-3380-3-0201) were processed with fluidized regeneration and up-flow simulated LAW introduction before down-flow simulated LAW processing. The bed voidage and permeability of the scale-up and 100-gallon batch resins were ~0.41 and $\sim 2.3 \times 10^{-10}$ m^2. Introducing simulated LAW down-flow constrained the bed as it expanded following its initial contraction in LAW. The bed was therefore compressed, leading to a lower voidage than when the simulated LAW was introduced up-flow, and the bed was allowed to freely expand. The lower permeability of the scale-up and 100-gallon resin batches was caused by their smaller bead size. No breakage of the spherical RF resins was observed.
- For a spherical RF bed with height to diameter ratio of 1.6, the radial and axial bed pressures were up to ten times the differential pressure during down-flow regeneration, which is indicative of the residual stresses from the beds constrained expansion. The average radial to axial pressure ratio of 2.4 indicates an angle of internal friction of 25^o. For the same bed, bed pressures were approximately five times the differential pressure when the simulated LAW was immediately processed down-flow following down-flow regeneration,. The latter phenomenon is again indicative of stresses in the bed induced by its re-expansion following initial re-expansion in LAW. Up-flow LAW introduction allowed unrestrained re-expansion of the bed so that its pressures were comparable to the differential pressure.
- SL644 bed voidage and permeability were lower than those for the development spherical RF resin. During regeneration, SL644 bed voidage and permeability were 0.25 and $\sim 1 \times 10^{-10}$ m^2, respectively, and 0.32 and $\sim 2.4 \times 10^{-10}$ m^2, respectively, processing simulated LAW. Breakage of the granular SL644 resin particles led to the accumulation of fine material in the bed and decreasing bed voidage and permeability with increasing cycle number. Bed pressures were significantly higher than the differential pressure during regeneration, which is indicative of the stresses induced by constrained bed expansion. There was little change in the bed volume when processing LAW so the bed pressures were comparable to the differential pressure.
- Down-flow regenerated ion exchange beds could not be subsequently fluidized with simulated AP101 LAW, except where assisted by bubbles entrained in the feed, and the beds behaved as plugs adhering to the column walls. Up-flow LAW could be introduced without fluidization, but the observed partial break-up of the bed may potentially lead to fissures in the bed that would have channeled LAW and led to unacceptably early cesium breakthrough. Two methods for fluidizing the beds with simulated AP101 were successfully tested to achieve a level settled bed:

  - Relieve the radial pressures by alternately pumping and terminating up-flow simulated LAW while the bed undergoes initial contraction in simulated LAW. The bed can then be fluidized with simulated LAW.
  - Eliminate the radial pressures exerted by the bed by performing up-flow regeneration before introducing up-flow LAW. Bed expansion and sodium consumption tracked one another during up-flow regeneration, and the time for the bed to become fully regenerated was proportionate to the flow rate.

- Fluidized elution was successfully accomplished in Wave 4 with a range of velocities.
- A summary of the derived resin capacities is provided below in Table 10-1. Average capacity of the Wave 3 resin from a 100-gallon production batch was 1.55 mol/L wet sodium-form resin bed in contact with sodium hydroxide of final concentration ~0.1 M. Average capacities of the Wave 4 resin from the 100-gallon production batches were somewhat higher being of the order 1.8 mol/L wet sodium-form resin bed in contact with either nitric acid or sodium hydroxide of final concentration ~0.1 M.

Resin	Capacity (mol/L) and contact solution
5E-370/641 (Wave 3)	1.55 / 0.12 M sodium hydroxide
5J-370/686 (Wave 4)	1.72 / 0.10 M sodium hydroxide
	1.86 / 0.077 M nitric acid
	1.65 / 0.11 M nitric acid
BSC-3380-3-0200 and BSC-3380-3-0201 blend (Wave 4)	1.84 / 0.10 M sodium hydroxide
	1.94 / 0.066 M nitric acid
	1.65 / 0.11 M nitric acid

Table 10-1. Comparison of ion exchange capacities

- The density of the bed in the 3-inch column used in these tests appears to be 10% lower than that measured in the 2-cm columns of TSS A225. This difference is most likely caused by the 2-cm column being tapped until a constant volume is achieved whereas no such configuring of the bed was attempted in the 3-inch column to be representative of actual conditions expected in the WTP.
- There was no impact of chemical cycling up to 10 cycles on the equilibrium performance of the BRF15 spherical RF resin, as measured in batch contacts. Extrapolating this conclusion to the other spherical RF batches appears reasonable since Fiskum et al. (2006)[18] report a 9% reduction in column performance after 17 cycles for resin 5E-370/641.

---

[18] Fiskum, SK, ST Arm, WC Buchmiller, T Trang-Le, JE Martinez, J Matyas, MJ Steele, KK Thomas, DL Blanchard. 2006. *Comparison Testing of Multiple Spherical Resorcinol Formaldehyde Resins for the River Protection Project – Waste Treatment Plant.* WTP-RPT-143 (to be published), Battelle—Pacific Northwest Division, Richland, WA.

11.0 References

Adamson DJ, MD Fowley, JL Steimke, TJ Steeper, M Williams, CE Duffey and F Fondeur. 2006. *Pilot Scale Hydraulic Testing of Resorcinol Formaldehyde Ion Exchange Resin*. WSRC-TR-2005-00570, Savannah River National Laboratory, Savannah River Site, Aiken, SC.

Arm ST, DL Blanchard, PK Berry, SJ Bos, SA Bryan, JR DesChane, GS Klinger, AV Mitroshkov, KB Olsen, BM Rapko, RL Russell, and RL Sell. 2003a. *Radiation Stability Testing of SuperLig® 639 and SuperLig® 644 Resins.* PNWD-3239, Battelle—Pacific Northwest Division, Richland, WA.

Arm ST, DL Blanchard, SK Fiskum, and DR Weier. 2003b. *Chemical Degradation of SuperLig®644 Ion Exchange Resin*. PNWD-3315, Battelle—Pacific Northwest Division, Richland, WA.

Arm ST, and DL Blanchard. 2004. *Pre-conditioning and Regeneration Requirements of Ground Gel Resorcinol Formaldehyde Ion Exchange Resin.* PNWD-3390, Battelle—Pacific Northwest Division, Richland, WA.

Brown GN, LA Bray, and RJ Elovich. 1995. *Evaluation and Comparison of SuperLig®644, Resorcinol Formaldehyde and CS-100 Ion Exchange Materials for the Removal of Cesium from Simulated Alkaline Supernate.* PNL-10486, Pacific Northwest National Laboratory, Richland, WA.

Burgeson IE, DL Blanchard, BJ Cook, and JR Deschane. 2004. *Elution Testing of Resorcinol Formaldehyde Resins with AN-105 Simulant.* PNWD-3388, Battelle—Pacific Northwest Division, Richland, WA.

Coulson JM and JF Richardson. 1996. *Chemical Engineering*. Butterworth – Heinemann, Oxford, United Kingdom.

Ergun S. 1952. *Fluid Flow Through Packed Columns*. Chemical Engineering Progress 48(2), pages 89-94.

Fiskum SK, DL Blanchard Jr., MJ Steele, and JJ Wagner. 2003a. *Analysis of SuperLig® 644 Resin Used in Hanford Tank Waste Processing.* PNWD-3353, Battelle—Pacific Northwest Division, Richland, WA. See also references therein.

Fiskum SK, ST Arm, and DL Blanchard, Jr. 2003b. *Small Column Ion Exchange Testing of SuperLig®644 for Removal of ^{137}Cs from Hanford Waste Tank 241-AZ-102 Concentrate (Envelope B).* PNWD-3267, Battelle—Pacific Northwest Division, Richland, WA.

Fiskum SK, BS Augsberger, KP Brooks, WC Buchmiller, RL Russell, MJ Schweiger, LA Snow, MJ Steele, KK Thomas, DE Wallace, NH Wong, JD Yeager, and DL Blanchard. 2004. *Comparison Testing of Multiple Resorcinol Formaldehyde Resins for the River Protection Project – Waste Treatment Plant*. PNWD-3387, Battelle—Pacific Northwest Division, Richland, WA.

Hassan NM, WD King, DJ McCabe, and ML Crowder. 2001. *Small-Scale Ion Exchange Removal of Cesium and Technetium from Envelope B Hanford Tank 241-AZ-102.* WSRC-TR-2000-00419, Westinghouse Savannah River Company, Aiken, SC.

Kurath DE, DL Blanchard, and JR Bontha. 2000a. *Small Column Ion Exchange Testing of Superlig 644 for Removal of* ^{137}*Cs from Hanford Tank Waste Envelope A (Tank 241-AW-101).* PNWD-3001, Battelle—Pacific Northwest Division, Richland, WA.

Kurath DE, DL Blanchard, and JR Bontha. 2000b. *Small Column Ion Exchange Testing of Superlig 644 for Removal of* ^{137}*Cs from Hanford Tank Waste Envelope C (Tank 241-AN-107).* PNWD-3039, Battelle—Pacific Northwest Division, Richland, WA.

Leva M. 1959. *Fluidization*. McGraw-Hill, New York.

Lide DR (editor). 2004. *CRC Handbook of Chemistry and Physics*. 85th Edition. CRC Press, Boca Raton, FL.

Nedderman RM. 1992. *Statics and Kinematics of Granular Materials*. Cambridge University Press, Cambridge, United Kingdom.

Poloski AP, PR Bredt, RC Daniel and AE Saez. 2006. *The Contribution of Frictional Contacts to the Shear Strength of Coarse Glass Bead Powders and Slurries*. Rheologica Acta, January, 2006.

Russell RL, SK Fiskum, LK Jagoda, and AP Poloski. 2003. *AP-101 Diluted Feed (Envelope A) Simulant Development Report*. PNWD-3248, Battelle—Pacific Northwest Division, Richland, WA.

Appendix A: Batch-Contact Data

Appendix A: Batch-Contact Data

Tables A.1 and A.2 summarize the batch-contact equilibrium data input values. The contact solution was simulated AP101 LAW, and the contact media was acid-form BRF-14 RF resin. The equilibrium test used simulated LAW at an initial cesium concentration of 5.93 mg/L and the virgin resin. The raw data used to generate these data points are maintained in the project file 42365 at Battelle—Pacific Northwest Division.

Table A.1. Equilibrium Confirmation of Batch Contacts

Sample ID	Contact Time (hours)	Resin mass, g	F Factor, Water Loss	Simulant Volume*, mL	Equil. Sample Activity, mCi/L	Fraction Cs Remaining	Equil. Cs Molarity	Na/Cs Mole Ratio	Equil Cs, µg/mL	K_d, mL/g	Avg Kd, mL/g	RPD
390-AP-S1-C	NA	none	NA	19.5550	2.08E-2	Not applicable						0.5
390-AP-S1-CD	NA	none	NA	14.0539	2.07E-2							
390-AP-S1-VT1A	24	0.3304	0.5281	19.6681	3.39E-3	0.164	7.30E-6	6.85E+5	9.70E-1	576	582	2.1
390-AP-S1-VT1B	24	0.3317	0.5281	19.5717	3.31E-3	0.160	7.12E-6	7.03E+5	9.46E-1	588		
390-AP-S1-VT2A	48	0.3358	0.5281	19.5075	3.43E-3	0.165	7.38E-6	6.78E+5	9.80E-1	555	564	3.3
390-AP-S1-VT2B	48	0.3672	0.5281	19.6979	3.12E-3	0.150	6.71E-6	7.45E+5	8.92E-1	573		
390-AP-S1-VT3A	72	0.3519	0.5281	19.8125	3.30E-3	0.159	7.09E-6	7.05E+5	9.42E-1	564	570	2.2
390-AP-S1-VT3B	72	0.3429	0.5281	19.7487	3.30E-3	0.159	7.09E-6	7.05E+5	9.43E-1	577		

Table A.2. Batch-Contact Data for the Hydraulic-Tested and Virgin Materials

Sample ID	IX Material	Free-Flowing Resin Mass, g	F factor, Water Loss	Contact Volume, mL	Analysis Volume, mL	Sample Count Rate, cpm	% Count Error	cpm/mL	Avg cpm/mL	Fraction Cs Remaining	Equil Cs, mg/mL	Equil. Cs in Resin, mg/g	K_d, mL/g
390-AP-S1-C	None	none	NA	19.2290	2.0113	20,925	0.18	10,393		Not applicable			
390-AP-S1-CD	None	none	NA	13.8197	1.9902	20,720	0.18	10,400	10,396				
390-AP-S2-C	None	none	NA	13.5487	2.0098	18,410	0.19	9,149					
390-AP-S2-CD	None	none	NA	14.1892	2.0031	18,355	0.19	9,152	9,151				
390-AP-S3-C	None	none	NA	14.5719	1.9991	21,902	0.17	10,945					
390-AP-S3-CD	None	none	NA	14.4092	1.9992	21,944	0.17	10,965	10,955				
390-AP-S1-H	H	0.3311	0.5027	19.9721	2.0083	3,650	0.43	1,807	Not applicable	0.174	1.03E-3	5.88E-1	570
390-AP-S1-HD	H	0.3330	0.5027	19.9955	1.9962	3,641	0.43	1,813		0.174	1.03E-3	5.84E-1	565
390-AP-S2-H	H	0.3305	0.5027	20.4075	1.9965	5,249	0.36	2,618		0.286	4.47E-2	1.37E+1	306
390-AP-S2-HD	H	0.3618	0.5027	20.4398	1.9926	4,845	0.37	2,421		0.265	4.13E-2	1.29E+1	312
390-AP-S2-HT	H	0.3606	0.5027	20.4277	1.9958	4,846	0.37	2,417		0.264	4.13E-2	1.29E+1	314
390-AP-S3-H	H	0.3839	0.5027	20.4291	1.9856	8,171	0.29	4,104		0.375	2.63E-1	4.65E+1	177
390-AP-S3-HD	H	0.3603	0.5027	20.1609	1.9847	8,496	0.28	4,270		0.390	2.74E-1	4.77E+1	174
390-AP-S1-V	VR	0.3746	0.5281	19.7078	1.9941	3,041	0.47	1,514		0.146	8.64E-4	5.05E-1	584
390-AP-S1-VD	VR	0.3573	0.5281	19.7031	1.9799	3,201	0.46	1,606		0.154	9.16E-4	5.23E-1	572
390-AP-S2-V	VR	0.3524	0.5281	20.1380	1.9906	4,512	0.38	2,256		0.247	3.85E-2	1.27E+1	331
390-AP-S2-VD	VR	0.3413	0.5281	20.1350	1.9919	4,679	0.38	2,338		0.256	3.99E-2	1.30E+1	326
390-AP-S3-V	VR	0.3517	0.5281	20.1074	1.9854	8,022	0.29	4,030		0.368	2.58E-1	4.80E+1	186
390-AP-S3-VD	VR	0.3335	0.5281	20.0814	1.9839	8,328	0.28	4,187		0.382	2.68E-1	4.95E+1	184

Distribution

No. of Copies

OFFSITE

1 Savannah River National Laboratory
Richard Edwards
Savannah River National Laboratory
Westinghouse SA
Aiken, SC 29808-0001

No. of Copies

ONSITE

No. of Copies	Name	Location
12	Battelle—Pacific Northwest Division	
	S. T. Arm	P7-28
	D. L. Blanchard	P7-25
	W. C. Buchmiller	K6-24
	B. J. Cook	P7-25
	J. M. Cuta	K7-15
	S. K. Fiskum	P7-22
	D. E. Kurath	P7-28
	A. A. Schepmoes	K6-24
	Project Office (2)	P7-28
	Information Release (2)	K1-06
4	Bechtel National, Inc.	
	S. M. Barnes	H4-02
	D. L Gier (2)	H4-02
	M. R. Thorson	H4-02